Technische Universität München

Fakultät für Medizin

Mechanisms of tissue-specific T cell tolerance in diabetes

Maike Becker

Vollstänter Abdruck der von der Fakultät für Medizin

der Technischen Universität München zur Erlangung des

akademischen Grades eines Doktors der Naturwissenschaften

genehmigten Dissertation.

Vorsitzender: Prof. Dr. Percy A. Knolle

Prüfende der Dissertation:

1. Prof. Dr. Anette-Gabriele Ziegler

2. Prof. Dr. Hannelore Daniel

Mechanisms of tissue-specific T cell tolerance in diabetes

Dissertation zu Erlangung des

Doktorgrades der Naturwissenschaften

Maike Becker

geboren am 10. August 1990

in Heidenheim an der Brenz

Technische Universität München, Fakultät für Medizin

Helmholtz Zentrum München, Institut für Diabetesforschung

Betreuer: Prof. Dr. Anette-Gabriele Ziegler, Prof. Dr. Carolin Daniel

April 2016 – August 2019

Eidesstattliche Erklärung

Ich erkläre an Eides statt, dass ich die bei der promotionsführenden Einrichtung Technische Universität München, Fakultät für Medizin der TUM zur Promotionsprüfung vorgelegte Arbeit mit dem Titel **„Mechanisms of tissue-specific T cell tolerance in diabetes"** in Fakultät für Medizin, Lehrstuhl für Diabetes und Gestationsdiabetes unter der Anleitung und Betreuung durch Prof. Dr. Anette-Gabriele Ziegler ohne sonstige Hilfe erstellt und bei der Abfassung nur die gemäß § 6 Ab. 6 und 7 Satz 2 angebotenen Hilfsmittel benutzt habe.

Ich habe keine Organisation eingeschaltet, die gegen Entgelt Betreuerinnen und Betreuer für die Anfertigung von Dissertationen sucht, oder die mir obliegenden Pflichten hinsichtlich der Prüfungsleistungen für mich ganz oder teilweise erledigt.

Ich habe die Dissertation in dieser oder ähnlicher Form in keinem anderen Prüfungsverfahren als Prüfungsleistung vorgelegt.

Ich habe den angestrebten Doktorgrad noch nicht erworben und bin nicht in einem früheren Promotionsverfahren für den angestrebten Doktorgrad endgültig gescheitert.

Die öffentlich zugängliche Promotionsordnung der TUM ist mir bekannt, insbesondere habe ich die Bedeutung von § 28 (Nichtigkeit der Promotion) und § 29 (Entzug des Doktorgrades) zur Kenntnis genommen. Ich bin mir der Konsequenzen einer falschen Eidesstattlichen Erklärung bewusst.

Mit der Aufnahme meiner personenbezogenen Daten in die Alumni-Datei der TUM bin ich einverstanden.

München, den 05. August 2019

....
(Unterschrift) / (Signature)

Mentor: Prof. Dr. Carolin Daniel

1. Prüfer: Prof. Dr. Anette-Gabriele Ziegler

2. Prüfer: Prof. Dr. Hannelore Daniel

Table of Contents

List of Abbreviations

Abbreviation	
°C	degree Celsius
μ	micro-
aka	also known as
APC	antigen presenting cell
Areg	amphiregulin
ATP	adenosine triphosphate
BAT	brown adipose tissue
BSA	bovine serum albumin
BW	body weight
CD	cluster of differentiation
CK2	casein kinase 2
CNS	central nervous system
CNS2	conserved non-coding DNA sequence 2 (aka TSDR)
d	day(s)
PBS	Dulbecco's phosphate-buffered saline
EDTA	Ethylenediaminetetraacetic acid
eGFP	enhanced green fluorescent protein
et al.	*et alii*, and others
EtOH	ethanol
FACS	fluorescence-activated cell sorting
Foxp3	Forkhead box protein 3 (aka Scurfin)
FREECE	effect of the FTO-genotype on resting energy expenditure after defined cold exposure
GATA3	trans-acting T cell-specific transcription factor GATA-3
h	hour(s)
HBSS	Hank's balanced salt solution
HDAC	histone deacetylase
HEPES	4-(2-hydroxyethyl)-1-piperazineethanesulfonic acid

Abbreviation	
IL	Interleukin
IL-2Rα	Interleukin 2 receptor α (aka CD25)
IPEX	immune dysregulation, polyendocrinopathy, enteropathy, X-linked
IVC	individually ventilated cages
LIPSTIC	labelling immune partnerships by sortagging intercellular contacts
Lkb1	liver kinase b1
MACS	magnetic-activated cell separation
MAPK	mitogen-activated protein kinase
MBH	mediobasal hypothalamus
min	minute(s)
mTOR	mechanistic target of rapamycin
mTORC1	mechanistic target of rapamycin complex 1
Myf	myogenic factor
NEA	non-essential amino acids
NFAT	nuclear factor of activated T cells
NGS	next generation sequencing
Nlk	Nemo-like kinase
NST	non-shivering thermogenesis
OXPHOS	oxidative phosphorylation
PBMC	peripheral blood mononuclear cell
Pen/Strep	penicillin/streptomycin
PI3K	phosphoinositide 3 kinase
Pparγ	peroxisome proliferator-activated receptor gamma
Pten	phosphatase and tensin homologue
qPCR	quantitative real time polymerase chain reaction
RPMI	Roswell Park Memorial Institute medium
SAT	subcutaneous adipose tissue (also: scWAT)
SPF	specific pathogen free
ST2	IL-33 receptor (aka IL33R), encoded by *Il1rl1*
Stat	signal transducer and activator of transcription

Abbreviation	
STED	stimulated emission depletion
T2D	type 2 diabetes
Tbet	T-box transcription factor TBX21, encoded by *Tbx21*
Tbx21	T-box transcription factor TBX21, encodes for Tbet
Tak1	TGFβ-activated kinase 1
TCA	tricarboxylic acid
TCR	T cell receptor
TNFα	tumor necrosis factor α
TGFβ	transforming growth factor β
Treg	CD4$^+$Foxp3$^+$ regulatory T cell
TSDR	Treg-specific demethylated region; aka CNS2 of *Foxp3* locus
Ucp1	uncoupling protein 1
VAT	visceral adipose tissue
WAT	white adipose tissue
wk	week(s)

Publications included in this thesis

Peer-reviewed publications:

A Stat6/Pten Axis Links Regulatory T Cells with Adipose Tissue Function

Stefanie Kälin*, **Maike Becker***, Verena B. Ott, Isabelle Serr, Fabian Hosp, Mohammad M.H. Mollah, Susanne Keipert, Daniel Lamp, Francoise Rohner-Jeanrenaud, Victoria K. Flynn, Martin G. Scherm, Lucas F.R. Nascimento, Katharina Gerlach, Vanessa Popp, Sarah Dietzen, Tobias Bopp, Purna Krishnamurthy, Mark H. Kaplan, Manuel Serrano, Stephen C. Woods, Philipp Tripal, Ralf Palmisano, Martin Jastroch, Matthias Blüher, Christian Wolfrum, Benno Weigmann, Anette-Gabriele Ziegler, Matthias Mann, Matthias H. Tschöp, and Carolin Daniel.

Cell Metabolism *26*, 475-492, September 5, 2017

* equal contribution

Short-term cold exposure supports human Treg induction *in vivo*

Maike Becker, Isabelle Serr, Victoria K. Salb, Verena B. Ott, Laura Mengel, Anette-G. Ziegler, Matthias Blüher, Benno Weigmann, Hans Hauner, Matthias H. Tschöp and Carolin Daniel.

Molecular Metabolism, https://doi.org/10.1016/j.molmet.2019.08.002. Accepted for publication on August 1st, 2019

Publications not included in this thesis

Peer-reviewed publications:

A miRNA181a/NFAT5 axis links impaired T cell tolerance induction with autoimmune type 1 diabetes

Isabelle Serr, Martin G. Scherm, Adam M. Zahm, Jonathan Schug, Victoria K. Flynn, Markus Hippich, Stefanie Kälin, **Maike Becker**, Peter Achenbach, Alexei Nikolaev, Katharina Gerlach, Nicole Liebsch, Brigitta Loretz, Claus-Michael Lehr, Benedikt Kirchner, Melanie Spornraft, Bettina Haase, James Segars, Christoph Küper, Ralf Palmisano, Ari Waisman, Richard A. Willis, Wan-Uk Kim, Benno Weigmann, Klaus H. Kaestner, Anette-Gabriele Ziegler, Carolin Daniel

Science Translational Medicine *10*, eaag1782, January 3, 2018

Adipose-tissue regulatory T cells: Critical players in adipose-immune crosstalk

Maike Becker, Megan K. Levings and Carolin Daniel

European Journal of Immunology *47*, 1867-1874, September 20, 2017

Regulatory T cells control hypothalamic innate immune responsiveness to high calorie environments

Maike Becker, Stefanie Kälin, Victoria K. Flynn, Verena B. Ott, Roland E. Kälin, Markus Hippich, Martin G. Scherm, Lucas F. R. Nascimento, Isabelle Serr, Fabian Hosp, Alexei Nikolaev, Alma Mohebiany, Martin Krüger, Beata Legutko, Michael Pfaffl, Bettina Haase, Chun-Xia Yi, Sarah Dietzen, Tobias Bopp, Stephen C. Woods, Christian Wolfrum, Ari Waisman, Benno Weigmann, Ingo Bechmann, Matthias Mann, Matthias H. Tschöp and Carolin Daniel.

Manuscript in revision

Posters presented at international conferences:

Maike Becker, Stefanie Kälin, Victoria K. Flynn, Verena B. Ott, Isabelle Serr, Martin G. Scherm, Lucas F. R. do Nascimento, Anette-Gabriele Ziegler, Matthias H. Tschöp and Carolin Daniel. High-caloric feeding impairs immune homeostasis in the hypothalamus. *Deutsches Zentrum für Diabetesforschung (DZD), Summer Research School*; **2016** Sep 11-12; Freising, Germany.

Isabelle Serr, Victoria K. Flynn, **Maike Becker**, Peter Achenbach, Markus Hippich, Eva-Maria Sedlmeier, Benno Weigmann, Anette-Gabriele Ziegler and Carolin Daniel. A miRNA181a/NFAT5 axis links T cell tolerance with autoimmune Type 1 diabetes. *Immunology of Diabetes Society Congress (IDS)*; **2017** Jan 19-23; San Francisco, USA.

Maike Becker, Stefanie Kälin, Victoria K. Flynn, Verena B. Ott, Isabelle Serr, Martin G. Scherm, Fabian Hosp, Chun-Xia Yi, Anette-Gabriele Ziegler, Ingo Bechmann, Matthias Mann, Matthias H. Tschöp and Carolin Daniel. Impairment of hypothalamic immune homeostasis by high-caloric feeding. *Immunometabolism and Chronic Disease Conference (IMCD);* **2017** Aug 13-16; Coral Coast, Fiji.

Maike Becker, Stefanie Kälin, Victoria K. Flynn, Verena B. Ott, Isabelle Serr, Martin G. Scherm, Fabian Hosp, Chun-Xia Yi, Anette-Gabriele Ziegler, Ingo Bechmann, Matthias Mann, Matthias H. Tschöp and Carolin Daniel. Abstract 261 - Impairment of hypothalamic immune homeostasis by high-caloric feeding. *Jahrestagung der Deutschen Gesellschaft für Immunologie (DGfI);* **2017** Sep 12-15; Erlangen, Germany.

Verena B. Ott, Isabelle Serr, **Maike Becker**, Klaus H. Kaestner, Matthias H. Tschöp and Carolin Daniel. Insulin limits differentiation of naive $CD4^+$T cells into $Foxp3^+$Tregs from both WT and ob/ob mice. *Cell Symposia on Translational Immunometabolism Conference;* **2018** June 24-26; Basel, Switzerland.

Maike Becker, Isabelle Serr, Laura Mengel, Hans Hauner, Matthias H. Tschöp and Carolin Daniel. Short-term cold acclimation enhances human Treg induction. *European Congress of Immunology;* **2018** Sep 02-05; Amsterdam, The Netherlands.

Maike Becker, Isabelle Serr, Laura Mengel, Hans Hauner, Matthias H. Tschöp and Carolin Daniel. Short-term cold acclimation enhances human Treg induction. *Harald von Boehmer Midwinter Conference – Advances in Immunobiology*; **2019** Jan 19-23; Seefeld, Austria.

Abstract

Obesity and type 2 diabetes (T2D) are increasing worldwide at alarming rates. It is established now that obesity is a main factor that contributes to a chronic, low-grade inflammation in adipose tissues, leading to local and systemic insulin resistance and thus, resulting in the development of T2D. Especially the inflammation in the visceral adipose tissue (VAT) contributes here, highlighting its importance for therapeutic intervention.

Regulatory T cells (Tregs) are the main cellular mediators of immune tolerance and in addition, they are critically involved in maintaining tissue homeostasis. Tregs are able to modulate and dampen aberrant immune activation. In obese VAT, there is a progressive decline of Tregs observed, further promoting immune activation instead of maintaining immune and tissue homeostasis. In obesity, this decline in Treg frequencies in obese fat is correlative to impaired metabolic indices, such as elevated insulin resistance and hyperglycemia. The adipose-immune crosstalk is out of kilter. The restoration of a functional adipose-immune crosstalk is of major interest in order to dampen the obesity-associated inflammation with the final aim to improve metabolic health. To achieve that, a greater understanding of the molecular mechanisms underlying the environmental-adipose-immune crosstalk is of superior relevance for the development of potential future preventive or therapeutic approaches.

To fill that knowledge gap, the herein described experiments aimed at gaining a better understanding of immunological alterations of adipose tissue-resident T cell populations when they are exposed to different environmental stimuli. As potential mean to reduce immune activation and to increase the amount of calories being burned, the environmental cue cold was investigated. While it is known that cold induces browning in fat depots, the effects of cold on adipose tissue-residing immune cells have not been characterized yet and therefore, nothing is known about cold-induced alterations of the adipose-immune crosstalk. By modulating Treg cell frequencies experimentally in mice, I found that the presence of fat-residing Tregs is required for proper adipose tissue function. Using various sophisticated gain- and loss-of-function mouse models, I identified a Stat6/Pten signaling axis that links Tregs with adipose tissue function. Cold exposure or beta3-adrenergic signaling supported Treg function and improved adipose tissue metabolism. These experiments enabled the identification of molecular mechanisms that underlie the integration of environmental signals in T cells and that are shared between mice and humans; and thus, might help to reveal new potential therapeutic

approaches to limit the obesity-associated inflammation within fat compartments and thereby, improve immune-metabolic health by supporting Tregs in guiding adipose tissue function.

Zusammenfassung

Übergewicht und Typ 2 Diabetes nehmen weltweit dramatisch zu. In adipösem viszeralen Fett trägt eine chronische, leichte Entzündung entscheidend zur Verschlechterung der metabolischen Indices bei. Regulatorische T Zellen (Tregs) sind wichtige Mediatoren der Immunhomöostase und unterdrücken überschießende und fehlgeleitete Immunreaktionen. Des Weiteren ist seit Kurzem die Rolle der Tregs in der Erhaltung der Gewebshomöostase bekannt. Adipöses viszerales Fettgewebe ist durch einen signifikanten Rückgang der Tregs geprägt, dessen Ursache bis heute ungeklärt ist. Diese immunologischen Veränderungen und insbesondere die Abnahme an fettgewebsspezifischen Tregs tragen grundlegend zur Verschlechterung des Fettgewebszustands und zur Entwicklung von Insulinresistenz und Hyperglykämie bei. Aus diesem Grund stellt die Wiederherstellung der Immunhomöostase im Fettgewebe ein wichtiges therapeutisches Ziel zur Verbesserung der Entzündungsprozesse und metabolischen Indices bei Übergewicht und Typ 2 Diabetes dar. Für die Entwicklung neuer Strategien zur Therapie der fettgewebsspezifischen Entzündungsreaktionen ist ein umfangreicheres Verständnis der zugrundeliegenden molekularen Mechanismen von essentieller Bedeutung.

Um diese Wissenslücke zu schließen beschäftigt sich diese Doktorarbeit mit Experimenten, die zu einem besseren Verständnis beitragen sollen, welchen Einfluss äußere Faktoren auf die Wechselwirkung zwischen Fettgewebe und Immunzellen ausüben. Als Mittel zur Reduzierung der Immunaktivität und gleichzeitigen Erhöhung der Stoffwechselaktivität wurde der Fokus auf Kälte und beta3-adrenerge Stimulation gelegt. Während die aktivierende Wirkung von Kälte auf braunes Fettgewebe und die damit verbundene Erhöhung des Grundenergieumsatzes ausführlich beschrieben wurde, wurden deren Effekte auf gewebsspezifische Immunzellen und die Wechselwirkungen zwischen Gewebe und Immunzellen weitgehend ignoriert. Durch experimentelle Modulation von Treg Frequenzen in Mäusen konnte ich zeigen, dass Tregs für einen funktionalen Fettstoffwechsel von grundlegender Bedeutung sind. Mit Hilfe mehrerer durchdachter Funktionsverlust- und Funktionsgewinn-Modelle konnte ich zeigen, dass durch Stat6-, Pten- und C17orf59-vermittelte Signalwege in Tregs zur Unterstützung der Fettgewebsfunktionen beitragen. Sowohl Kälte als auch pharmakologische beta3-adrenerge Stimulation förderten hierdurch gewebsspezifische Tregs und dadurch wiederum die metabolische Funktionalität der Fettgewebe.

Die in dieser Thesis beschriebenen Experimente ermöglichten die Identifikation molekularer Mechanismen, welche der Integration von extrinsischen Faktoren wie Kälte oder beta3-adrenerger Stimulation in T Zellen sowohl in Mäusen als auch im Menschen zugrunde liegen. Die gewonnenen Einblicke könnten daher für neue therapeutische Ansätze zur Reduzierung der Entzündungsprozesse in adipösem Fettgewebe genutzt werden, indem sie gezielt Tregs unterstützen und dadurch die immun-metabolische Homöostase bei Übergewicht und Typ 2 Diabetes wiederherstellen.

1 Introduction

1.1 The immune system

The immune system is responsible to defend an organism against the myriad of infectious invaders it constantly confronts. To ensure that, innate and adaptive immune cells together with the complement system work in concert. When an infectious agent conquers the body, a hierarchical series of immune responses are raised to eliminate it. This process involves regulatory T cells (Tregs) that ensure that the immune attack raised is not at the expense of being controlled.

Immune homeostasis and immunological tolerance are maintained by two main mechanisms: recessive tolerance versus dominant tolerance (Sakaguchi et al., 2008). Recessive tolerance occurs during immune cell development and ensures that autoreactive cells that respond to self-antigens die by apoptosis or become anergic before their maturation to fully functional immune cells (Ramsdell and Fowlkes, 1990; Surh and Sprent, 1994). For T cells, this cell-intrinsic process prevents the egress of autoreactive T cells from the thymus – it is tightly controlled, however not fully fail-safe. The second mechanism that plays an important role to prevent aberrant immune activation is dominant tolerance, mediated by Tregs.

1.2 Regulatory T cells

As mentioned above, CD4$^+$Tregs are the main cellular mediators of dominant tolerance. They are characterized by high expression of the high-affinity interleukin 2 (IL-2) receptor α chain (IL-2Rα; also known as CD25) (Sakaguchi et al., 1995) and of Forkhead box protein 3 (Foxp3), their lineage-defining transcription factor (Fontenot et al., 2003; Hori et al., 2003; Khattri et al., 2003; Khattri et al., 2001). Tregs can be either thymus-derived or peripherally induced. In a simplified model, Tregs in the thymus originate from T cells that have a high affinity/avidity to self-antigens but have not undergone apoptosis or anergy (Klein et al., 2019). Furthermore, Tregs can also be induced in the periphery from naïve T cells (Apostolou et al., 2002; Daniel and von Boehmer, 2011; Kretschmer et al., 2005). The peripheral Treg induction works best with strong-agonistic ligands under sub-immunogenic conditions provided to naïve CD4$^+$T cells (Daniel et al., 2011b; Daniel et al., 2010; Sauer et al., 2008). Sub-immunogenic conditions resemble a scenario where a fine-tuned balance of T cell receptor (TCR) signaling together with

limited costimulatory signals induces signaling within cells but is below the threshold of full immunogenic activation and cellular proliferation. Here, the activity of the phosphoinositide 3 kinase (PI3K)/Akt/mechanistic target of rapamycin (mTOR) signaling pathway plays a crucial role since it supports immune activation but limits successful Treg induction (Daniel et al., 2011a; Gottschalk et al., 2010; Haxhinasto et al., 2008; Sauer et al., 2008; Serr et al., 2016b; Serr et al., 2018; von Boehmer and Daniel, 2013). Therefore, modulation of the PI3K/Akt/mTOR pathway is a promising tool to improve Treg induction efficacy. This can be achieved by different strategies: among others, direct pharmacological inhibition of mTOR by using established compounds such as rapamycin or everolimus is an option (Sauer et al., 2008), as well as by manipulating phosphates of the enzymes involved in this pathway and thereby influencing downstream signaling. The antagonist of PI3K activity is phosphatase and tensin homolog (Pten). Pten counteracts PI3K activity by cleaving the activating phosphorylation of Akt and thereby, limits signaling via the PI3K/Akt/mTOR pathway, promoting Treg induction.

Since peripheral Treg induction is a relevant therapeutic approach to treat or prevent aberrant immune activation, several markers have been proposed to distinguish thymus-derived vs. peripherally induced Tregs. Especially Helios (encoded by *Ikzf2*) and Neuropilin 1 (encoded by *Nrp1)* were suggested (Haribhai et al., 2009; Thornton et al., 2010; Weiss et al., 2012), however, none of the proposed markers was completely conclusive/convincing for all Tregs induced in different peripheral sites under different circumstances.

The importance of Tregs in maintaining immune homeostasis is best evident when they fail: Mutations in the *Foxp3* gene (former known as *Scurfin*) lead to a severe form of autoimmunity in mice (so-called scurfy mice) (Brunkow et al., 2001; Godfrey et al., 1991; Khattri et al., 2003; Khattri et al., 2001) and men (immune dysregulation, polyendocrinopathy, enteropathy, X-linked syndrome (IPEX)) (Bennett et al., 2001). Likewise, when Tregs are depleted experimentally in newborn mice, fatal autoimmune disease occurs (Kim et al., 2007; Lahl et al., 2007). Due to the global defect in Tregs and the resulting deregulation of the immune system, the multi-organ autoimmune attack raised early after birth is life threatening if left untreated.

1.2.1 Canonical and non-canonical functions of regulatory T cells

Tregs have several modes of action to exert their immune-regulatory function: 1) by direct contact-dependent inhibition of antigen-presenting cells (APCs) and effector cells (Misra et al., 2004), 2) by lysis of effector T cells through secretion of enzymes e.g. granzyme B or perforin

(Gondek et al., 2005), 3) by secretion of anti-inflammatory cytokines, especially of IL-10 (Asseman et al., 1999) and transforming growth factor β (TGFβ) (Fahlen et al., 2005; Green et al., 2003) 4) by consumption of IL-2 and with all that together, Tregs critically limit effector responses. Since Tregs secrete and consume soluble immune mediators such as interleukins, their suppressive function is not dependent on cell-cell-interactions but they can also manipulate cells in their proximity – a feature called bystander suppression (Miller, 1991).

In addition to the canonical function of suppressing effector immune cells described above, Tregs also fulfill non-canonical functions such as contributing to tissue homeostasis as further specified in section 1.3 Tissue Tregs. With regard to their multifaceted function, Tregs were shown to be critically involved in dampening allergic responses (Bacher et al., 2016; Hartl et al., 2007), to be induced by oral antigens and gut commensals (Sun et al., 2007), to contribute to the prevention of aberrant immune activation in autoimmunity (Asano et al., 1996) and transplant rejection (Ohki et al., 1987), to contribute to tissue repair after injury (Burzyn et al., 2013b; Haertel et al., 2018; Kuswanto et al., 2016) and to maintain fetal tolerance during pregnancy (Aluvihare et al., 2004; Sasaki et al., 2004; Zenclussen et al., 2005). These findings demonstrate the highly adaptable phenotype and functions of Tregs.

1.2.2   Treg stability and functional regulatory networks

In order to maintain self-tolerance and to prevent aberrant immune activation, Tregs have to persist and stay functional for long periods. Sustained Foxp3 expression is crucial for Treg function (Williams and Rudensky, 2007) and therefore, Treg stability can be monitored by epigenetic analysis of the Treg-specific demethylated region (TSDR, also referred to as conserved non-coding DNA sequence 2 (CNS2)) of the *Foxp3* locus (Floess et al., 2007; Polansky et al., 2008; Toker et al., 2013). Here, a demethylated TSDR represents a stable Foxp3 expression and can be found in *ex vivo* isolated Tregs, while naïve and effector T cells present with partially or fully methylated TSDR. Epigenetic analysis of TSDR methylation also allow the differentiation of human activated effector T cells which express intermediate levels of FOXP3 versus human Tregs that express high levels of FOXP3 and have a fully demethylated TSDR (Baron et al., 2007). The methylation state of the TSDR is especially important for scenarios where Tregs are induced *de novo* and shall be maintained for long periods as therapeutic strategy. It is known for example that Treg induction strategies *in vitro* that try to differentiate Tregs from naïve T cells in the presence of TGFβ result in high Treg frequencies but with only partially demethylated

TSDR (Floess et al., 2007). When being transferred *in vivo,* these TGFβ-induced Tregs lose their Foxp3 expression and suppressive phenotype (Floess et al., 2007). In contrast, Treg differentiation of naïve T cells to Tregs under sub-immunogenic conditions *in vivo* results in Tregs that can be isolated weeks after induction and thus, resemble a more stably induced Treg (Serr et al., 2016b; Serr et al., 2018). Additionally to epigenetic control, Foxp3 stability is regulated by post-transcriptional modifications of the protein, namely phosphorylation, acetylation or ubiquitination. Here, phosphorylation of multiple serines and threonines stabilizes Foxp3 by preventing its ubiquitination (Fleskens et al., 2019), which marks proteins for proteasomal degradation. Stabilizing phosphorylation of Fopx3 depends on the action of nemo-like kinase (Nlk) that gets activated when TGFβ-activated kinase 1 (Tak1) is activated downstream of TCR signaling (Fleskens et al., 2019). Not only the presence of Foxp3 itself is critically important, but a complex protein network is involved in regulation of gene expression and effector function of Tregs as it has been shown by the group of Alexander Rudensky (Rudra et al., 2012). They identify several transcription factors, proteins involved in chromatin remodeling (e.g. histone deacetylases (HDACs)), proteins of the MLL and of the SWI-SNIF complex to form higher-order complexes together with Foxp3 or to be directly interacting with Foxp3. Foxp3 even binds the promoter of many proteins involved in this Foxp3 protein network and by that tunes their transcription and functionality.

To summarize these complex regulatory networks, different processes on the epigenetic and protein level work in concert to ensure proper immune regulation and to prevent aberrant immune activation.

1.2.3 T cell and Treg metabolism

Not only certain proteins are regulated by epigenetic and posttranslational modifications, but the whole T cell has to adapt to its specific function in a spatiotemporal manner. When T cells recognize their cognate antigen to induce an immune response, adaptations in their transcriptome and metabolome are required. Antigen-unexperienced naïve T cells do not express many effector T cell molecules and their metabolism is reduced to a minimum. Naïve T cells mainly rely on glycolysis and oxidative phosphorylation (OXPHOS) and this quiescent state is maintained until they recognize their cognate antigen and become effector T cells (Blagih et al., 2015; Macintyre et al., 2014; Michalek et al., 2011). Activated effector T cells migrate through tissues, produce effector cytokines and undergo rapid clonal expansion. The

acquisition of these effector T cell functions requires huge adaptations of cellular transcription, translation and metabolism. To meet these demands, activated effector T cells have more nutrient transporters to import fuel, mainly oxidize glucose (glycolysis) to produce adenosine triphosphate (ATP), but also rely on the oxidation of glutamine (glutaminolysis), the tricarboxylic acid (TCA) cycle and fatty acid oxidation to fuel OXPHOS (Buck et al., 2016; Macintyre et al., 2014; Pearce and Pearce, 2013).

For Tregs, several transcription factors have been implicated in control of their metabolism: among them, the lineage-defining transcription factor Foxp3 itself is involved in regulating Treg metabolism (Angelin et al., 2017), together with Lkb1 that not only stabilizes Foxp3 expression in Tregs (Wu et al., 2017), but also renders their metabolism towards more fatty acid oxidation (Yang et al., 2017). Thus, the metabolism of Tregs is special; it mainly relies on fatty acid oxidation and OXPHOS while glycolysis is dispensable (Angelin et al., 2017; Gerriets et al., 2015; Michalek et al., 2011). This is similar to the metabolic profile found in long-lasting memory T cells (Gerriets et al., 2015) and reflects the adaptation for extended persistence of Tregs within the organism.

1.2.4 Human FOXP3^{high} regulatory T cells

While most basic immunological research is done in mice, the translational relevance of those findings to humans has to be proven. Human T cells do not exactly behave as murine immune cells and this has to be taken into account. As example, human activated T cells express intermediate levels of FOXP3 although they are not functioning as immunosuppressive Tregs (Allan et al., 2007; Morgan et al., 2005; Walker et al., 2003; Wang et al., 2007), a phenomenon that is not observed in the mouse. However, the inclusion of additional markers next to FOXP3 enables the discrimination between activated T cells and immunosuppressive Tregs. Therefore, human Tregs are characterized as CD3^{+}CD4^{+}CD127^{low}CD25^{hi}FOXP3^{hi} (Cossarizza et al., 2017; Liu et al., 2006; Ruprecht et al., 2005). Similar to the murine system, human Tregs can be induced *in vitro* under sub-immunogenic conditions from naïve CD3^{+}CD4^{+}CD45RA^{+}CD45RO^{-}CD127^{+}CD25^{-} T cells (Serr et al., 2016b; Serr et al., 2018).

1.3 Tissue Tregs

Additionally to their localization in lymphoid organs, it was shown that T cells and Tregs are residing in various non-lymphoid tissues in health and disease (Burzyn et al., 2013a; Panduro

et al., 2016). These tissue-residing Tregs harbor unique phenotypes and functions, which are not restricted to classical tasks of immune modulation but include non-canonical functions such as maintenance of tissue homeostasis. Evidence is arising, that those tissue-specific Tregs function as critical players to control inflammation locally within peripheral tissues (Cipolletta, 2014; Liston and Gray, 2014).

In general, tissue-residing Tregs have adapted their transcriptome and metabolome to the environment they reside in. This includes a 'generalized tissue Treg signature' with genes commonly transcribed in all tissue-residing Tregs but is different from Tregs residing in lymphoid organs; and additionally a gene signature special for each non-lymphoid tissue (Delacher et al., 2017; Miragaia et al., 2019). So far, it is difficult to define which genes belong to the generalized tissue Treg signature and which genes can be clearly classified as adaptation to the environment in a certain tissue. Tissue-residing Tregs have been described for skin (MacDonald et al., 2015), muscle (Burzyn et al., 2013b), colonic lamina propria (Schiering et al., 2014), lung (Arpaia et al., 2015), brain (Ito et al., 2019) and different adipose tissues (Feuerer et al., 2009; Kalin et al., 2017; Kolodin et al., 2015; Medrikova et al., 2015; Vasanthakumar et al., 2015). Located at these peripheral sites, Tregs closely adapt their transcriptome and metabolome to the local environment. This includes the expression of additional transcription factors that were initially thought to be specific for certain effector T cells; such as expression of T-box transcription factor Tbx21 ((Tbx21) also known as Tbet) that is classically defining TH1 cells; Trans-acting T cell-specific transcription factor GATA-3 (GATA3) which is crucial for TH2-mediated immune responses or a similar suppression mode of Tregs controlling TH17 responses (Levine et al., 2017). Tregs phenotypically "mirror" effector T cells (Duhen et al., 2012). The continued release of new studies analyzing tissue Treg signatures leads to the withdrawal of genes that had been proposed to be tissue-specific adaptations of Tregs (Burzyn et al., 2013b; Cipolletta et al., 2012; DiSpirito et al., 2018; Ito et al., 2019; Magnuson et al., 2018; Miragaia et al., 2019) and hence, further research is needed to precisely define specific tissue Treg subsets.

1.3.1 Tregs residing in visceral adipose tissues

Lean VAT in young male mice is populated with a tissue-specific subtype of Tregs (Feuerer et al., 2009). These VAT-residing Tregs express high amounts of the IL-33 receptor ST2 (encoded by *Il1rl1*) (Kolodin et al., 2015), amphiregulin (Areg; encoded by *Areg*) and Peroxisome

proliferator-activated receptor gamma (Pparγ; encoded by *Pparg*) (Cipolletta et al., 2012; Li et al., 2018). Pparγ is known as master regulator of adipocyte differentiation, modulating fatty acid uptake and adipogenesis (Hu et al., 1995; Tontonoz et al., 1994). The expression of Pparγ by VAT-residing Tregs is thought to resemble a typical adaptation to the local environment, enabling these Tregs to catabolize free fatty acids – the main nutrient available in adipose tissue depots. In male C57Bl/6 mice, the Treg frequency in VAT increases with age and peaks around 24-30 weeks of age (Cipolletta et al., 2015; Cipolletta et al., 2012; Feuerer et al., 2009).

Until now, the understanding is very limited what drives Tregs to take residency in peripheral tissues such as VAT. Lymphoid organ T cells and Tregs present with a polyclonal TCR repertoire. In contrast, the TCR repertoire of tissue Tregs is highly biased with a high prevalence of certain Vα/Vβ/CDR3 chains that are in most cases not found in naïve or effector T cells (Bergot et al., 2015; Kolodin et al., 2015). This indicates that Tregs such as those residing in VAT recognize specific cognate antigens, get activated there and undergo clonal expansion – resembling another characteristic of tissue Tregs. This theory was supported by work from Diane Mathis' group that generated a transgenic mouse in which most T cells express a TCR that was derived from a Treg that was originally isolated from VAT (Li et al., 2018). While splenic Treg frequencies remain unchanged, these transgenic mice present with enriched VAT Treg fractions, suggesting a TCR-driven accumulation of VAT Tregs. In addition, this accumulation was dependent on the presence of the ST2 on VAT Tregs, since a Treg-specific loss of ST2 led to dramatically reduced Treg numbers in VAT, but not in spleen (Li et al., 2018). Application of the ST2 agonist IL-33 leads to expansion of VAT-residing Tregs and thereby, contributes to metabolic health (Kolodin et al., 2015; Li et al., 2018; Vasanthakumar et al., 2015).

Tissue Tregs are important for tissue homeostasis; however, extrinsic signals such as environmental-metabolic cues affect their number and functionality.

1.4 Environmental-immunemetabolic cues and how they affect tissue-residing Tregs

In the last decades, obesity has reached epidemic proportions in several regions of the world, which includes a doubling of the worldwide prevalence of obesity between 1980 and 2014 (WHO, 2015). This occurred partly due to increased intake of energy-dense foods with a high fat and high sugar content. The persistent imbalance between caloric intake and energy

expenditure consequently leads to disease progression. Excess body weight is considered as major risk factor contributing to the development of obesity-related comorbidities such as type 2 diabetes (T2D), hypertension, heart failure, dyslipidemia, arteriosclerosis and some forms of cancer (Daniels, 2009; Haslam and James, 2005; Tsiros et al., 2009).

As described previously, Tregs survey and migrate throughout the body and take up residence in various tissues, followed by tissue-specific adaptations of their functions. Importantly, Tregs possess like other cells in the body the ability to respond to environmental and metabolic signals. Examples for such environmental and metabolic cues are ambient temperature, the surrounding cytokine milieu or hypercaloric challenges. However, if and how Tregs link such environmental-metabolic cues with tissue homeostasis and function remains largely unclear.

1.4.1 Obesity-associated low grade inflammation in the adipose-immune crosstalk

An increase in body weight and adipose tissue mass due to persistent hypercaloric intake is accompanied by an accumulation of immune cells within VAT. This immune cell infiltration critically contributes to the local chronic low-grade inflammation observed specifically in obese VAT and that was shown to substantially contribute to metabolic dysfunction (i.e. insulin resistance for instance) (Xu et al., 2003). In the lean state, Tregs, M2-polarized macrophages (Morris et al., 2013), few B and T cells, type 2 innate lymphoid cells (ILC2s) (Molofsky et al., 2013) and eosinophils (Molofsky et al., 2013; Wu et al., 2011) are the predominant immune cells in VAT, while upon hypercaloric challenge, the immune equilibrium shifts towards pro-inflammatory M1 macrophages, type 1 innate lymphoid cells (ILC1s) (Boulenouar et al., 2017; O'Sullivan et al., 2016), an increase in effector B and T cell numbers and at the same time, a reduction of Tregs (Becker et al., 2017; Feuerer et al., 2009). The immune activation and adipose tissue mass expansion induces a local and systemic increase of pro-inflammatory mediators such as tumor necrosis factor (TNF) α, IL-6 and an altered adipokine secretion. Although the inflammation resulting from the expansion of the adipose tissue mass differs from the classical definition of inflammation as response to a pathogen, since is lacks signs of rubor, dolor, color and tumor (Larson and Henson, 1983), this 'sterile' inflammation in the absence of a pathogen has still detrimental effects on the whole organism. The chronic low-grade inflammation critically contributes to the development of the metabolic syndrome and type 2 diabetes (T2D) (Rosen and Spiegelman, 2014; Xu et al., 2003). Considering the enlargement of the adipose

tissue as consequence of excess energy consumption, these findings highlight that adipose tissue is not only responsible for the storage of lipids, but also a remarkable endocrine organ that can exert negative effects on immune homeostasis and systemic metabolism.

Keeping the global obesity epidemic and its health cost burden at the back of one's mind, many studies have been performed to understand the immune-adipose crosstalk; however, the dissection of the complex layers of the obesity-associated adipose-immune dysregulation is still in its infancy. As described in the previous chapter, the VAT of young lean mice harbors a distinct population of Tregs that express Foxp3, Pparγ, Areg and ST2 (Cipolletta et al., 2012; DiSpirito et al., 2018; Feuerer et al., 2009; Li et al., 2018). The Treg frequency in VAT increases in male C57Bl/6J mice with age and peaks around 24-30 weeks of age (Cipolletta et al., 2015; Cipolletta et al., 2012; Feuerer et al., 2009). These Tregs are crucial for tissue homeostasis and when mice are exposed to high-caloric feeding, this specialized Treg population is dramatically reduced upon diet-induced weight gain (Deiuliis et al., 2011; Feuerer et al., 2009). It was shown that modulation of Tregs especially in the VAT compartment affects insulin resistance, hyperglycemia and related metabolic indices. An increase in Treg frequencies was shown to improve systemic metabolism, while Treg depletion impairs it and, as a proof of concept, elevates inflammatory markers within the fat depot (Cipolletta et al., 2012; Eller et al., 2011; Feuerer et al., 2009; Ilan et al., 2010).

In order to dissect the mechanisms influencing adipose tissue-resident Tregs, one has to consider the local microenvironment these Tregs reside in. There are three types of adipocytes present in mice and men: white, brown and beige (also known as brite ('brown-in-white')) fat cells. The main function of white adipocytes is the storage of energy in form of lipids and they appear with a characteristic unilocular lipid droplet and only few mitochondria (Cushman, 1970). White adipose tissue (WAT) is mainly located in subcutaneous (SAT) and VAT depots and derives from Myogenic factor 5 (Myf5)$^-$ precursor cells (Seale et al., 2008). In contrast, brown adipose tissue (BAT) critically contributes to adaptive non-shivering thermogenesis (NST), meaning it burns calories and dissipates heat when needed. This is facilitated by the expression of Uncoupling protein 1 (UCP1) that uncouples mitochondrial respiration from ATP synthesis and thereby allows the dissipation of energy as heat (Fedorenko et al., 2012; Rosen and Spiegelman, 2014; Ussar et al., 2014). Brown adipocytes derive from Myf5$^+$ adipomyogenic precursors, they are related to skeletal muscle cells, have a high mitochondria content, catabolize lipids and thus, are fundamentally different from white adipocytes (Seale et al., 2008;

Timmons et al., 2007). Accordingly, environmental-metabolic cues exert critical effects on the adipose tissue and therefore, impact the local microenvironment adipose tissue-Tregs reside in, again highlighting the important contribution of adipose-immune crosstalk.

1.4.2 The fat-brain-axis and how environmental cold stimuli link immune function with adipose tissue adaptations

From a metabolic perspective, caloric intake and cold exposure play a major role in the regulation of energy expenditure and have a significant impact on diverse metabolic processes in fat tissues. A specialized area of the brain links afferent signals related to feeding state, ambient temperature and stress to systemic metabolism. Here, mainly the mediobasal hypothalamic area signals via the efferent sympathetic nervous system (SNS) to the periphery and by that, controls systemic metabolism. Adipose tissues are highly innervated with nerves from the SNS and upon environmental triggers such as cold, these nerves release catecholamines (such as norepinephrine) that bind to beta-adrenergic receptors on brown adipocytes and mediate an increase in adaptive NST (reviewed in detail in (Bartness et al., 2010; Cannon and Nedergaard, 2004))(Ryu et al., 2015; Youngstrom and Bartness, 1995; Zeng et al., 2015). Additionally, upon exposure to cold or beta3-adreneric signaling, white adipocytes can acquire a brown-like signature and are then named beige/brite adipocytes – a process referred to as browning (Jespersen et al., 2013; Wu et al., 2012). The resulting induction of beige adipocytes mediated by the environmental cue cold is more prominent in the subcutaneous fat depot while VAT is for the most part resistant to browning upon cold exposure (Nagase et al., 1996). Since beige adipocytes arise after conversion from white adipocytes, the SAT is interspersed with beige cells while BAT depots are precise compartments that are densely packed with brown adipocytes. Although being derived from white adipocytes, beige adipose tissue is able to contribute to adaptive NST (Wu et al., 2012).

In rodents and murine cell lines, treatment with the highly specific β3-adrenergic receptor agonist CL316,243 (Bloom et al., 1992; David C. Humber et al., 1992; Himms-Hagen et al., 1994; Himms-Hagen et al., 2000) or with the broad β-adrenergic receptor agonist isoproterenol (Miller et al., 2015) induces browning of white adipocytes. Furthermore, adipose tissue browning can be supported by the application of Pparγ agonists such as rosiglitazone and pioglitazone (Wang et al., 2016). For both, brown and beige adipocytes, Ucp1 expression is crucial, while Prdm16 expression can be used to discriminate both (Harms et al., 2014; Ohno et

al., 2012; Seale et al., 2008). As mentioned above, immunologists found Ppary being expressed specifically in VAT-residing Tregs (Cipolletta et al., 2012). These Ppary[+]Tregs were expanded when mice were treated with pioglitazone (Cipolletta et al., 2012), indicating that browning of adipose tissue by pioglitazone could also be not solely due to effects on adipocytes, but also mediated – or at least supported – by the expanded Treg population via immune-adipose crosstalk. A blunted Ppary response in Tregs clearly dampens the metabolic response of the adipose tissue to pioglitazone treatment (Cipolletta et al., 2012), pointing out that Tregs are indeed critical mediators of insulin-sensitizing agents (such as thiazolidinediones) and that Tregs are required for proper immune-adipose crosstalk and adipose tissue homeostasis.

For long time it was thought that only mice and human newborns have amounts of BAT worth mentioning, until BAT was rediscovered to be present and also functional in human adults (Cypess et al., 2009; Cypess et al., 2013; Heaton, 1972; Nedergaard et al., 2007; Virtanen et al., 2009). Later on, it was shown that human BAT is activated by cold exposure (Saito et al., 2009; van Marken Lichtenbelt et al., 2009), as well as by mirabegron, a pharmacological beta3-adrenergic receptor agonist that mimics cold exposure (Cypess et al., 2015). Analysis of marker gene expression showed that these BAT depots that are located in the supraclavicular (Jespersen et al., 2013), peri-vascular, para-spinal and the deep neck region (Cypess et al., 2013; Zingaretti et al., 2009), present with high amounts of *UCP1*.

In order to combat obesity, one therapeutic approach is the exploitation of adipose tissue browning to increase daily energy expenditure. However, it was shown for humans that obese subjects show a reduced response to cold or beta3-adrenergic stimulation when compared with lean controls (Saito et al., 2009; van Marken Lichtenbelt et al., 2009), curtailing this therapeutic strategy.

Cold exposure or short-term cryostimulation were used to activate beta3-adrenergic receptors in clinical situations, e.g. in immunological diseases such as rheumatoid arthritis (Guillot et al., 2017; Guillot et al., 2014) or multiple sclerosis (Miller et al., 2016; Miller et al., 2010). Furthermore, short-term high caloric challenges supports BAT thermogenesis and interestingly, an increased anti-inflammatory cytokine production has been reported upon short-term cryostimulation (Rothwell and Stock, 1979).

Since especially the obesity-associated inflammation in the VAT contributes to the metabolic dysfunction observed in obesity and T2D, targeting these inflammatory responses and

specifically the regulation of adipose-immune crosstalk might open new avenues in therapeutic interventions to interfere with metabolic disease.

2 Objective

A greater understanding of the molecular mechanisms underlying the environmental-adipose-immune crosstalk is of superior relevance for the development of potential future preventive or therapeutic approaches to interfere with aberrant immune activation as observed in obese fat. Thus, the herein described experiments aim at gaining a better understanding of immunological alterations of adipose tissue-resident T cell populations when they are exposed to different environmental stimuli, as well as how these immunological alterations affect the adipose tissue function.

As first objective, in order to dissect the role of regulatory T cells in supporting adipose tissue function, I aim to modulate Treg frequencies experimentally using sophisticated gain- and loss-of-function models. This includes transgenic mice, Treg transfers, Treg expansions, as well as Treg-depletion strategies *in vivo*.

As second objective, in order to dissect the adipose-immune crosstalk further and to especially test how the different local tissue microenvironments imprint on T cell differentiation, *ex vivo* analyses of tissue-residing T cells and *in vitro* differentiation assays are used.

As third objective, the environmental cues cold and hypercaloric feeding are investigated as a means to modulate the adipose-immune crosstalk. The focus is set on the molecular underpinnings how the environmental cue cold is integrated in T cells and how this helps Tregs in guiding adipose tissue metabolism. These experiments first will focus on unbiased approaches such as RNA sequencing and quantitative tandem mass spectrometry and will then be confirmed using knockout and transgenic mouse models upon identification of key molecules involved in integrating environmental cues in T cells.

As last objective, the identified pathways and signaling molecules identified in murine models are probed for their translatability into human disease using both, next generation humanized mouse models and human samples of the FREECE study.

All experiments aim at the identification of molecular mechanisms that underlie the integration of environmental signals in Tregs and therefore have the goal to contribute to the identification of new potential therapeutic approaches to limit the obesity-associated inflammation within fat compartments and thereby, improving immune-metabolic health.

3 Methods

3.1 Animal experiments

Mice were bred and maintained in individually ventilated cages (IVC) under specific pathogen free (SPF) conditions in the animal facility of the Helmholtz Zentrum München, Munich, Germany. Mice were maintained group-housed with a 12h/12h light dark cycle at 25 °C. All mice had *ad libitum* excess to water and food (Altromin #1314).

Mice were randomized to test groups.

In case of hypercaloric challenge, mice were fed *ad libitum* with food composed of 58% kcal fat and 25.5% kcal carbohydrates (including 8% sucrose) (Research Diet #D12331i).

For beta3-adrenergic stimulation or blockade, mice were injected i.p. with 1 mg/kg body weight CL316,243 or 0.3 mg/kg body weight cyanopindolol on three consecutive days. 0.9% NaCl was used as vehicle control.

For cold exposure experiments, mice were acclimated group housed to either 8°C for one week or 4°C for 24 h.

Humanized NOD-*scid IL2Rγ^{null}* (NSG) mice are immune deficient due to the *severe combined immunodeficiency* (*scid*) mutation they're harboring in combination with a knockout for the common gamma chain that is required for cytokine signaling (Shultz et al., 2005). Therefore, these mice lack functional murine B, T and natural killer (NK) cells, together with severe impairments in murine innate immunity (Shultz et al., 2005). Upon engraftment with CD34^{+} human stem cells or PBMCs, NSG mice develop a human immune system. They present with functional CD3^{+}CD4^{+}, CD3^{+}CD8^{+} T cells, Ig^{+} B cells, myeloid cells, NK cells and plasmacytoid DCs. Therefore, NSG mice are an interesting tool to study therapeutic approaches with regard to their translational relevance to human disease *in vivo*. Humanized mice were reconstituted with PBMCs and two weeks post reconstitution, mice were treated with either 1 mg/kg bodyweight mirabegron to induce beta3-adrenergic receptor signaling or with 0.9% NaCl as vehicle on three consecutive days.

For Treg depletion experiments, DEREG mice (mice harboring bacterial artificial chromosome containing the simian diphtheria toxin receptor fused to an eGFP reporter under control of the endogenous Treg-specific *Foxp3* promoter/enhancer) (Kim et al., 2009) were injected i.p. with

50 µg/kg body weight diphtheria toxin (Merck Millipore) for three days.

For Treg depletion in WT mice, 250 µg anti-mCD25 antibodies (BioXCell) were injected i.p. on three consecutive days according to established protocols (Setiady et al., 2010).

For Treg expansion, 6 µg anti-IL2/IL2 antibody complexes were injected s.c. for three days according to published protocols (Webster et al., 2009).

Investigators were not blinded to group allocations or to the assessment of experimental end points. All experiments were executed according to the guidelines established by the Institutional Animal Committees and ethical approval has been received by the corresponding local animal welfare authorities. The approval numbers of the district government of Upper Bavaria are: ROB-55.2-2532.Vet_02-14-32, ROB-55.2-2532.Vet_02-14-33, ROB-55.2-2532.Vet_02-17-63 and ROB-55.2-2532.Vet_02-18-173.

The following mouse strains were used for experiments (strain, background, genotype, provider/reference): Borcs6 het, C57Bl/6N, B6N(Cg)-*Borcs6*$^{tm1.1(KOMP)Vlcg}$/J, Jackson Laboratory, 028178; DEREG, C57Bl/6J, C57BL/6-Tg(Foxp3-DTR/EGFP)23.2Spar/Mmjax, Jackson Laboratory, 011003; Stat6KO, Balb/c, C.129S2-*Stat6*^{tm1Gru}/J, Jackson Laboratory, 002828 (Kaplan et al., 1996); Stat6VT, C57Bl/6, Tg(CD2-Stat6*V625A*T626A)78Mhk, provided by Mark H. Kaplan (Bruns et al., 2003); ob/ob, C57Bl/6J, B6.Cg-*Lep*^{ob}/J, Jackson Laboratory, 000632; PtenTg, C57Bl/6, Tg(Pten)1Srn, provided by Manuel Serrano, Spanish National Cancer Research Center (CNIO), Spain; Betaless, C57Bl/6, β1, β2, β3 adrenergic receptor triple knockout, provided by Francoise Rohner-Jeanrenaud, Faculty of Medicine, University of Geneva, Switzerland (Asensio et al., 2005); Foxp3-eGFP, C57Bl/6J, B6.Cg-*Foxp3*^{tm2Tch}/J, Jackson Laboratory, 006772; Foxp3-eGFP, Balb/c, Balb/c.Cg-*Foxp3*^{tm2Tch}/J, Jackson Laboratory, 006769; HLA-DR4, NSG, NOD.Cg-*Prkdc*^{scid}*Il2rg*^{tm1Wjl}*H2-Ab1*^{tm1Doi}Tg(HLA-DRB1)31Dmz/SzJ, provided by Leonard Shultz, Jackson Laboratory, 017637, herein referred to as NOD-*scid IL2Rγ*^{null} (NSG); HLA-DQ8, NSG, NOD.Cg-*Prkdc*^{scid}*H2-Ab1*^{tm1Gru}*Il2rg*^{tm1Wjl}Tg(HLA-DQA1,HLA-DQB1)1Dv/SzJ, provided by Leonard Shultz, Jackson Laboratory, 026561, herein referred to as NOD-*scid IL2Rγ*^{null} (NSG); CD45.1, C57Bl/6J, B6.SJL-*Ptprc*^{a}*Pepc*^{b}/BoyJ, Jackson Laboratory, 002014; CD90.1, Balb/c, CBy.PL(B6)-*Thy1*^{a}/ScrJ, Jackson Laboratory, 005443; CD90.2 Balb/c, Balb/cByJ, Jackson Laboratory, 001026.

3.2 Human subjects and samples

All human subjects gave informed written consent. Subjects consented to the Munich

Bioresource project (approval number #5049/11, Technische Universität München, Munich, Germany), the Effect of the FTO-Genotype on Resting Energy Expenditure after defined Cold Exposure (FREECE) study (approval numbers #236/16S and #113/19S, Technische Universität München, Munich, Germany), or the Obesity Leipzig Cohort (approval numbers #159-12-21052012 and #017-12-23012012, University of Leipzig, Leipzig, Germany). All experiments involving humans were performed in accordance with the Declaration of Helsinki.

3.3   T cell isolation

3.3.1   Preparation of T cells from murine lymphoid organs

The respective lymph nodes were collected and stored in HBSS+ (hanks balanced salt solution supplemented with 5% heat inactivated fetal calf serum and 10 mM HEPES (4-(2-hydroxyethyl)-1-piperazineethanesulfonic acid)) on ice until use. Single cell suspensions were obtained by straining tissues through 70 μm cell strainers with the plunger of a syringe into HBSS+ provided. After centrifugation (400xg, 4°C, 5 min) cells were resuspended in HBSS+ and stored on ice.

3.3.2   Isolation of T cells from adipose tissues

Adipose tissues were harvested and stored on ice in buffer containing Dulbecco's phosphate buffered saline (PBS) and 0.5 % (w/v) bovine serum albumin (BSA). SAT and VAT were digested using Collagenase II in HBSS supplemented with 10 mM $CaCl_2$ on a rotator in a 37°C incubator. After 8-15 min, digestion was stopped by adding cold MACS-PBS (PBS supplemented with 0.5 % (w/v) BSA and 2 mM EDTA) and the stromal vascular fraction was filtered through 200 μm nylon meshes. After centrifugation (400xg, 4°C, 5 min), adipocytes and free fatty acids were removed and cells stored in HBSS on ice until further processing.

For isolation of T cells from BAT, a Collagenase D solution (1 mg/ml in HBSS+) was injected into the tissue; the tissue was finely minced using scissors and then incubated 2-3 times for 20 min on a rotator in a 37°C incubator. The stromal vascular fraction was filtered through 200 μm nylon meshes and after centrifugation (400xg, 4°C, 5 min), adipocytes and free fatty acids were removed and cells stored in HBSS+ on ice until further processing.

3.3.3 Isolation of human T cells from peripheral blood

Venous peripheral blood was collected in heparinized tubes (Beckton Dickinson). Peripheral blood mononuclear cells (PBMCs) were isolated by density centrifugation over Ficoll Paque PLUS (GE Healthcare). For sorting, CD4$^+$T cells were magnetically enriched (MACS) using either the EasySep Human CD4 T cell enrichment kit (Stem Cell) or the CD4 Microbeads Human Kit (Miltenyi) according to the manufacturer's instructions.

3.4 *In vitro* Treg induction

For murine *in vitro* Treg induction, 96 well plates were coated with 5 µg/ml anti-CD3 (clone: 145-2C11) and 5 µg/ml anti-CD28 (clone: 37.51) antibodies in sodium bicarbonate buffer (pH= 8.2); and for human *in vitro* Treg induction, 5 µg/ml anti-CD3 (clone: UCHT1, BioLegend) and 15 µg/ml anti-CD28 (clone: CD28.1, BioLegend) antibodies were used. Human naïve T cells (gated as live CD3$^+$CD4$^+$CD45RA$^+$CD45RO$^-$CD127^{high}CD25^{low}) or murine naïve T cells (gated as live CD4$^+$CD25$^-$CD44^{low} or live CD4$^+$CD25$^-$CD44^{low}Foxp3 eGFP$^-$) were sorted for purity with the BD FACS AriaIII into tubes with HBSS+ provided. Murine naïve T cells were seeded into pre-coated wells in RPMI+ media (RPMI 1640, Gibco; supplemented with 10% (v/v) heat inactivated fetal calf serum, 1 mM sodium pyruvate, 50 µM β-mercaptoethanol, 1x Pen/Strep (100 U/ml Penicillin, 100 µg/ml Streptomycin), 1X non-essential amino acids) in the presence of 100 U/ml recombinant human IL-2; while x-vivo+ media (x-vivo, Lonza; supplemented with 10% (v/v) heat inactivated human serum, 1x Glutamax, 1 mM sodium pyruvate, 1x non-essential amino acids, 1x Pen/Strep (100 U/ml Penicillin, 100 µg/ml Streptomycin) and 2 µg/ml Fungizone) in the presence of 100 U/ml recombinant human IL-2 was used for human naïve T cells. A humidified incubator with 37°C and 5% (v/v) CO$_2$ was used for cell culture. For optimal Treg induction mimicking sub-immunogenic TCR stimulation, T cells were transferred into uncoated wells after 18 h and cultured without TCR stimulation for further 36 h prior to analysis. Treg induction capacity was analyzed by flow cytometry.

3.5 Flow Cytometry

Single cell solutions were pre-incubated with Fc-Block (BioLegend) for 10 min on ice. Afterwards, antibodies were added for surface staining for 30 min on ice in the dark and then washed with HBSS+. Dead cells were excluded by using viability stains (Sytox Blue/Red Live Dead Stain (Invitrogen) for unfixed cells; fixable viability dye eFluor450 (Invitrogen) for fixed

cells). For intracellular staining, the Foxp3 Staining Buffer Kit (eBioscience) was used with a slightly modified protocol. In brief, cells were fixated for 30-40 min on ice in the dark. After centrifugation (400xg, 4°C, 5 min), cells were resuspended in Perm buffer (diluted to 1x with PBS) and intracellular antibodies were added. Intracellular staining was performed for 30-40 min on ice in the dark. Cells were washed twice with Perm buffer, followed by two washing steps with HBSS+. Finally, single cell suspensions were filtered in FACS tubes through 40 µm nylon mesh and acquired or sorted for purity with the FACS AriaIII (Beckton Dickinson) using FACS DIVA software (Beckton Dickinson). All datasets were initially gated on forward-scatter and on side-scatter to exclude cell doublets from analysis. Dead cells were excluded based on live/dead staining. All data were analyzed using FlowJo Software (V10.0.8r1 or V7.6.1; TreeStar Inc.) and further processed with Prism 6, 7 and 8 (GraphPad) for statistical analyses.

3.6   Proteomics

For proteome analyses, CD4$^+$T cells were used. In order to separate CD4-Bio-labelled T cells, magnetic streptavidin microbeads and biotinylated anti-CD4 antibodies were used. 50 µl Streptavidin Microbeads were added to the single cell suspension and incubated for 15 min at 4 °C. Cells were washed with 5 ml MACS-PBS and resuspended in 3 ml MACS-PBS. A Miltenyi LS column was placed on the quadroMACS™ magnetic separator and rinsed with 3 ml MACS-PBS. The cell suspension was added to the column and washed three times with 3 ml MACS-PBS. For Elution, the column was put on a 15 ml Falcon tube and CD4$^+$ enriched cells were eluted with 5 ml MACS-PBS by quickly pressing the plunger down. The supernatant was discarded; cells were resuspended in 30 µl PBS and stored in protein low-binding Eppendorf tubes at -80 °C. Cell lysis, sample alkylation, tryptic digest and LC-MS/MS analysis was performed by Dr. Fabian Hosp, Max Planck Institute for Biochemistry, Martinsried, Germany. Mass spectrometry data analysis was performed using MaxQuant (1.5.3.29) (Cox and Mann, 2008) using the UniprotKB *Mus musculus* database with 2014_07 release together with 262 common contaminants by the integrated Andromeda search engine (Cox et al., 2011). All further analyses were performed using Perseus software package (Tyanova et al., 2016) and proteomics data were deposited to the ProteomeXchange Consortium via the PRIDE partner repository with dataset identifier ProteomeXchange PXD004671.

3.7   Quantitative real-time PCR

For quantitative real time PCR (qPCR), defined T cell populations were sorted for purity or T cells used after CD4$^+$T cell MACS enrichment. Whole tissues were snap frozen in liquid nitrogen or on dry ice and pre-processed with QIAshredders (Qiagen). RNA was isolated using Trizol and the miRNeasy micro Kit (Qiagen) according to the manufacturer's instructions. RNA quantity and quality was determined on an EPOCH microplate spectrophotometer (BioTek) using Take3 plate (BioTek) and Gen5 software (BioTek; v2.01.14). 200 ng RNA were reverse transcribed with the iScript Advanced cDNA Synthesis Kit (BioRad) according to the manufacturer's instructions. For very low cell numbers, the SMARTer Ultra Low Input Kit-v4 (Takara Clontech) was used for direct cDNA synthesis from cells. For qPCR analyses, the SsoFast Evagreen Supermix (BioRad) was used on a CFX96 Touch/C1000 real time system (BioRad) with self-designed primers (Sigma Aldrich). Histone and/or 18S rRNA Ct values were used for normalization.

3.8   RNA-Sequencing

CD4$^+$T cells were sorted for purity with the FACS Aria III (BD) and stored at -80 °C until sample preparation. cDNA was reverse transcribed and amplified directly from sorted cells using the SMARTer ultra-low input RNA kit for sequencing – v4 (Takara Clontech) according to the manufacturer's instructions. cDNA concentration and quality was assessed with the Bioanalyzer 2100 and High Sensitivity DNA Chips (Agilent Technologies). Library preparation was done according to the Nextera XT Kit (Illumina) and the manufacturer's instructions. 75 bp single end reads were acquired on a NextSeq (Illumina). Quality was assessed by FastQC (Andrews, 2010) and reads were mapped against the mouse genome (mm10) using BWA-mem with default configuration. Read count lists were created with SAMTools and HTSeq-count and normalized with DESeq2.

3.9   Statistical analyses

Where appropriate Students *t*-test was used to determine statistical significance. For >2 groups, one-way ANOVA with Dunnett's or Bonferroni post hoc test was used. GraphPad Prism 6, 7 or 8 was used for statistical analyses. Statistical methods are stated in detail in figure legends and/or methods section of each publication. Two-tailed analyses were performed and a (adjusted) *p* value <0.05 was regarded as significant. *=p<0.05; **= p ≤0.01; ***= p ≤ 0.001.

4 Results

4.1 Summary of 'A Stat6/Pten Axis Links Regulatory T cells with Adipose Tissue Function'

Given the aforementioned critical role of chronic low-grade inflammation in contributing to metabolic diseases such as obesity and T2D, in the first part of my thesis I focused on the dissection of involved molecular mechanisms that can shape the adipose-immune crosstalk and thereby, guide T cell phenotypes in adipose tissues. Specifically, in this publication I analyzed the role of environmental-metabolic cues in guiding adipose tissue Tregs. In line with a key impact of environmental cold in regulating energy expenditure, the focus was set on the question how environmental cold affects both, immune cell function and adipose metabolism. In order to dissect how the local tissue microenvironment imprints on immune function, naïve T cells from different fat depots were tested for their *de novo* Treg induction potential using limited TCR stimulation. The highest Treg induction capacity had naïve T cells from BAT>SAT>VAT, what interestingly inversely reflects the susceptibility of each tissue to be prone towards obesity-associated inflammation with VAT being especially prone and lowest Treg induction efficacy. This indicates that the tissue T cells reside in impinges on the differentiation potential of naïve T cells and therefore, raises question how environmental cues can be used to target and manipulate immune cells selectively.

Although it has been described in great detail that environmental cold exposure in mice leads to BAT activation and browning of white fat depots, not much is known about its influence on the adipose-immune crosstalk. *In vivo* cold exposure increased numbers of *ex vivo* Tregs residing in all fat depots and a significantly improved *in vitro* Treg induction capacity using naïve T cells from these adipose tissues after an *in vivo* cold stimulus. Similar effects on *ex vivo* Treg frequencies in adipose tissues, as well as on improving the Treg induction capacity were observed when environmental cold was mimicked pharmacologically by treating the mice with CL316,243, a highly specific beta3-adrenergic receptor agonist that is well described for its browning-inducing properties. By using different gain- and loss-of-function models, I modulated Treg frequencies in order to dissect the role of adipose-residing Tregs in supporting adipose tissue function. Using anti-mCD25 antibody or diphtheria toxin-mediated Treg depletion protocols, I found a blunted adipose tissue response to environmental cold or

27

pharmacological beta3-adrenergic stimulation. Vice versa, Treg expansion with anti-IL2/IL2 antibody complexes improved metabolic adaptations in response to cold within BAT and in line with this, a Treg transfer *in vivo* alone was sufficient to improve BAT activity as indicated by increased expression of *Ucp1, Adrb3, Pparg, Prdm16* and other markers related to fat metabolism. These findings stress the importance of tissue-residing Tregs in maintaining tissue homeostasis and here specifically, underline their contribution in integrating environmental signals with proper adipose tissue function.

In order to dissect the intrinsic molecular mechanisms that are differentially affected in T cells isolated from BAT vs. VAT, we performed a pilot RNAseq experiment with CD4$^+$T cells. *Signal transducer and activator of transcription 6 (Stat6)* was the most differentially upregulated transcript in BAT vs. VAT T cells. This was confirmed by analyzing Stat6 abundance by flow cytometry and I found both: a successive reduction in Stat6 expression from BAT>SAT>VAT, as well as an increase in Stat6 abundance after cold exposure. Together with the direct proof that Stat6 signaling is triggered by cold exposure by analyzing Stat6 phosphorylation at tyrosine 641 (Y641) after cold exposure/CL316,243 treatment, I used mice that have either a global knockout of Stat6 or mice that harbor a modified Stat6(VT) that constitutively signals. Stat6KO mice presented with reduced *ex vivo* Treg frequencies in all adipose tissues, a decline in Treg induction efficacy and a blunted response to cold/beta3-adrenergic stimulation. In line with these findings, constitutive Stat6 signaling using cells from Stat6VT mice greatly improved Treg induction efficacy and fat Treg numbers. These findings indicate a crucial role of Stat6 signaling for the adipose tissue and immune homeostasis in response to environmental cold/beta3-adrenergic signaling.

In addition, we found that *Pten* as negative modulator of the PI3K/Akt/mTOR signaling pathway is differentially expressed in T cells from BAT>SAT>VAT, explaining the improved Treg induction capacity observed in T cells from BAT. Accordingly, Pten-transgenic (PtenTg) mice presented with high fat-residing Treg frequencies and beta3-adrenergic stimulation did not improve Treg induction further, nor further increased *ex vivo* Treg frequencies after *in vivo* treatment. In line with this, Pten inhibition by SF1670 significantly reduced Treg induction capacities. These findings call attention to the importance of PI3K/Akt/mTOR signaling modulation as it occurs in T cells residing in adipose tissues and especially when they are exposed to environmental stimuli such as cold.

To dissect the complex intracellular signaling pathways that are triggered by such environmental stimuli further, we next choose an unbiased approach and analyzed CD4$^+$T cells with and without cold/beta3-adreneric stimulation by quantitative label-free tandem mass spectrometry. Here we found the protein C17orf59 to be significantly induced by cold exposure. C17orf59 is encoded by the gene *BLOC-1 related complex subunit 6 (Borcs6)* and it was confirmed by qRT-PCR and flow cytometric analyses that mRNA and protein are more abundant after cold exposure or beta3-adrenergic stimulation. C17orf59 modulates mTORC1 signaling by competing with its interaction with Ragulator and by that, prevents mTORC1 activation at lysosomal surfaces. Since strong mTOR signaling limits successful Treg induction, more *Borcs6* mRNA expression and higher C17orf59 abundance results in improved Treg induction capacity due to reduced mTOR signaling.

These different intracellular signaling modules contribute in concert to the improved Treg induction that I have observed in T cells isolated from BAT vs SAT and VAT. These proteins and their related signaling pathways respond to environmental cues such as cold or pharmacological beta3-adrenergic signaling and together, fine tune T cell-intrinsic signaling pathways, thereby impacting Treg function and differentiation locally within adipose tissues.

With these experiments, I have shown in mice that the adipose-immune crosstalk responds to stimuli such as environmental cold or beta3-adrenergic stimulation and that this has an effect on both, immune cell differentiation and adipose tissue function. Therapeutic modulation of these newly identified proteins that are involved in linking cold exposure/beta3-adrenergic signaling with Treg differentiation potentially enables the identification of potential strategies to counteract obesity-associated inflammation by enabling Tregs.

4.1.1 Authors' contributions

Maike Becker: designed and performed *in vitro*, *ex vivo* and *in vivo* experiments, analyzed and interpreted data and wrote the manuscript. Fig. 1A-G, J-O; Fig. 2C-I; Fig. 3A, C, H-K; Fig. 4A, F-N; Fig. 5D-J; Fig. 6A-G sample preparation, J, K; Fig. S1A, B, E; Fig. S2C; Fig. S4A-C; Fig. S5A-E,L.

Stefanie Kälin: designed and performed experiments, analyzed data

Verena B. Ott: analyzed adipose tissue function by qPCR and prepared samples for RNAseq

Isabelle Serr: performed *in vivo* experiments

Fabian Hosp: performed proteomic profiling of CD4$^+$ T cells

Mohammad Hasan Mollah: performed *in vitro* experiments

Susanne Keipert: supported BAT analyses

Daniel Lamp: supported T cell analyses by Western Blot

Francoise Rohner-Jeanrenaud.: provided beta-less mice

Victoria K. Flynn: performed *in vitro* experiments

Martin G. Scherm: performed Treg induction analyses

Lucas Ribeiro do Nascimento: performed *in vitro* experiments

Katharina Gerlach: analyzed immunostainings of T cells

Vanessa Popp: analyzed immunostainings of T cells

Sarah Dietzen: supported experiments with Foxp3 DTR (DEREG) mice

Tobias Bopp: provided Foxp3 DTR (DEREG) mice

Mark H. Kaplan and Purna Krishnamurthy: provided Stat6VT mice and supported analyses of mice

Manuel Serrano: provided PtenTg mice and supported analyses of animals

Stephen C. Woods: contributed to the writing of the manuscript

Philipp Tripal and Ralf Palmisano: performed STED microscopy and related analyses

Martin Jastroch: supported analyses of BAT tissues

Matthias Blüher: supported analyses of AT function

Christian Wolfrum: performed experiments with *in vivo* cold exposure

Benno Weigmann: performed gain- and loss-of-function experiments for Treg analyses, immunofluorescence and confocal microscopy

Anette-Gabriele Ziegler: contributed to conceptualization and discussion of the project

Matthias Mann: supervised proteomic analyses

Matthias H. Tschöp: provided substantial conceptualization and contributed to writing of the manuscript

Carolin Daniel: conceptualized, designed, and performed *in vivo* experiments; analyzed and interpreted data; and wrote the manuscript.

4.1.2   Permission statement of the journal

Copyright Clearance Center — RightsLink®

Title:	A Stat6/Pten Axis Links Regulatory T Cells with Adipose Tissue Function
Author:	Stefanie Kälin, Maike Becker, Verena B. Ott, Isabelle Serr, Fabian Hosp, Mohammad M.H. Mollah, Susanne Keipert, Daniel Lamp, Francoise Rohner-Jeanrenaud, Victoria K. Flynn, Martin G. Scherm, Lucas F.R. Nascimento, Katharina Gerlach, Vanessa Popp, Sarah Dietzen et al.
Publication:	Cell Metabolism
Publisher:	Elsevier
Date:	5 September 2017

© 2017 Elsevier Inc.

BACK   CLOSE WINDOW

4.1.3   PDF: Kälin*, Becker* et al., Cell Metabolism 2017

For full-length PDF version, see Appendix **Fehler! Verweisquelle konnte nicht gefunden werden.**.

4.2 Summary of 'Short-term cold exposure supports human Treg induction in vivo'

To probe the translational relevance of my murine findings of cold/beta3-adrenergic stimulation in supporting adipose tissue Tregs, I subjected next generation humanized mice to pharmacologic beta3-adrenergic stimulation with mirabegron. Mirabegron shows in comparison to CL316,243 an improved binding affinity to the human beta3-adrenergic receptor and although tissues in humanized mice expresses the murine beta3-adrenergic receptor, I found that mirabegron was indeed able to induce browning in VAT of humanized mice as observed by a significant increase in *Ucp1* expression. Furthermore, beta3-adrenergic signaling by *in vivo* mirabegron treatment significantly improved the Treg induction capacity of naïve T cells accompanied by increased *ex vivo* Treg frequencies following beta3-adrenergic stimulation. These findings provided evidence that the signaling that is induced by beta3-adrenergic stimulation in T cells is conserved between mice and men. We further confirmed the ability of human T cells to respond to beta3-adrenergic stimulation by dose-titration experiments using human naïve T cells and *in vitro* Treg induction in the presence or absence of mirabegron. Mirabegron was able to improve the Treg induction efficacy in human naïve T cells, opening its potential utility for therapeutic use against aberrant inflammation.

In order to dissect the translational relevance of *in vivo* cold exposure in supporting human Treg function in further detail, I analyzed human samples of the FREECE study before and after exposure to individualized defined cooling protocols. Interestingly, I found improved Treg induction capacity using cells from subjects after they had been exposed to *in vivo* cold. Furthermore, *ex vivo* Treg frequencies in peripheral blood were increased after cold exposure.

Consistent with my murine data, I found an increase in *BORCS6* expression and C17orf59 abundance after *in vivo* cold exposure, indicating that the signaling pathway that links cold exposure with improved Treg induction capacity is conserved between species. A significant increase in Tregs residing in SAT biopsies after this very short and mild *in vivo* cold exposure was not observed. However, these findings highlight that intrinsic signaling mechanisms that are triggered by environmental cues such as cold or beta3-adrenergic are likely conserved between mice and men. Therefore, the identified molecular mechanisms might open path for potential therapeutic approaches using Tregs induced by cold or beta3-adrenergic signaling to reduce obesity-associated inflammation and thereby, improve metabolic health.

4.2.1   Authors' contributions

Maike Becker: performed *in vivo* and *in vitro* experiments, analyzed gene expression, analyzed and interpreted data and wrote the manuscript. Fig. 1A-E, Fig. 2, Fig. 3, Fig. 4B-C, Fig. 5A.

Isabelle Serr: performed *in vivo* and *in vitro* experiments.

Victoria K. Salb: performed human dose-response titration (Fig. 1F).

Verena B. Ott: analyzed human SAT/VAT gene expression (Fig. 4A).

Laura Mengel: recruited subjects to and performed the FREECE study.

Benno Weigmann: performed and analyzed immunefluorescence on cytospins.

Matthias Blüher: is PI of the Leipzig Obesity Cohort and provided human SAT/VAT samples.

Hans Hauner: is PI of the FREECE study and provided human blood and SAT samples.

Matthias H. Tschöp: supported conception of the manuscript.

Carolin Daniel: analyzed data, conceptualized and wrote the manuscript.

4.2.2   Permission statement of the journal

from https://www.elsevier.com/about/policies/copyright on July 2, 2019

4.2.3   PDF: Becker et al., Molecular Metabolism 2019

For full-length PDF version, see Appendix **Fehler! Verweisquelle konnte nicht gefunden werden.**.

5 Discussion

In the present thesis, I aimed at the dissection of environmental cues that can integrate the immune-metabolic crosstalk with a goal of identifying relevant molecular underpinnings that impinge on Treg induction in target tissues of metabolic disease, such as fat.

VAT-residing Tregs are known to support adipose tissue function and to be significantly reduced in obesity (Deiuliis et al., 2011; Feuerer et al., 2009). With a focus on the underlying mechanisms that contribute to the observed decline in Tregs in obese VAT compared to lean VAT, several hypotheses are currently discussed: 1) a scenario where an altered chemokine expression within VAT affects Treg immigration; 2) altered local (micro-)environment with more free fatty acids/triglycerides and potential insulin resistance that requires an adapted T cell metabolism as various nutrients are limited; 3) a hindered Treg proliferation or increase in apoptosis due to changes in the local microenvironment.

With regard to the inflammation within visceral fat depots that accompanies obesity and critically contributes to the development of insulin resistance, T2D and related co-morbidities, it would be of major interest to know the antigen specificity of invading T cells. There is strong evidence, that VAT-residing T cells recognize certain antigens and then undergo clonal expansion, since T cells isolated from VAT show a clonally expanded TCR repertoire (Bergot et al., 2015; Kolodin et al., 2015). This concept was further supported by transgenic mice (Li et al., 2018) that harbor a TCR that was originally derived from a VAT-residing Treg clone. These TCR-transgenic T cells mainly relocate to VAT and present with higher Treg frequencies also in lymphoid organs (Li et al., 2018). This indicates that a (or several) certain antigen(s) is recognized by VAT-residing Tregs and that this recognition is critically involved in Treg differentiation and retention at that site. This raises the question what the source of the antigen is: 1) driven by adipocyte death that releases antigens which then get presented by professional APCs to circulating T cells; 2) is it derived from adipocytes that get hypertrophic upon high-caloric feeding and present (lipid-derived?) antigens in a CD1d-restricted manner; or is it 3) a bystander effect of the immune reaction in lean versus obese VAT that also involves other immune subsets such as macrophages, DCs, ILCs, B and CD8^{+}T cells? The identification of the antigen(s) potentially allows an antigen-specific *de novo* induction of VAT-specific Tregs as it has been done for insulin-specific Tregs using strong-agonistic ligands under sub-immunogenic conditions (Daniel et al., 2011b; Serr et al., 2016a).

In order to identify the APCs that interact with T cells/Tregs in adipose tissues, the kiss-and-run LIPSTIC technique (for Labelling Immune Partnerships by SorTagging Intercellular Contacts) could be useful (Pasqual et al., 2018). This technique enables the identification of *in vivo* interactions between different cell types by intercellular enzymatic labelling. The system has been validated in OT-II transgenic mice where APC-T cell interactions have been successfully visualized few hours after experimental antigen delivery (Pasqual et al., 2018). After identification of APCs that stimulate T cells in adipose tissues, presented peptide repertoires have to be eluted and identified by techniques such as tandem mass spectrometry. While this has been done recently with human thymus-derived APCs (Adamopoulou et al., 2013), the number of required cells ($\sim 3 \times 10^7$-10^8) limits its usage for murine VAT ligandomics. Thus, further improvements of methodological aspects as well as of detection sensitivity are required to enable the identification of (adipose-derived?) peptides that drive immune responses in obese VAT.

With regard to the contribution of soluble mediators that are elevated in obese VAT, adipokine and cytokine compositions and levels adopt according to chronic alterations in energy balance, which correlates with insulin sensitivity and glucose tolerance. TNFα and IL-6 are important immune-modulators that are upregulated in chronic inflammation as apparent in obesity and diabetes. Immunologically, IL-6 employs different signaling modes: classical signaling occurs through binding of IL-6 to the membrane-bound IL6Rα and gp130; trans-signaling is mediated through soluble sIL6Rα:IL-6 that was shed from the cell surface and triggers activation of any gp130$^+$ cell (Rose-John, 2012; Timper et al., 2017); or by trans-presentation to T cells mediated by DCs (Heink et al., 2017). However, in the setting of different environmental-immunemetabolic cues, such as during endurance exercise, IL-6 functions as a rather anti-inflammatory myokine with significantly increased levels, while TNFα levels are constant (Febbraio and Pedersen, 2002; Lancaster and Febbraio, 2014; Pal et al., 2014; Steensberg et al., 2000). Under exercise conditions, IL-6 signaling is involved in mediating weight loss since IL-6 depletion results in blunted weight-reducing effects of exercise (Wedell-Neergaard et al., 2018). Specifically, intramuscular IL-6 expression was shown to be regulated by signaling cascades that among other pathways are likely to involve crosstalk between the Ca^{2+}/nuclear factor of activated T cells (NFAT) and glycogen/p38 mitogen-activated protein kinase (MAPK) pathways. In contrast to IL-6 produced by macrophages which elicits an pro-inflammatory response, upon exercised muscle-derived IL-6 does not trigger activation of classical pro-inflammatory

pathways such as TNFα and IL-1β, but rather involves anti-inflammatory cytokines such as IL-10 (Pedersen and Febbraio, 2008). Therefore, IL-6 has context-dependent either pro- or anti-inflammatory properties that, among others, likely rely on the co-emergence of other cytokine signaling networks.

Interestingly, in preliminary results not included in this thesis I found that classical IL-6 signaling is important to maintain the VAT Treg population in lean male mice and more specifically, Foxp3$^+$ST2$^+$Tregs. Upon T cell-specific depletion of IL6Rα, which specifically abolishes classical IL-6 signaling, lean VAT presents with clearly reduced Treg frequencies and numbers (Becker et al., manuscript in preparation). Accordingly, the role of IL-6 in obesity and obesity-associated inflammation might not solely be disadvantageous, but required to maintain VAT Foxp3$^+$ST2$^+$Tregs.

In contrast to VAT-residing Tregs, the population of Tregs located in BAT is distinct (Kalin et al., 2017; Medrikova et al., 2015). Specifically, BAT Tregs do not vanish when mice are exposed to high-caloric feeding and importantly, they exert a supporting effect on adipose tissue function. These intercellular effects are not uni-directional but resemble an active adipose-immune crosstalk since the local environment within fat depots imprints on T cell function and *vice versa*, Tregs influence fat metabolism (Kalin et al., 2017). With regard to the intrinsic molecular mechanisms that are differentially affected in T cells isolated from different adipose tissue depots, we found *Stat6* the most differentially upregulated transcript in BAT vs. VAT T cells (Kalin et al., 2017).

In order to dissect the contribution of environmental-metabolic signaling cues in integrating Treg induction with metabolic tissue function, I focused on acute cold stimulation. Cold-induced recruitment of active BAT was studied in detail for its use as potential anti-obesity agent by increasing energy expenditure (van der Lans et al., 2013; van Marken Lichtenbelt et al., 2009; Yoneshiro et al., 2013). Specifically, here I provide evidence that short-term cold acclimation induces pro-tolerogenic signaling pathways in adipose tissue that exert their function via Stat6, Pten and C17orf59/BORCS6, thereby resulting in a significant induction of local Tregs.

Using gain- and loss-of-function mice, I identified a crucial role of Stat6 signaling for the adipose tissue and immune response in response to environmental cold. These findings add to the existing knowledge of Stat6 being involved in cold-induced remodeling of fat, that is

impaired when Stat6 is absent (Qiu et al., 2014). From an immunological perspective, Stat6 has been mainly described in the context of promoting Th2 and Th9 immunity (Goenka and Kaplan, 2011) and interestingly, in being involved as second signal in antigen-specific Treg induction (Chapoval et al., 2010; Pillemer et al., 2009; Sanchez-Guajardo et al., 2007). Constitutive activation of Stat6 signaling (by Stat6VT mutation) was found to increase the frequencies of antigen-specific Tregs in secondary lymphoid organs (Sanchez-Guajardo et al., 2007), which is in line with our observation of elevated Treg frequencies in fat depots of Stat6VT-transgenic mice, as well as when Stat6 signaling is triggered by environmental stimuli such as cold or beta3-adrenergic stimulation (Kalin et al., 2017).

These mechanistic insights revealed a first glimpse on distinct intrinsic signaling differences and how these differences integrate local and global environmental signals to influence T cell differentiation in a tissue-specific manner. Since the strength of the PI3K/Akt/mTOR signaling pathway (that is modulated by the PI3K antagonist Pten amongst others) plays a central role for successful Treg induction, the identified differences in *Pten* mRNA expression levels in BAT>SAT>VAT explain the improved Treg induction in BAT, since this results in an increase in PI3K/Akt/mTOR inhibition. Interestingly, PtenTg mice with high *Pten* expression were resistant to further improvements in Treg induction upon beta3-adrenergic stimulation. These findings call attention to the importance of PI3K/Akt/mTOR signaling modulation as it occurs in T cells residing in adipose tissues, especially when they are exposed to environmental stimuli such as cold or as it can be modulated using the pharmacological Pten inhibitor SF1670 (Kalin et al., 2017; Serr et al., 2016c; Serr et al., 2018).

In line with this, the protein C17orf59 that is encoded by the gene *BLOC-1 related complex subunit 6 (Borcs6)* is critically involved in regulating mTORC1 activity. C17orf59 was found to be increased in T cells after exposure to environmental cold or beta3-adrenergic stimulation (Becker et al., 2019; Kalin et al., 2017). mTORC1 activation requires co-localization with the Ragulator complex at lysosomal surfaces and C17orf59 competes with this interaction by occupying the Ragulator complex and by that, prevents mTORC1 activation (Pu et al., 2015; Schweitzer et al., 2015; Zhang et al., 2017). As outlined above, strong mTOR signaling limits successful Treg induction (Daniel et al., 2011b; Daniel et al., 2010; Sauer et al., 2008; Serr et al., 2016b) and consequently, more *Borcs6* mRNA expression and higher C17orf59 abundance improves Treg induction due to reduced mTOR signaling.

Since it is established that not only the local environment (i.e. the adipose tissue) but also cellular metabolism impinges on T cell differentiation potentials, it is interesting that we found first evidence that proteins related to fatty acid oxidation are increased upon beta3-adrenergic stimulation in CD4^{+}T cells (Kalin et al., 2017). As mentioned in the introduction, fatty acid oxidation fuels OXPHOS and was shown to be crucial for Treg homeostasis (Angelin et al., 2017; Gerriets et al., 2015; Michalek et al., 2011). Thus, the pro-tolerogenic effects of beta3-adrenergic stimulation might be in part triggered by metabolic adaptations within immune cells.

The here described different intracellular signaling modules contribute in concert to the improved Treg induction that we have observed in T cells isolated from BAT>SAT>VAT. These proteins and their related signaling pathways respond to environmental cues such as cold or pharmacological beta3-adrenergic signaling and together, fine tune T cell-intrinsic signaling pathways, thereby impacting Treg function and differentiation. With these experiments, I have shown in mice that the adipose-immune crosstalk responds to stimuli such as environmental cold or beta3-adrenergic stimulation and that it has an effect on both, immune cell differentiation and adipose tissue function. Therapeutic modulation of these newly identified proteins that are involved in linking cold exposure or beta3-adrenergic signaling with Treg differentiation potentially enables the identification of strategies to counteract obesity-associated inflammation by enabling Tregs.

From a perspective of Treg targeting, the exploitation of these pathways could also contribute to an improvement of Treg induction during activating immune conditions. Accordingly, and from a rather therapeutic perspective in the human setting, the environmental cue cold has been described for its beneficial effects on reducing aberrant immune inflammation in rheumatic diseases (Guillot et al., 2014; Lange et al., 2008). Here, cold is usually applied locally or as whole-body cryotherapy by using cold gas or exposure to ice. Both techniques showed analgesic, anti-phlogistic, myorelaxing, vasoconstrictive and anti-inflammatory effects. A pilot study with subjects that underwent a ten day training in meditation, breathing techniques and exposure to cold found a more pronounced anti-inflammatory response to experimental endotoxemia that was preceded by an elevated increase in epinephrine levels (Kox et al., 2014; van Marken Lichtenbelt, 2017). Here, flu-like symptoms and pro-inflammatory mediators (TNFα, IL-6, IL-8) were reduced in the trained group. However, these subjects were not exposed to a defined cold stimulus that takes individual differences in cold sensation and in adaptive NST into account. Instead, voluntary self-exposure to standing in the snow barefoot, lying in

the snow bar chested, daily dipping or swimming in ice cold water, as well as bare chested and barefoot hiking on snowy mountains were used as cold stimulus (Kox et al., 2014). The non-standardized cold exposure protocols are a drawback of these particular studies and besides that, these studies did not analyze the effects of cold exposure on adaptive immune cells such as CD4$^+$T cells or Tregs. Interestingly, but also without analyzing markers related to inflammation, the group of Patrick Schrauwen found that short-term cold acclimation improves insulin sensitivity in type 2 diabetics (Hanssen et al., 2015). Therefore, the here presented molecular studies of this thesis add depth to the existing knowledge of cold being involved in BAT activation and its anti-inflammatory properties.

An open question remains how the here described molecular pathways can be exploited to improve metabolic health by supporting Tregs. Cold triggers the release of catecholamines via the SNS and thereby, induces beta3-adrenergic signaling. It is widely accepted that catecholamine release in adipose tissues plays a substantial role in inducing metabolic activity upon cold exposure and as mentioned in the introduction, the SNS is critically involved in integrating afferent signals related to metabolism and environment and responding to them via efferent signaling. With regard to the environmental stimulus cold, this includes signaling with noradrenaline and adrenaline (i.e. catecholamines), as it was shown that mice lacking both signaling molecules (due to a knockout of the synthesizing enzyme dopamine beta-hydroxylase) cannot respond to thermal stress in an adequate manner (Thomas and Palmiter, 1997). These mice are unable to increase *Ucp1* expression in BAT upon cold exposure and when being exposed to prolonged environmental cold, the constant heat loss leads to lethargy, shivering and ultimately to death due to hypothermia (Thomas and Palmiter, 1997). In line with this, mice that lack all beta-adrenergic receptors present with cold sensitivity and spontaneous obesity (Jimenez et al., 2002), highlighting the crucial role of BAT activity and NST to maintain organismal homeostasis and prevent obesity. Interestingly, both, white and brown adipocytes respond to stimulation of beta-adrenergic receptors by catecholamines. Although lipolysis is induced on both cell types, catecholamine signaling preferentially induces thermogenesis in brown adipocytes. The mechanisms underlying this differential downstream signaling remained elusive for a long time until the Kajimura lab found differences in casein kinase 2 (CK2) expression/activity between white and beige/brown adipocytes (Shinoda et al., 2015). Genetic or pharmacological inhibition of CK2 shifted the signaling to favor beige adipogenesis and thermogenesis over inducing lipolysis in white adipocytes in response to norepinephrine

or to a hypercaloric diet (Shinoda et al., 2015). Interestingly, CK2 was also shown to enable Tregs in suppressing overshooting Th2 responses *in vivo* (Ulges et al., 2015) and also Pten stability is regulated by CK2 (Patsoukis et al., 2013). These data show that although CK2 inhibition might be considered as favorable approach to induce adipose tissue browning and by that to increase metabolic activity, its potential therapeutic use is likely limited due to unwanted side effects on impairing Treg function and by that, supporting inflammation.

It was reported that obese humans present with impaired lipolytic response to beta-adrenergic stimulation triggered by catecholamines (Large et al., 1999), while weight reduction normalized catecholamine sensitivity and lipolytic responses without changing the total number of beta-adrenergic receptors present on adipocytes (Martin et al., 1990; Reynisdottir et al., 1995). This impaired response in obese patients correlates with significantly reduced adenylate cyclase activity – a downstream mediator of beta-adrenergic stimulation (Martin et al., 1990). Adenylate cyclase activity reverted close to normal levels upon weight loss after gastric stapling (Martin et al., 1990), indicating that although weight loss is clearly beneficial for health, an obese period in life imprints on intrinsic/core adipocyte function and by that, may contribute to persistent obesity. Interestingly, it was shown that the number of adipocytes is set in childhood or adolescence and then constant in lean and obese individuals, demonstrating that the adipose mass expansion in obesity is mainly driven by hypertrophic adipocytes (Spalding et al., 2008).

From an immune-metabolic perspective, specific targeting of tissue-residing Tregs enables a precise tailored intervention strategy to limit obesity-associated inflammation and its related co-morbidities. Their potential has already been shown for murine diet-induced obesity where Treg expansion e.g. by IL-2/anti-IL-2 antibody complexes (Feuerer et al., 2009), anti-CD3 mAbs (Ilan et al., 2010; Winer et al., 2009), pioglitazone treatment (Cipolletta et al., 2012) or IL-33 administration (Delacher et al., 2017; Han et al., 2015; Kolodin et al., 2015) resulted in improved metabolic indices such as reduced insulin resistance and improved glucose tolerance. However, these generalized immune-modulatory therapies bear the risk of unwanted immunological side effects due to co-expansion of other immune subsets and therefore, precise targeting strategies to specifically and exclusively expand VAT-residing Tregs are critically needed. In line with these assumptions, in an unbiased approach I focused therefore on pharmacological agents that can significantly improve Treg induction also under pro-inflammatory conditions. In a side project, by screening 25,000 chemical compounds for their potential to improve antigen-specific Treg induction, I identified 344 candidates that generally supported the Treg

induction efficacy. Further testing of these compounds might lead to selection of applicable compounds that are able to induce and/or expand Tregs in a pro-inflammatory environment such as obese VAT. The identified compounds might act on either side that is involved in antigen-specific Treg induction: namely the APCs or the naïve T cells. While it was shown that Treg conversion works best with minute antigen doses delivered to APCs (Kretschmer et al., 2005), addition of compounds might broaden the window of opportunity for successful Treg induction under activating conditions.

In addition to the adipose tissue and the contribution of locally residing Tregs to its immunemetabolic functions, the brain and more specifically the brain-fat-axis was identified as a key regulator of systemic metabolism. Here, the hypothalamic area of the brain functions as control center, responsible for sensible integration of afferent signals to maintain organismal homeostasis via efferent signaling. The SNS not only activates BAT function upon cold exposure and beta3-adrenergic stimulation, but also as response to overnutrition (Rothwell and Stock, 1979). Of note, it was reported that especially the mediobasal area of the hypothalamus (mediobasal hypothalamus; MBH) gets affected by hypercaloric diets and obesity (De Souza et al., 2005; Kälin et al., 2015; Thaler et al., 2012; Velloso et al., 2008). While hypothalamic neuropathy is contributing to the development of the obesity and its related co-morbidities, the specific causes of such neuronal malfunction remain ill described. Within the CNS, the MBH lies next to the median eminence, which is one of the circumventricular organs and has a highly fenestrated vascular endothelium that lacks a blood brain barrier (BBB). For this reason, this area is highly sensitive to blood-borne factors such as insulin, leptin, fatty acids and C-reactive protein (Cottrell and Ferguson, 2004; Hsuchou et al., 2012; Milanski et al., 2009; Verkhratsky and Butt, 2007). The MBH regulates food intake and energy expenditure through its neural circuitry and peptides. Thus, impaired hypothalamic control leads to lipid accumulation within fat depots and accelerated body weight gain (Jastroch et al., 2014; Reis et al., 2015; Thaler et al., 2012). Neuronal homeostasis is maintained by brain-resident glial cells that are mainly microglia and astrocytes. They critically contribute to neuronal homeostasis by synaptic pruning, waste clearance, nutrient supply and repair processes after injury. Within the CNS, microglia are the first line of defense and respond rapidly to any type of brain injury (Hanisch and Kettenmann, 2007; Kreutzberg, 1996; Streit, 2002; Vinet et al., 2012). The prerequisite for all APCs, that is the expression of major histocompatibility complex II, was reported for microglia (Gehrmann et al., 1993; Hayes et al., 1987; Sedgwick et al., 1993) and an increase in

expression was observed upon activation in response to neuronal damage, infection or inflammation resulting in co-expression of co-stimulatory molecules (Frei et al., 1987; Gerritse et al., 1996; Hall et al., 1999; Kreutzberg, 1996; Williams et al., 1994). This enables microglia to functionally interact with T cells, to activate them and therefore, to modulate immune and metabolic homeostasis. Despite these insights, the role of the adaptive immune system and specifically the contribution of T cells and Tregs in regulating these metabolic alterations remain currently unknown. Therefore, in a manuscript currently in revision and not specifically included in this thesis, I dissected the brain-immune crosstalk in the context of hypercaloric challenges (Becker et al.). These studies become even more important since lymphatic vessels draining the brain meninges were re-discovered only recently (Aspelund et al., 2015; Louveau et al., 2015). Although connections between the meninges and peripheral lymphatics had been described by Paolo Mascagni in late 1780s ((Mascagni, 1787); for English translation see (Sandrone et al., 2019)), the knowledge of their existence was lost for almost 200 years. These meningeal lymphatic vessels provide an opportunity of T cells and Tregs to affect neuronal homeostasis. This does not necessarily mean that these T cells or Tregs have to migrate into the parenchyma as it is observed during autoimmune inflammation in multiple sclerosis, but they could also secrete soluble mediators that influence neuronal or glial homeostasis. Treg frequencies are significantly reduced upon hypercaloric feeding specifically in the hypothalamic area of the brain, but neither in other brain areas nor in the periphery (Becker et al.). With gain- and loss-of-function experiments using Treg expansion (Webster et al., 2009) or depletion protocols (Setiady et al., 2010) I was able to show that Treg frequencies impact parenchymal immune homeostasis as indicated by increased microglial activation and macrophage infiltration upon Treg depletion (Becker et al.). Although total numbers of T cells and Tregs are relatively low compared to immune cells numbers found in multiple sclerosis patients or mice suffering from experimental autoimmune encephalitis (EAE), our findings indicate that the decline of hypothalamic Tregs contributes to the neuronal disorder observed upon hypercaloric feeding and obesity – a hypothesis that is supported by Steinman's observations that (even) rare tissue-specific T cells in an autoimmune brain infiltrate have the capacity to regulate both, the influx and efflux of other immune cells and by that, are able to critically control the ongoing immune reaction (Steinman, 1996).

In sum, the findings of this thesis underline the critical role of Tregs in metabolic tissues such as fat and brain in interfering with local inflammation and their support of tissue homeostasis

and function. Specifically, this thesis substantially contributes to a better understanding which T cell-intrinsic signaling pathways are affected by environmental cold or beta3-adrenergic stimulation and how this environmental cue improves adipose tissue function by supporting Tregs in the adipose-immune crosstalk. In the future, targeting these key signaling pathways might be utilized to develop new preventive or therapeutic approaches to limit obesity-associated inflammation and therefore, to improve metabolic indices in obesity and T2D.

6 References

Adamopoulou, E., Tenzer, S., Hillen, N., Klug, P., Rota, I.A., Tietz, S., Gebhardt, M., Stevanovic, S., Schild, H., Tolosa, E., *et al.* (2013). Exploring the MHC-peptide matrix of central tolerance in the human thymus. Nat Commun *4*, 2039.

Allan, S.E., Crome, S.Q., Crellin, N.K., Passerini, L., Steiner, T.S., Bacchetta, R., Roncarolo, M.G., and Levings, M.K. (2007). Activation-induced FOXP3 in human T effector cells does not suppress proliferation or cytokine production. Int Immunol *19*, 345-354.

Aluvihare, V.R., Kallikourdis, M., and Betz, A.G. (2004). Regulatory T cells mediate maternal tolerance to the fetus. Nat Immunol *5*, 266-271.

Andrews, S. (2010). FastQC: a quality control tool for high throughput sequence data. Available online at: http://www.bioinformatics.babraham.ac.uk/projects/fastqc.

Angelin, A., Gil-de-Gomez, L., Dahiya, S., Jiao, J., Guo, L., Levine, M.H., Wang, Z., Quinn, W.J., 3rd, Kopinski, P.K., Wang, L., *et al.* (2017). Foxp3 Reprograms T Cell Metabolism to Function in Low-Glucose, High-Lactate Environments. Cell Metab.

Apostolou, I., Sarukhan, A., Klein, L., and von Boehmer, H. (2002). Origin of regulatory T cells with known specificity for antigen. Nat Immunol *3*, 756-763.

Arpaia, N., Green, J.A., Moltedo, B., Arvey, A., Hemmers, S., Yuan, S., Treuting, P.M., and Rudensky, A.Y. (2015). A Distinct Function of Regulatory T Cells in Tissue Protection. Cell *162*, 1078-1089.

Asano, M., Toda, M., Sakaguchi, N., and Sakaguchi, S. (1996). Autoimmune disease as a consequence of developmental abnormality of a T cell subpopulation. The Journal of Experimental Medicine *184*, 387-396.

Asensio, C., Jimenez, M., Kuhne, F., Rohner-Jeanrenaud, F., and Muzzin, P. (2005). The Lack of beta-Adrenoceptors Results in Enhanced Insulin Sensitivity in Mice Exhibiting Increased Adiposity and Glucose Intolerance. Diabetes *54*, 3490-3495.

Aspelund, A., Antila, S., Proulx, S.T., Karlsen, T.V., Karaman, S., Detmar, M., Wiig, H., and Alitalo, K. (2015). A dural lymphatic vascular system that drains brain interstitial fluid and macromolecules. J Exp Med *212*, 991-999.

Asseman, C., Mauze, S., Leach, M.W., Coffman, R.L., and Powrie, F. (1999). An Essential Role for Interleukin 10 in the Function of Regulatory T Cells That Inhibit Intestinal Inflammation. The Journal of Experimental Medicine *190*, 995-1004.

Bacher, P., Heinrich, F., Stervbo, U., Nienen, M., Vahldieck, M., Iwert, C., Vogt, K., Kollet, J., Babel, N., Sawitzki, B., *et al.* (2016). Regulatory T Cell Specificity Directs Tolerance versus Allergy against Aeroantigens in Humans. Cell *167*, 1067-1078 e1016.

Baron, U., Floess, S., Wieczorek, G., Baumann, K., Grutzkau, A., Dong, J., Thiel, A., Boeld, T.J., Hoffmann, P., Edinger, M., *et al.* (2007). DNA demethylation in the human FOXP3 locus

discriminates regulatory T cells from activated FOXP3(+) conventional T cells. Eur J Immunol *37*, 2378-2389.

Bartness, T.J., Shrestha, Y.B., Vaughan, C.H., Schwartz, G.J., and Song, C.K. (2010). Sensory and sympathetic nervous system control of white adipose tissue lipolysis. Molecular and Cellular Endocrinology *318*, 34-43.

Becker, M., Kälin, S., Flynn, V.K., Ott, V.B., Kälin, R.E., Hippich, M., Scherm, M.G., Nascimento, L.F.R., Serr, I., Hosp, F*., et al.* Regulatory T cells control hypothalamic innate immune responsiveness to high calorie environments. Manuscript in revision.

Becker, M., Levings, M.K., and Daniel, C. (2017). Adipose-tissue regulatory T cells: Critical players in adipose-immune crosstalk. Eur J Immunol *47*, 1867-1874.

Becker, M., Serr, I., Salb, V.K., Ott, V.B., Mengel, L., Blüher, M., Weigmann, B., Hauner, H., Tschöp, M.H., and Daniel, C. (2019). Short-term cold exposure supports human Treg induction in vivo. Molecular Metabolism.

Bennett, C.L., Christie, J., Ramsdell, F., Brunkow, M.E., Ferguson, P.J., Whitesell, L., Kelly, T.E., Saulsbury, F.T., Chance, P.F., and Ochs, H.D. (2001). The immune dysregulation, polyendocrinopathy, enteropathy, X-linked syndrome (IPEX) is caused by mutations of FOXP3. Nature genetics *27*, 20-21.

Bergot, A.S., Chaara, W., Ruggiero, E., Mariotti-Ferrandiz, E., Dulauroy, S., Schmidt, M., von Kalle, C., Six, A., and Klatzmann, D. (2015). TCR sequences and tissue distribution discriminate the subsets of naive and activated/memory Treg cells in mice. Eur J Immunol *45*, 1524-1534.

Blagih, J., Coulombe, F., Vincent, E.E., Dupuy, F., Galicia-Vazquez, G., Yurchenko, E., Raissi, T.C., van der Windt, G.J., Viollet, B., Pearce, E.L*., et al.* (2015). The energy sensor AMPK regulates T cell metabolic adaptation and effector responses in vivo. Immunity *42*, 41-54.

Bloom, J.D., Dutia, M.D., Johnson, B.D., Wissner, A., Burns, M.G., Largis, E.E., Dolan, J.A., and Claus, T.H. (1992). Disodium (R,R)-5-[2-[[2-(3-chlorophenyl)-2-hydroxyethyl]-amino] propyl]-1,3-benzodioxole-2,2-dicarboxylate (CL 316,243). A potent beta-adrenergic agonist virtually specific for beta 3 receptors. A promising antidiabetic and antiobesity agent. Journal of medicinal chemistry *35*, 3081-3084.

Boulenouar, S., Michelet, X., Duquette, D., Alvarez, D., Hogan, A.E., Dold, C., O'Connor, D., Stutte, S., Tavakkoli, A., Winters, D*., et al.* (2017). Adipose Type One Innate Lymphoid Cells Regulate Macrophage Homeostasis through Targeted Cytotoxicity. Immunity *46*, 273-286.

Brunkow, M.E., Jeffery, E.W., Hjerrild, K.A., Paeper, B., Clark, L.B., Yasayko, S.A., Wilkinson, J.E., Galas, D., Ziegler, S.F., and Ramsdell, F. (2001). Disruption of a new forkhead/winged-helix protein, scurfin, results in the fatal lymphoproliferative disorder of the scurfy mouse. Nature genetics *27*, 68-73.

Bruns, H.A., Schindler, U., and Kaplan, M.H. (2003). Expression of a Constitutively Active Stat6 In Vivo Alters Lymphocyte Homeostasis with Distinct Effects in T and B Cells. The Journal of Immunology *170*, 3478-3487.

Buck, M.D., O'Sullivan, D., Klein Geltink, R.I., Curtis, J.D., Chang, C.H., Sanin, D.E., Qiu, J., Kretz, O., Braas, D., van der Windt, G.J., *et al.* (2016). Mitochondrial Dynamics Controls T Cell Fate through Metabolic Programming. Cell *166*, 63-76.

Burzyn, D., Benoist, C., and Mathis, D. (2013a). Regulatory T cells in nonlymphoid tissues. Nat Immunol *14*, 1007-1013.

Burzyn, D., Kuswanto, W., Kolodin, D., Shadrach, J.L., Cerletti, M., Jang, Y., Sefik, E., Tan, T.G., Wagers, A.J., Benoist, C., *et al.* (2013b). A special population of regulatory T cells potentiates muscle repair. Cell *155*, 1282-1295.

Cannon, B., and Nedergaard, J. (2004). Brown adipose tissue: function and physiological significance. Physiol Rev *84*, 277-359.

Chapoval, S., Dasgupta, P., Dorsey, N.J., and Keegan, A.D. (2010). Regulation of the T helper cell type 2 (Th2)/T regulatory cell (Treg) balance by IL-4 and STAT6. Journal of Leukocyte Biology *87*, 1011-1018.

Cipolletta, D. (2014). Adipose tissue-resident regulatory T cells: phenotypic specialization, functions and therapeutic potential. Immunology *142*, 517-525.

Cipolletta, D., Cohen, P., Spiegelman, B.M., Benoist, C., and Mathis, D. (2015). Appearance and disappearance of the mRNA signature characteristic of Treg cells in visceral adipose tissue: age, diet, and PPARgamma effects. Proc Natl Acad Sci U S A *112*, 482-487.

Cipolletta, D., Feuerer, M., Li, A., Kamei, N., Lee, J., Shoelson, S.E., Benoist, C., and Mathis, D. (2012). PPAR-gamma is a major driver of the accumulation and phenotype of adipose tissue Treg cells. Nature *486*, 549-553.

Cossarizza, A., Chang, H.D., Radbruch, A., Andra, I., Annunziato, F., Bacher, P., Barnaba, V., Battistini, L., Bauer, W.M., Baumgart, S., *et al.* (2017). Guidelines for the use of flow cytometry and cell sorting in immunological studies. Eur J Immunol *47*, 1584-1797.

Cottrell, G.T., and Ferguson, A.V. (2004). Sensory circumventricular organs: central roles in integrated autonomic regulation. Regulatory Peptides *117*, 11-23.

Cox, J., and Mann, M. (2008). MaxQuant enables high peptide identification rates, individualized p.p.b.-range mass accuracies and proteome-wide protein quantification. Nat Biotechnol *26*, 1367-1372.

Cox, J., Neuhauser, N., Michalski, A., Scheltema, R.A., Olsen, J.V., and Mann, M. (2011). Andromeda: a peptide search engine integrated into the MaxQuant environment. Journal of proteome research *10*, 1794-1805.

Cushman, S.W. (1970). STRUCTURE-FUNCTION RELATIONSHIPS IN THE ADIPOSE CELL: I. Ultrastructure of the Isolated Adipose Cell. The Journal of Cell Biology *46*, 326-341.

Cypess, A.M., Lehman, S., Williams, G., Tal, I., Rodman, D., Goldfine, A.B., Kuo, F.C., Palmer, E.L., Tseng, Y.H., Doria, A., *et al.* (2009). Identification and importance of brown adipose tissue in adult humans. New England Journal of Medicine *360*, 1509-1517.

Cypess, A.M., Weiner, L.S., Roberts-Toler, C., Franquet Elia, E., Kessler, S.H., Kahn, P.A., English, J., Chatman, K., Trauger, S.A., Doria, A., *et al.* (2015). Activation of human brown adipose tissue by a beta3-adrenergic receptor agonist. Cell Metab *21*, 33-38.

Cypess, A.M., White, A.P., Vernochet, C., Schulz, T.J., Xue, R., Sass, C.A., Huang, T.L., Roberts-Toler, C., Weiner, L.S., Sze, C., *et al.* (2013). Anatomical localization, gene expression profiling and functional characterization of adult human neck brown fat. Nature Medicine *19*, 635-639.

Daniel, C., and von Boehmer, H. (2011). Extrathymic generation of regulatory T cells--chances and challenges for prevention of autoimmune disease. Adv Immunol *112*, 177-213.

Daniel, C., Weigmann, B., Bronson, R., and Boehmer, H.v. (2011a). Prevention of type 1 diabetes in mice by tolerogenic vaccination with a strong agonist insulin mimetope. J Exp Med *208*, 1501-1510.

Daniel, C., Weigmann, B., Bronson, R., and von Boehmer, H. (2011b). Prevention of type 1 diabetes in mice by tolerogenic vaccination with a strong agonist insulin mimetope. J Exp Med *208*, 1501-1510.

Daniel, C., Wennhold, K., Kim, H.J., and von Boehmer, H. (2010). Enhancement of antigen-specific Treg vaccination in vivo. Proc Natl Acad Sci U S A *107*, 16246-16251.

Daniels, S.R. (2009). Complications of obesity in children and adolescents. Int J Obes (Lond) *33 Suppl 1*, S60-65.

David C. Humber, Cammack, N., Coates, A.V., Cobley, K.N., Orr, D.C., Storer, R., Weingarten, G.G., and Weir, M.P. (1992). Disodium (R,R)-5-[2-[[2-(3-chlorophenyl)-2-hydroxyethyl]amino]propyl]-1,3-benzodioxole-2,2-dicarboxylate (CL 316,243). A potent .beta.-adrenergic agonist virtually specific for .beta.3 receptors. A promising antidiabetic and antiobesity agent. Journal of Medical Chemistry *35*, 3081–3084.

De Souza, C.T., Araujo, E.P., Bordin, S., Ashimine, R., Zollner, R.L., Boschero, A.C., Saad, M.J., and Velloso, L.A. (2005). Consumption of a fat-rich diet activates a proinflammatory response and induces insulin resistance in the hypothalamus. Endocrinology *146*, 4192-4199.

Deiuliis, J., Shah, Z., Shah, N., Needleman, B., Mikami, D., Narula, V., Perry, K., Hazey, J., Kampfrath, T., Kollengode, M., *et al.* (2011). Visceral adipose inflammation in obesity is associated with critical alterations in tregulatory cell numbers. PLoS One *6*, e16376.

Delacher, M., Imbusch, C.D., Weichenhan, D., Breiling, A., Hotz-Wagenblatt, A., Trager, U., Hofer, A.C., Kagebein, D., Wang, Q., Frauhammer, F., *et al.* (2017). Genome-wide DNA-methylation landscape defines specialization of regulatory T cells in tissues. Nat Immunol *18*, 1160-1172.

DiSpirito, J.R., Zemmour, D., Ramanan, D., Cho, J., Zilionis, R., Klein, A.M., Benoist, C., and Mathis, D. (2018). Molecular diversification of regulatory T cells in nonlymphoid tissues. Science immunology *3*.

Duhen, T., Duhen, R., Lanzavecchia, A., Sallusto, F., and Campbell, D.J. (2012). Functionally distinct subsets of human FOXP3+ Treg cells that phenotypically mirror effector Th cells.

Blood *119*, 4430-4440.

Eller, K., Kirsch, A., Wolf, A.M., Sopper, S., Tagwerker, A., Stanzl, U., Wolf, D., Patsch, W., Rosenkranz, A.R., and Eller, P. (2011). Potential role of regulatory T cells in reversing obesity-linked insulin resistance and diabetic nephropathy. Diabetes *60*, 2954-2962.

Fahlen, L., Read, S., Gorelik, L., Hurst, S.D., Coffman, R.L., Flavell, R.A., and Powrie, F. (2005). T cells that cannot respond to TGF-beta escape control by CD4(+)CD25(+) regulatory T cells. J Exp Med *201*, 737-746.

Febbraio, M.A., and Pedersen, B.K. (2002). Muscle-derived interleukin-6: mechanisms for activation and possible biological roles. Faseb j *16*, 1335-1347.

Fedorenko, A., Lishko, P.V., and Kirichok, Y. (2012). Mechanism of fatty-acid-dependent UCP1 uncoupling in brown fat mitochondria. Cell *151*, 400-413.

Feuerer, M., Herrero, L., Cipolletta, D., Naaz, A., Wong, J., Nayer, A., Lee, J., Goldfine, A.B., Benoist, C., Shoelson, S.*, et al.* (2009). Lean, but not obese, fat is enriched for a unique population of regulatory T cells that affect metabolic parameters. Nat Med *15*, 930-939.

Fleskens, V., Minutti, C.M., Wu, X., Wei, P., Pals, C., McCrae, J., Hemmers, S., Groenewold, V., Vos, H.J., Rudensky, A.*, et al.* (2019). Nemo-like Kinase Drives Foxp3 Stability and Is Critical for Maintenance of Immune Tolerance by Regulatory T Cells. Cell Rep *26*, 3600-3612 e3606.

Floess, S., Freyer, J., Siewert, C., Baron, U., Olek, S., Polansky, J., Schlawe, K., Chang, H.D., Bopp, T., Schmitt, E.*, et al.* (2007). Epigenetic control of the foxp3 locus in regulatory T cells. PLoS Biol *5*, e38.

Fontenot, J.D., Gavin, M.A., and Rudensky, A.Y. (2003). Foxp3 programs the development and function of CD4+CD25+ regulatory T cells. Nat Immunol *4*, 330-336.

Frei, K., Siepl, C., Groscurth, P., Bodmer, S., Schwerdel, C., and Fontana, A. (1987). Antigen presentation and tumor cytotoxicity by interferon-γ-treated microglial cells. European Journal of Immunology *17*, 1271-1278.

Gehrmann, J., Banati, R.B., and Kreutzberg, G.W. (1993). Microglia in the immune surveillance of the brain: Human microglia constitutively express HLA-DR molecules. Journal of Neuroimmunology *48*, 189-198.

Gerriets, V.A., Kishton, R.J., Nichols, A.G., Macintyre, A.N., Inoue, M., Ilkayeva, O., Winter, P.S., Liu, X., Priyadharshini, B., Slawinska, M.E.*, et al.* (2015). Metabolic programming and PDHK1 control CD4+ T cell subsets and inflammation. J Clin Invest *125*, 194-207.

Gerritse, K., Laman, J.D., Noelle, R.J., Aruffo, A., Ledbetter, J.A., Boersma, W.J., and Claassen, E. (1996). CD40-CD40 ligand interactions in experimental allergic encephalomyelitis and multiple sclerosis. Proc Natl Acad Sci U S A *93*, 2499-2504.

Godfrey, V.L., Wilkinson, J.E., and Russell, L.B. (1991). X-linked lymphoreticular disease in the scurfy (sf) mutant mouse. The American journal of pathology *138*, 1379-1387.

Goenka, S., and Kaplan, M.H. (2011). Transcriptional regulation by STAT6. Immunologic research *50*, 87-96.

Gondek, D.C., Lu, L.F., Quezada, S.A., Sakaguchi, S., and Noelle, R.J. (2005). Cutting Edge: Contact-Mediated Suppression by CD4+CD25+ Regulatory Cells Involves a Granzyme B-Dependent, Perforin-Independent Mechanism. The Journal of Immunology *174*, 1783-1786.

Gottschalk, R.A., Corse, E., and Allison, J.P. (2010). TCR ligand density and affinity determine peripheral induction of Foxp3 in vivo. J Exp Med *207*, 1701-1711.

Green, E.A., Gorelik, L., McGregor, C.M., Tran, E.H., and Flavell, R.A. (2003). CD4+ CD25+ T regulatory cells control anti-islet CD8+ T cells through TGF-β–TGF-β receptor interactions in type 1 diabetes. Proceedings of the National Academy of Sciences *100*, 10878-10883.

Guillot, X., Martin, H., Seguin-Py, S., Maguin-Gate, K., Moretto, J., Totoson, P., Wendling, D., Demougeot, C., and Tordi, N. (2017). Local cryotherapy improves adjuvant-induced arthritis through down-regulation of IL-6 / IL-17 pathway but independently of TNFalpha. PLoS One *12*, e0178668.

Guillot, X., Tordi, N., Mourot, L., Demougeot, C., Dugue, B., Prati, C., and Wendling, D. (2014). Cryotherapy in inflammatory rheumatic diseases: a systematic review. Expert Rev Clin Immunol *10*, 281-294.

Haertel, E., Joshi, N., Hiebert, P., Kopf, M., and Werner, S. (2018). Regulatory T cells are required for normal and activin-promoted wound repair in mice. Eur J Immunol *48*, 1001-1013.

Hall, G.L., Girdlestone, J., Compston, D.A.S., and Wing, M.G. (1999). Recall antigen presentation by g-interferon-activated microglia results in T cell activation and propagation of the immune response. Journal of Neuroimmunology *98*, 105-111.

Han, J.M., Wu, D., Denroche, H.C., Yao, Y., Verchere, C.B., and Levings, M.K. (2015). IL-33 Reverses an Obesity-Induced Deficit in Visceral Adipose Tissue ST2+ T Regulatory Cells and Ameliorates Adipose Tissue Inflammation and Insulin Resistance. J Immunol *194*, 4777-4783.

Hanisch, U.K., and Kettenmann, H. (2007). Microglia: active sensor and versatile effector cells in the normal and pathologic brain. Nat Neurosci *10*, 1387-1394.

Hanssen, M.J., Hoeks, J., Brans, B., van der Lans, A.A., Schaart, G., van den Driessche, J.J., Jorgensen, J.A., Boekschoten, M.V., Hesselink, M.K., Havekes, B.*, et al.* (2015). Short-term cold acclimation improves insulin sensitivity in patients with type 2 diabetes mellitus. Nat Med *21*, 863-865.

Haribhai, D., Lin, W., Edwards, B., Ziegelbauer, J., Salzman, N.H., Carlson, M.R., Li, S.H., Simpson, P.M., Chatila, T.A., and Williams, C.B. (2009). A central role for induced regulatory T cells in tolerance induction in experimental colitis. J Immunol *182*, 3461-3468.

Harms, M.J., Ishibashi, J., Wang, W., Lim, H.W., Goyama, S., Sato, T., Kurokawa, M., Won, K.J., and Seale, P. (2014). Prdm16 is required for the maintenance of brown adipocyte identity and function in adult mice. Cell Metab *19*, 593-604.

Hartl, D., Koller, B., Mehlhorn, A.T., Reinhardt, D., Nicolai, T., Schendel, D.J., Griese, M., and Krauss-Etschmann, S. (2007). Quantitative and functional impairment of pulmonary CD4+CD25hi regulatory T cells in pediatric asthma. J Allergy Clin Immunol *119*, 1258-1266.

Haslam, D.W., and James, W.P.T. (2005). Obesity. The Lancet *366*, 1197-1209.

Haxhinasto, S., Mathis, D., and Benoist, C. (2008). The AKT-mTOR axis regulates de novo differentiation of CD4+Foxp3+ cells. J Exp Med *205*, 565-574.

Hayes, G.M., Woodroofe, M.N., and Cuzner, M.L. (1987). Microglia are the major cell type expressing MHC class II in human white matter. Journal of the Neurological Sciences *80*, 25-37.

Heaton, J.M. (1972). The distribution of brown adipose tissue in the human. Journal of anatomy *112*, 35-39.

Heink, S., Yogev, N., Garbers, C., Herwerth, M., Aly, L., Gasperi, C., Husterer, V., Croxford, A.L., Moller-Hackbarth, K., Bartsch, H.S., *et al.* (2017). Trans-presentation of IL-6 by dendritic cells is required for the priming of pathogenic TH17 cells. Nat Immunol *18*, 74-85.

Himms-Hagen, J., Cui, J., Danforth, E., Taatjes, D.J., Lang, S.S., Waters, B.L., and Claus, T.H. (1994). Effect of CL-316,243, a thermogenic beta 3-agonist, on energy balance and brown and white adipose tissues in rats. American Journal of Physiology-Regulatory, Integrative and Comparative Physiology *266*, R1371-R1382.

Himms-Hagen, J., Melnyk, A., Zingaretti, M.C., Ceresi, E., Barbatelli, G., and Cinti, S. (2000). Multilocular fat cells in WAT of CL-316243-treated rats derive directly from white adipocytes. American Journal of Physiology-Cell Physiology *279*, C670-C681.

Hori, S., Nomura, T., and Sakaguchi, S. (2003). Control of regulatory T cell development by the transcription factor Foxp3. Science *299*, 1057-1061.

Hsuchou, H., Kastin, A.J., and Pan, W. (2012). Blood-borne metabolic factors in obesity exacerbate injury-induced gliosis. J Mol Neurosci *47*, 267-277.

Hu, E., Tontonoz, P., and Spiegelman, B.M. (1995). Transdifferentiation of myoblasts by the adipogenic transcription factors PPAR gamma and C/EBP alpha. Proc Natl Acad Sci U S A *92*, 9856-9860.

Ilan, Y., Maron, R., Tukpah, A.M., Maioli, T.U., Murugaiyan, G., Yang, K., Wu, H.Y., and Weiner, H.L. (2010). Induction of regulatory T cells decreases adipose inflammation and alleviates insulin resistance in ob/ob mice. Proc Natl Acad Sci U S A *107*, 9765-9770.

Ito, M., Komai, K., Mise-Omata, S., Iizuka-Koga, M., Noguchi, Y., Kondo, T., Sakai, R., Matsuo, K., Nakayama, T., Yoshie, O., *et al.* (2019). Brain regulatory T cells suppress astrogliosis and potentiate neurological recovery. Nature *565*, 246-250.

Jastroch, M., Morin, S., Tschop, M.H., and Yi, C.X. (2014). The hypothalamic neural-glial network and the metabolic syndrome. Best Pract Res Clin Endocrinol Metab *28*, 661-671.

Jespersen, N.Z., Larsen, T.J., Peijs, L., Daugaard, S., Homoe, P., Loft, A., de Jong, J., Mathur, N., Cannon, B., Nedergaard, J*., et al.* (2013). A classical brown adipose tissue mRNA signature partly overlaps with brite in the supraclavicular region of adult humans. Cell Metab *17*, 798-805.

Jimenez, M., Leger, B., Canola, K., Lehr, L., Arboit, P., Seydoux, J., Russell, A.P., Giacobino, J.P., Muzzin, P., and Preitner, F. (2002). Beta(1)/beta(2)/beta(3)-adrenoceptor knockout mice are obese and cold-sensitive but have normal lipolytic responses to fasting. FEBS Lett *530*, 37-40.

Kalin, S., Becker, M., Ott, V.B., Serr, I., Hosp, F., Mollah, M.M.H., Keipert, S., Lamp, D., Rohner-Jeanrenaud, F., Flynn, V.K*., et al.* (2017). A Stat6/Pten Axis Links Regulatory T Cells with Adipose Tissue Function. Cell Metab *26*, 475-492 e477.

Kälin, S., Heppner, F.L., Bechmann, I., Prinz, M., Tschop, M.H., and Yi, C.X. (2015). Hypothalamic innate immune reaction in obesity. Nat Rev Endocrinol *11*, 339-351.

Kaplan, M.H., Schindler, U., Smiley, S.T., and Grusby, M.J. (1996). Stat6 is required for mediating responses to IL-4 and for development of Th2 cells. Immunity *4*, 313-319.

Khattri, R., Cox, T., Yasayko, S.A., and Ramsdell, F. (2003). An essential role for Scurfin in CD4+CD25+ T regulatory cells. Nat Immunol *4*, 337-342.

Khattri, R., Kasprowicz, D., Cox, T., Mortrud, M., Appleby, M.W., Brunkow, M.E., Ziegler, S.F., and Ramsdell, F. (2001). The Amount of Scurfin Protein Determines Peripheral T Cell Number and Responsiveness. The Journal of Immunology *167*, 6312-6320.

Kim, J., Lahl, K., Hori, S., Loddenkemper, C., Chaudhry, A., deRoos, P., Rudensky, A., and Sparwasser, T. (2009). Cutting edge: depletion of Foxp3+ cells leads to induction of autoimmunity by specific ablation of regulatory T cells in genetically targeted mice. J Immunol *183*, 7631-7634.

Kim, J.M., Rasmussen, J.P., and Rudensky, A.Y. (2007). Regulatory T cells prevent catastrophic autoimmunity throughout the lifespan of mice. Nat Immunol *8*, 191-197.

Klein, L., Robey, E.A., and Hsieh, C.S. (2019). Central CD4(+) T cell tolerance: deletion versus regulatory T cell differentiation. Nat Rev Immunol *19*, 7-18.

Kolodin, D., van Panhuys, N., Li, C., Magnuson, A.M., Cipolletta, D., Miller, C.M., Wagers, A., Germain, R.N., Benoist, C., and Mathis, D. (2015). Antigen- and cytokine-driven accumulation of regulatory T cells in visceral adipose tissue of lean mice. Cell Metab *21*, 543-557.

Kox, M., van Eijk, L.T., Zwaag, J., van den Wildenberg, J., Sweep, F.C., van der Hoeven, J.G., and Pickkers, P. (2014). Voluntary activation of the sympathetic nervous system and attenuation of the innate immune response in humans. Proc Natl Acad Sci U S A *111*, 7379-7384.

Kretschmer, K., Apostolou, I., Hawiger, D., Khazaie, K., Nussenzweig, M.C., and von Boehmer, H. (2005). Inducing and expanding regulatory T cell populations by foreign antigen. Nat Immunol *6*, 1219-1227.

Kreutzberg, G.W. (1996). Microglia: a sensor for pathological events in the CNS. Trends

Neurosci *19*, 312-318.

Kuswanto, W., Burzyn, D., Panduro, M., Wang, K.K., Jang, Y.C., Wagers, A.J., Benoist, C., and Mathis, D. (2016). Poor Repair of Skeletal Muscle in Aging Mice Reflects a Defect in Local, Interleukin-33-Dependent Accumulation of Regulatory T Cells. Immunity *44*, 355-367.

Lahl, K., Loddenkemper, C., Drouin, C., Freyer, J., Arnason, J., Eberl, G., Hamann, A., Wagner, H., Huehn, J., and Sparwasser, T. (2007). Selective depletion of Foxp3+ regulatory T cells induces a scurfy-like disease. J Exp Med *204*, 57-63.

Lancaster, G.I., and Febbraio, M.A. (2014). The immunomodulating role of exercise in metabolic disease. Trends Immunol *35*, 262-269.

Lange, U., Uhlemann, C., and Muller-Ladner, U. (2008). [Serial whole-body cryotherapy in the criostream for inflammatory rheumatic diseases. A pilot study]. Med Klin (Munich) *103*, 383-388.

Large, V., Reynisdottir, S., Langin, D., Fredby, K., Klannemark, M., Holm, C., and Arner, P. (1999). Decreased expression and function of adipocyte hormone-sensitive lipase in subcutaneous fat cells of obese subjects. Journal of Lipid Research *40*, 2059-2065.

Larson, G.L., and Henson, P.M. (1983). Mediators of Inflammation. Annual Review of Immunology *1*, 335-359.

Levine, A.G., Medoza, A., Hemmers, S., Moltedo, B., Niec, R.E., Schizas, M., Hoyos, B.E., Putintseva, E.V., Chaudhry, A., Dikiy, S., *et al.* (2017). Stability and function of regulatory T cells expressing the transcription factor T-bet. Nature *546*, 421-425.

Li, C., DiSpirito, J.R., Zemmour, D., Spallanzani, R.G., Kuswanto, W., Benoist, C., and Mathis, D. (2018). TCR Transgenic Mice Reveal Stepwise, Multi-site Acquisition of the Distinctive Fat-Treg Phenotype. Cell.

Liston, A., and Gray, D.H. (2014). Homeostatic control of regulatory T cell diversity. Nat Rev Immunol *14*, 154-165.

Liu, W., Putnam, A.L., Xu-Yu, Z., Szot, G.L., Lee, M.R., Zhu, S., Gottlieb, P.A., Kapranov, P., Gingeras, T.R., Fazekas de St Groth, B., *et al.* (2006). CD127 expression inversely correlates with FoxP3 and suppressive function of human CD4+ T reg cells. J Exp Med *203*, 1701-1711.

Louveau, A., Smirnov, I., Keyes, T.J., Eccles, J.D., Rouhani, S.J., Peske, J.D., Derecki, N.C., Castle, D., Mandell, J.W., Lee, K.S., *et al.* (2015). Structural and functional features of central nervous system lymphatic vessels. Nature.

MacDonald, K.G., Dawson, N.A., Huang, Q., Dunne, J.V., Levings, M.K., and Broady, R. (2015). Regulatory T cells produce profibrotic cytokines in the skin of patients with systemic sclerosis. J Allergy Clin Immunol *135*, 946- e949.

Macintyre, A.N., Gerriets, V.A., Nichols, A.G., Michalek, R.D., Rudolph, M.C., Deoliveira, D., Anderson, S.M., Abel, E.D., Chen, B.J., Hale, L.P., *et al.* (2014). The glucose transporter Glut1 is selectively essential for CD4 T cell activation and effector function. Cell Metab *20*, 61-72.

Magnuson, A.M., Kiner, E., Ergun, A., Park, J.S., Asinovski, N., Ortiz-Lopez, A., Kilcoyne, A., Paoluzzi-Tomada, E., Weissleder, R., Mathis, D., *et al.* (2018). Identification and validation of a tumor-infiltrating Treg transcriptional signature conserved across species and tumor types. Proc Natl Acad Sci U S A.

Martin, L.F., Klim, C.M., Vannucci, S.J., Dixon, L.B., Landis, J.R., and LaNoue, K.F. (1990). Alterations in adipocyte adenylate cyclase activity in morbidly obese and formerly morbidly obese humans. Surgery *108*, 228-234; discussion 234-225.

Mascagni, P., & Ciro, S (1787). Vasorum lymphaticorum Corporis Humani Historia et Ichnographia. In Auctore Paulo Mascagni in Regio Senarum Lyceo Publico Anatomes Professore (Ex typographia Pazzini Carli.

Medrikova, D., Sijmonsma, T.P., Sowodniok, K., Richards, D.M., Delacher, M., Sticht, C., Gretz, N., Schafmeier, T., Feuerer, M., and Herzig, S. (2015). Brown adipose tissue harbors a distinct sub-population of regulatory T cells. PLoS One *10*, e0118534.

Michalek, R.D., Gerriets, V.A., Jacobs, S.R., Macintyre, A.N., MacIver, N.J., Mason, E.F., Sullivan, S.A., Nichols, A.G., and Rathmell, J.C. (2011). Cutting edge: distinct glycolytic and lipid oxidative metabolic programs are essential for effector and regulatory CD4+ T cell subsets. J Immunol *186*, 3299-3303.

Milanski, M., Degasperi, G., Coope, A., Morari, J., Denis, R., Cintra, D.E., Tsukumo, D.M., Anhe, G., Amaral, M.E., Takahashi, H.K., *et al.* (2009). Saturated fatty acids produce an inflammatory response predominantly through the activation of TLR4 signaling in hypothalamus: implications for the pathogenesis of obesity. J Neurosci *29*, 359-370.

Miller, A. (1991). Antigen-driven bystander suppression after oral administration of antigens. Journal of Experimental Medicine *174*, 791-798.

Miller, C.N., Yang, J.Y., England, E., Yin, A., Baile, C.A., and Rayalam, S. (2015). Isoproterenol Increases Uncoupling, Glycolysis, and Markers of Beiging in Mature 3T3-L1 Adipocytes. PLoS One *10*, e0138344.

Miller, E., Kostka, J., Wlodarczyk, T., and Dugue, B. (2016). Whole-body cryostimulation (cryotherapy) provides benefits for fatigue and functional status in multiple sclerosis patients. A case-control study. Acta neurologica Scandinavica *134*, 420-426.

Miller, E., Mrowicka, M., Malinowska, K., Zolynski, K., Kedziora, J., oacute, and zef (2010). Effects of the whole-body cryotherapy on a total antioxidative status and activities of some antioxidative enzymes in blood of patients with multiple sclerosis-preliminary study. The Journal of Medical Investigation *57*, 168-173.

Miragaia, R.J., Gomes, T., Chomka, A., Jardine, L., Riedel, A., Hegazy, A.N., Whibley, N., Tucci, A., Chen, X., Lindeman, I., *et al.* (2019). Single-Cell Transcriptomics of Regulatory T Cells Reveals Trajectories of Tissue Adaptation. Immunity.

Misra, N., Bayry, J., Lacroix-Desmazes, S., Kazatchkine, M.D., and Kaveri, S.V. (2004). Cutting Edge: Human CD4+CD25+ T Cells Restrain the Maturation and Antigen-Presenting Function of Dendritic Cells. The Journal of Immunology *172*, 4676-4680.

Molofsky, A.B., Nussbaum, J.C., Liang, H.E., Van Dyken, S.J., Cheng, L.E., Mohapatra, A., Chawla, A., and Locksley, R.M. (2013). Innate lymphoid type 2 cells sustain visceral adipose tissue eosinophils and alternatively activated macrophages. J Exp Med *210*, 535-549.

Morgan, M.E., van Bilsen, J.H., Bakker, A.M., Heemskerk, B., Schilham, M.W., Hartgers, F.C., Elferink, B.G., van der Zanden, L., de Vries, R.R., Huizinga, T.W.*, et al.* (2005). Expression of FOXP3 mRNA is not confined to CD4+CD25+ T regulatory cells in humans. Human immunology *66*, 13-20.

Morris, D.L., Cho, K.W., Delproposto, J.L., Oatmen, K.E., Geletka, L.M., Martinez-Santibanez, G., Singer, K., and Lumeng, C.N. (2013). Adipose tissue macrophages function as antigen-presenting cells and regulate adipose tissue CD4+ T cells in mice. Diabetes *62*, 2762-2772.

Nagase, I., Yoshida, T., Kumamoto, K., Umekawa, T., Sakane, N., Nikami, H., Kawada, T., and Saito, M. (1996). Expression of uncoupling protein in skeletal muscle and white fat of obese mice treated with thermogenic beta 3-adrenergic agonist. J Clin Invest *97*, 2898-2904.

Nedergaard, J., Bengtsson, T., and Cannon, B. (2007). Unexpected evidence for active brown adipose tissue in adult humans. Am J Physiol Endocrinol Metab *293*, E444-452.

O'Sullivan, T.E., Rapp, M., Fan, X., Weizman, O.E., Bhardwaj, P., Adams, N.M., Walzer, T., Dannenberg, A.J., and Sun, J.C. (2016). Adipose-Resident Group 1 Innate Lymphoid Cells Promote Obesity-Associated Insulin Resistance. Immunity *45*, 428-441.

Ohki, H., Martin, C., Corbel, C., Coltey, M., and Le Douarin, N.M. (1987). Tolerance induced by thymic epithelial grafts in birds. Science *237*, 1032-1035.

Ohno, H., Shinoda, K., Spiegelman, B.M., and Kajimura, S. (2012). PPARgamma agonists induce a white-to-brown fat conversion through stabilization of PRDM16 protein. Cell Metab *15*, 395-404.

Pal, M., Febbraio, M.A., and Whitham, M. (2014). From cytokine to myokine: the emerging role of interleukin-6 in metabolic regulation. Immunol Cell Biol *92*, 331-339.

Panduro, M., Benoist, C., and Mathis, D. (2016). Tissue Tregs. Annu Rev Immunol *34*, 609-633.

Pasqual, G., Chudnovskiy, A., Tas, J.M.J., Agudelo, M., Schweitzer, L.D., Cui, A., Hacohen, N., and Victora, G.D. (2018). Monitoring T cell-dendritic cell interactions in vivo by intercellular enzymatic labelling. Nature *553*, 496-500.

Patsoukis, N., Li, L., Sari, D., Petkova, V., and Boussiotis, V.A. (2013). PD-1 increases PTEN phosphatase activity while decreasing PTEN protein stability by inhibiting casein kinase 2. Mol Cell Biol *33*, 3091-3098.

Pearce, E.L., and Pearce, E.J. (2013). Metabolic pathways in immune cell activation and quiescence. Immunity *38*, 633-643.

Pedersen, B.K., and Febbraio, M.A. (2008). Muscle as an endocrine organ: focus on muscle-derived interleukin-6. Physiol Rev *88*, 1379-1406.

Pillemer, B.B., Qi, Z., Melgert, B., Oriss, T.B., Ray, P., and Ray, A. (2009). STAT6 activation confers upon T helper cells resistance to suppression by regulatory T cells. J Immunol *183*, 155-163.

Polansky, J.K., Kretschmer, K., Freyer, J., Floess, S., Garbe, A., Baron, U., Olek, S., Hamann, A., von Boehmer, H., and Huehn, J. (2008). DNA methylation controls Foxp3 gene expression. Eur J Immunol *38*, 1654-1663.

Pu, J., Schindler, C., Jia, R., Jarnik, M., Backlund, P., and Bonifacino, J.S. (2015). BORC, a multisubunit complex that regulates lysosome positioning. Dev Cell *33*, 176-188.

Qiu, Y., Nguyen, K.D., Odegaard, J.I., Cui, X., Tian, X., Locksley, R.M., Palmiter, R.D., and Chawla, A. (2014). Eosinophils and type 2 cytokine signaling in macrophages orchestrate development of functional beige fat. Cell *157*, 1292-1308.

Ramsdell, F., and Fowlkes, B. (1990). Clonal deletion versus clonal anergy: the role of the thymus in inducing self tolerance. Science *248*, 1342-1348.

Reis, W.L., Yi, C.X., Gao, Y., Tschop, M.H., and Stern, J.E. (2015). Brain innate immunity regulates hypothalamic arcuate neuronal activity and feeding behavior. Endocrinology *156*, 1303-1315.

Reynisdottir, S., Langin, D., Carlstrom, K., Holm, C., Rossner, S., and Arner, P. (1995). Effects of weight reduction on the regulation of lipolysis in adipocytes of women with upper-body obesity. Clinical science (London, England : 1979) *89*, 421-429.

Rose-John, S. (2012). IL-6 trans-signaling via the soluble IL-6 receptor: importance for the pro-inflammatory activities of IL-6. Int J Biol Sci *8*, 1237-1247.

Rosen, E.D., and Spiegelman, B.M. (2014). What we talk about when we talk about fat. Cell *156*, 20-44.

Rothwell, N.J., and Stock, M.J. (1979). A role for brown adipose tissue in diet-induced thermogenesis. Nature *281*, 31-35.

Rudra, D., deRoos, P., Chaudhry, A., Niec, R.E., Arvey, A., Samstein, R.M., Leslie, C., Shaffer, S.A., Goodlett, D.R., and Rudensky, A.Y. (2012). Transcription factor Foxp3 and its protein partners form a complex regulatory network. Nat Immunol *13*, 1010-1019.

Ruprecht, C.R., Gattorno, M., Ferlito, F., Gregorio, A., Martini, A., Lanzavecchia, A., and Sallusto, F. (2005). Coexpression of CD25 and CD27 identifies FoxP3+ regulatory T cells in inflamed synovia. J Exp Med *201*, 1793-1803.

Ryu, V., Garretson, J.T., Liu, Y., Vaughan, C.H., and Bartness, T.J. (2015). Brown adipose tissue has sympathetic-sensory feedback circuits. J Neurosci *35*, 2181-2190.

Saito, M., Okamatsu-Ogura, Y., Matsushita, M., Watanabe, K., Yoneshiro, T., Nio-Kobayashi, J., Iwanaga, T., Miyagawa, M., Kameya, T., Nakada, K., *et al.* (2009). High incidence of metabolically active brown adipose tissue in healthy adult humans: effects of cold exposure and adiposity. Diabetes *58*, 1526-1531.

Sakaguchi, S., Sakaguchi, N., Asano, M., Itoh, M., and Toda, M. (1995). Immunologic self-

tolerance maintained by activated T cells expressing IL-2 receptor alpha-chains (CD25). Breakdown of a single mechanism of self-tolerance causes various autoimmune diseases. The Journal of Immunology *155*, 1151-1164.

Sakaguchi, S., Yamaguchi, T., Nomura, T., and Ono, M. (2008). Regulatory T cells and immune tolerance. Cell *133*, 775-787.

Sanchez-Guajardo, V., Tanchot, C., O'Malley, J.T., Kaplan, M.H., Garcia, S., and Freitas, A.A. (2007). Agonist-Driven Development of CD4+CD25+Foxp3+ Regulatory T Cells Requires a Second Signal Mediated by Stat6. The Journal of Immunology *178*, 7550-7556.

Sandrone, S., Moreno-Zambrano, D., Kipnis, J., and van Gijn, J. (2019). A (delayed) history of the brain lymphatic system. Nat Med *25*, 538-540.

Sasaki, Y., Sakai, M., Miyazaki, S., Higuma, S., Shiozaki, A., and Saito, S. (2004). Decidual and peripheral blood CD4+CD25+ regulatory T cells in early pregnancy subjects and spontaneous abortion cases. Mol Hum Reprod *10*, 347-353.

Sauer, S., Bruno, L., Hertweck, A., Finlay, D., Leleu, M., Spivakov, M., Knight, Z.A., Cobb, B.S., Cantrell, D., O'Connor, E., *et al.* (2008). T cell receptor signaling controls Foxp3 expression via PI3K, Akt, and mTOR. Proc Natl Acad Sci U S A *105*, 7797-7802.

Schiering, C., Krausgruber, T., Chomka, A., Frohlich, A., Adelmann, K., Wohlfert, E.A., Pott, J., Griseri, T., Bollrath, J., Hegazy, A.N*., et al.* (2014). The alarmin IL-33 promotes regulatory T-cell function in the intestine. Nature *513*, 564-568.

Schweitzer, L.D., Comb, W.C., Bar-Peled, L., and Sabatini, D.M. (2015). Disruption of the Rag-Ragulator Complex by c17orf59 Inhibits mTORC1. Cell Rep *12*, 1445-1455.

Seale, P., Bjork, B., Yang, W., Kajimura, S., Chin, S., Kuang, S., Scime, A., Devarakonda, S., Conroe, H.M., Erdjument-Bromage, H*., et al.* (2008). PRDM16 controls a brown fat/skeletal muscle switch. Nature *454*, 961-967.

Sedgwick, J.D., Schwender, S., Gregersen, R., Dörries, R., and ter Meulen, V. (1993). Resident macrophages (ramified microglia) of the adult brown Norway rat central nervous system are constitutively major histocompatibility complex class II positive. The Journal of Experimental Medicine *177*, 1145-1152.

Serr, I., Furst, R.W., Achenbach, P., Scherm, M.G., Gokmen, F., Haupt, F., Sedlmeier, E.-M., Knopff, A., Shultz, L., Willis, R.A*., et al.* (2016a). Type 1 diabetes vaccine candidates promote human Foxp3+Treg induction in humanized mice. Nat Commun *7*.

Serr, I., Furst, R.W., Achenbach, P., Scherm, M.G., Gokmen, F., Haupt, F., Sedlmeier, E.M., Knopff, A., Shultz, L., Willis, R.A*., et al.* (2016b). Type 1 diabetes vaccine candidates promote human Foxp3(+)Treg induction in humanized mice. Nat Commun *7*, 10991.

Serr, I., Furst, R.W., Ott, V.B., Scherm, M.G., Nikolaev, A., Gokmen, F., Kalin, S., Zillmer, S., Bunk, M., Weigmann, B*., et al.* (2016c). miRNA92a targets KLF2 and the phosphatase PTEN signaling to promote human T follicular helper precursors in T1D islet autoimmunity. Proc Natl Acad Sci U S A *113*, E6659-E6668.

Serr, I., Scherm, M.G., Zahm, A.M., Schug, J., Flynn, V.K., Hippich, M., Kalin, S., Becker, M., Achenbach, P., Nikolaev, A., *et al.* (2018). A miRNA181a/NFAT5 axis links impaired T cell tolerance induction with autoimmune type 1 diabetes. Sci Transl Med *10*.

Setiady, Y.Y., Coccia, J.A., and Park, P.U. (2010). In vivo depletion of CD4+FOXP3+ Treg cells by the PC61 anti-CD25 monoclonal antibody is mediated by FcgammaRIII+ phagocytes. Eur J Immunol *40*, 780-786.

Shinoda, K., Ohyama, K., Hasegawa, Y., Chang, H.Y., Ogura, M., Sato, A., Hong, H., Hosono, T., Sharp, L.Z., Scheel, D.W., *et al.* (2015). Phosphoproteomics Identifies CK2 as a Negative Regulator of Beige Adipocyte Thermogenesis and Energy Expenditure. Cell Metab *22*, 997-1008.

Shultz, L.D., Lyons, B.L., Burzenski, L.M., Gott, B., Chen, X., Chaleff, S., Kotb, M., Gillies, S.D., King, M., Mangada, J., *et al.* (2005). Human lymphoid and myeloid cell development in NOD/LtSz-scid IL2R gamma null mice engrafted with mobilized human hemopoietic stem cells. J Immunol *174*, 6477-6489.

Spalding, K.L., Arner, E., Westermark, P.O., Bernard, S., Buchholz, B.A., Bergmann, O., Blomqvist, L., Hoffstedt, J., Naslund, E., Britton, T., *et al.* (2008). Dynamics of fat cell turnover in humans. Nature *453*, 783-787.

Steensberg, A., van Hall, G., Osada, T., Sacchetti, M., Saltin, B., and Klarlund Pedersen, B. (2000). Production of interleukin-6 in contracting human skeletal muscles can account for the exercise-induced increase in plasma interleukin-6. The Journal of physiology *529 Pt 1*, 237-242.

Steinman, L. (1996). A few autoreactive cells in an autoimmune infiltrate control a vast population of nonspecific cells: a tale of smart bombs and the infantry. Proc Natl Acad Sci U S A *93*, 2253-2256.

Streit, W.J. (2002). Microglia as neuroprotective, immunocompetent cells of the CNS. Glia *40*, 133-139.

Sun, C.M., Hall, J.A., Blank, R.B., Bouladoux, N., Oukka, M., Mora, J.R., and Belkaid, Y. (2007). Small intestine lamina propria dendritic cells promote de novo generation of Foxp3 T reg cells via retinoic acid. J Exp Med *204*, 1775-1785.

Surh, C.D., and Sprent, J. (1994). T-cell apoptosis detected in situ during positive and negative selection in the thymus. Nature *372*, 100-103.

Thaler, J.P., Yi, C.X., Schur, E.A., Guyenet, S.J., Hwang, B.H., Dietrich, M.O., Zhao, X., Sarruf, D.A., Izgur, V., Maravilla, K.R., *et al.* (2012). Obesity is associated with hypothalamic injury in rodents and humans. J Clin Invest *122*, 153-162.

Thomas, S.A., and Palmiter, R.D. (1997). Thermoregulatory and metabolic phenotypes of mice lacking noradrenaline and adrenaline. Nature *387*, 94-97.

Thornton, A.M., Korty, P.E., Tran, D.Q., Wohlfert, E.A., Murray, P.E., Belkaid, Y., and Shevach, E.M. (2010). Expression of Helios, an Ikaros transcription factor family member, differentiates

thymic-derived from peripherally induced Foxp3+ T regulatory cells. J Immunol *184*, 3433-3441.

Timmons, J.A., Wennmalm, K., Larsson, O., Walden, T.B., Lassmann, T., Petrovic, N., Hamilton, D.L., Gimeno, R.E., Wahlestedt, C., Baar, K.*, et al.* (2007). Myogenic gene expression signature establishes that brown and white adipocytes originate from distinct cell lineages. Proceedings of the National Academy of Sciences *104*, 4401-4406.

Timper, K., Denson, J.L., Steculorum, S.M., Heilinger, C., Engstrom-Ruud, L., Wunderlich, C.M., Rose-John, S., Wunderlich, F.T., and Bruning, J.C. (2017). IL-6 Improves Energy and Glucose Homeostasis in Obesity via Enhanced Central IL-6 trans-Signaling. Cell Rep *19*, 267-280.

Toker, A., Engelbert, D., Garg, G., Polansky, J.K., Floess, S., Miyao, T., Baron, U., Duber, S., Geffers, R., Giehr, P.*, et al.* (2013). Active demethylation of the Foxp3 locus leads to the generation of stable regulatory T cells within the thymus. J Immunol *190*, 3180-3188.

Tontonoz, P., Hu, E., and Spiegelman, B.M. (1994). Stimulation of adipogenesis in fibroblasts by PPARγ2, a lipid-activated transcription factor. Cell *79*, 1147-1156.

Tsiros, M.D., Olds, T., Buckley, J.D., Grimshaw, P., Brennan, L., Walkley, J., Hills, A.P., Howe, P.R., and Coates, A.M. (2009). Health-related quality of life in obese children and adolescents. Int J Obes (Lond) *33*, 387-400.

Tyanova, S., Temu, T., Sinitcyn, P., Carlson, A., Hein, M.Y., Geiger, T., Mann, M., and Cox, J. (2016). The Perseus computational platform for comprehensive analysis of (prote)omics data. Nat Methods.

Ulges, A., Klein, M., Reuter, S., Gerlitzki, B., Hoffmann, M., Grebe, N., Staudt, V., Stergiou, N., Bohn, T., Bruhl, T.J.*, et al.* (2015). Protein kinase CK2 enables regulatory T cells to suppress excessive TH2 responses in vivo. Nat Immunol *16*, 267-275.

Ussar, S., Lee, K.Y., Dankel, S.N., Boucher, J., Haering, M.F., Kleinridders, A., Thomou, T., Xue, R., Macotela, Y., Cypess, A.M.*, et al.* (2014). ASC-1, PAT2, and P2RX5 are cell surface markers for white, beige, and brown adipocytes. Sci Transl Med *6*, 247ra103.

van der Lans, A.A., Hoeks, J., Brans, B., Vijgen, G.H., Visser, M.G., Vosselman, M.J., Hansen, J., Jorgensen, J.A., Wu, J., Mottaghy, F.M.*, et al.* (2013). Cold acclimation recruits human brown fat and increases nonshivering thermogenesis. J Clin Invest *123*, 3395-3403.

van Marken Lichtenbelt, W. (2017). Who is the Iceman? Temperature (Austin) *4*, 202-205.

van Marken Lichtenbelt, W.D., Vanhommerig, J.W., Smulders, N.M., Drossaerts, J.M.A.F.L., Kemerink, G.J., Bouvy, N.D., Schrauwen, P., and Teule, G.J.J. (2009). Cold-Activated Brown Adipose Tissue in Healthy Men. New England Journal of Medicine *360*, 1500-1508.

Vasanthakumar, A., Moro, K., Xin, A., Liao, Y., Gloury, R., Kawamoto, S., Fagarasan, S., Mielke, L.A., Afshar-Sterle, S., Masters, S.L.*, et al.* (2015). The transcriptional regulators IRF4, BATF and IL-33 orchestrate development and maintenance of adipose tissue-resident regulatory T cells. Nat Immunol *16*, 276-285.

Velloso, L.A., Araujo, E.P., and de Souza, C.T. (2008). Diet-induced inflammation of the hypothalamus in obesity. Neuroimmunomodulation *15*, 189-193.

Verkhratsky, A., and Butt, A.M. (2007). Glial Neurobiology (Wiley).

Vinet, J., Weering, H.R., Heinrich, A., Kalin, R.E., Wegner, A., Brouwer, N., Heppner, F.L., Rooijen, N., Boddeke, H.W., and Biber, K. (2012). Neuroprotective function for ramified microglia in hippocampal excitotoxicity. J Neuroinflammation *9*, 27.

Virtanen, K.A., Lidell, M.E., Orava, J., Heglind, M., Westergren, R., Niemi, T., Taittonen, M., Laine, J., Savisto, N.J., Enerback, S., *et al.* (2009). Functional brown adipose tissue in healthy adults. The New England journal of medicine *360*, 1518-1525.

von Boehmer, H., and Daniel, C. (2013). Therapeutic opportunities for manipulating T(Reg) cells in autoimmunity and cancer. Nat Rev Drug Discov *12*, 51-63.

Walker, M.R., Kasprowicz, D.J., Gersuk, V.H., Benard, A., Van Landeghen, M., Buckner, J.H., and Ziegler, S.F. (2003). Induction of FoxP3 and acquisition of T regulatory activity by stimulated human CD4+CD25- T cells. J Clin Invest *112*, 1437-1443.

Wang, H., Liu, L., Lin, J.Z., Aprahamian, T.R., and Farmer, S.R. (2016). Browning of White Adipose Tissue with Roscovitine Induces a Distinct Population of UCP1(+) Adipocytes. Cell Metab *24*, 835-847.

Wang, J., Ioan-Facsinay, A., van der Voort, E.I., Huizinga, T.W., and Toes, R.E. (2007). Transient expression of FOXP3 in human activated nonregulatory CD4+ T cells. Eur J Immunol *37*, 129-138.

Webster, K.E., Walters, S., Kohler, R.E., Mrkvan, T., Boyman, O., Surh, C.D., Grey, S.T., and Sprent, J. (2009). In vivo expansion of T reg cells with IL-2-mAb complexes: induction of resistance to EAE and long-term acceptance of islet allografts without immunosuppression. J Exp Med *206*, 751-760.

Wedell-Neergaard, A.S., Lang Lehrskov, L., Christensen, R.H., Legaard, G.E., Dorph, E., Larsen, M.K., Launbo, N., Fagerlind, S.R., Seide, S.K., Nymand, S., *et al.* (2018). Exercise-Induced Changes in Visceral Adipose Tissue Mass Are Regulated by IL-6 Signaling: A Randomized Controlled Trial. Cell Metab.

Weiss, J.M., Bilate, A.M., Gobert, M., Ding, Y., Curotto de Lafaille, M.A., Parkhurst, C.N., Xiong, H., Dolpady, J., Frey, A.B., Ruocco, M.G., *et al.* (2012). Neuropilin 1 is expressed on thymus-derived natural regulatory T cells, but not mucosa-generated induced Foxp3+ T reg cells. J Exp Med *209*, 1723-1742, S1721.

WHO (2015). Report: Obesity and overweight, Fact Sheet No. 311.

Williams, K., Ulvestad, E., and Antel, J.P. (1994). B7/BB-1 antigen expression on adult human microglia studied in vitro and in situ. Eur J Immunol *24*, 3031-3037.

Williams, L.M., and Rudensky, A.Y. (2007). Maintenance of the Foxp3-dependent developmental program in mature regulatory T cells requires continued expression of Foxp3.

Nat Immunol *8*, 277-284.

Winer, S., Chan, Y., Paltser, G., Truong, D., Tsui, H., Bahrami, J., Dorfman, R., Wang, Y., Zielenski, J., Mastronardi, F.*, et al.* (2009). Normalization of obesity-associated insulin resistance through immunotherapy. Nat Med *15*, 921-929.

Wu, D., Luo, Y., Guo, W., Niu, Q., Xue, T., Yang, F., Sun, X., Chen, S., Liu, Y., Liu, J.*, et al.* (2017). Lkb1 maintains Treg cell lineage identity. Nat Commun *8*, 15876.

Wu, D., Molofsky, A.B., Liang, H.-E., Ricardo-Gonzalez, R.R., Jouihan, H.A., Bando, J.K., Chawla, A., and Locksley, R.M. (2011). Eosinophils Sustain Adipose Alternatively Activated Macrophages Associated with Glucose Homeostasis. Science *332*, 243.

Wu, J., Bostrom, P., Sparks, L.M., Ye, L., Choi, J.H., Giang, A.H., Khandekar, M., Virtanen, K.A., Nuutila, P., Schaart, G.*, et al.* (2012). Beige adipocytes are a distinct type of thermogenic fat cell in mouse and human. Cell *150*, 366-376.

Xu, H., Barnes, G.T., Yang, Q., Tan, G., Yang, D., Chou, C.J., Sole, J., Nichols, A., Ross, J.S., Tartaglia, L.A.*, et al.* (2003). Chronic inflammation in fat plays a crucial role in the development of obesity-related insulin resistance. J Clin Invest *112*, 1821-1830.

Yang, K., Blanco, D.B., Neale, G., Vogel, P., Avila, J., Clish, C.B., Wu, C., Shrestha, S., Rankin, S., Long, L.*, et al.* (2017). Homeostatic control of metabolic and functional fitness of Treg cells by LKB1 signalling. Nature.

Yoneshiro, T., Aita, S., Matsushita, M., Kayahara, T., Kameya, T., Kawai, Y., Iwanaga, T., and Saito, M. (2013). Recruited brown adipose tissue as an antiobesity agent in humans. J Clin Invest *123*, 3404-3408.

Youngstrom, T.G., and Bartness, T.J. (1995). Catecholaminergic innervation of white adipose tissue in Siberian hamsters. American Journal of Physiology-Regulatory, Integrative and Comparative Physiology *268*, R744-R751.

Zenclussen, A.C., Gerlof, K., Zenclussen, M.L., Sollwedel, A., Bertoja, A.Z., Ritter, T., Kotsch, K., Leber, J., and Volk, H.D. (2005). Abnormal T-cell reactivity against paternal antigens in spontaneous abortion: adoptive transfer of pregnancy-induced CD4+CD25+ T regulatory cells prevents fetal rejection in a murine abortion model. The American journal of pathology *166*, 811-822.

Zeng, W., Pirzgalska, R.M., Pereira, M.M., Kubasova, N., Barateiro, A., Seixas, E., Lu, Y.H., Kozlova, A., Voss, H., Martins, G.G.*, et al.* (2015). Sympathetic neuro-adipose connections mediate leptin-driven lipolysis. Cell *163*, 84-94.

Zhang, T., Wang, R., Wang, Z., Wang, X., Wang, F., and Ding, J. (2017). Structural basis for Ragulator functioning as a scaffold in membrane-anchoring of Rag GTPases and mTORC1. Nat Commun *8*, 1394.

Zingaretti, M.C., Crosta, F., Vitali, A., Guerrieri, M., Frontini, A., Cannon, B., Nedergaard, J., and Cinti, S. (2009). The presence of UCP1 demonstrates that metabolically active adipose tissue in the neck of adult humans truly represents brown adipose tissue. FASEB J *23*, 3113-3120.

Danksagung

Ich möchte mich von ganzem Herzen bei Carolin Daniel für die Betreuung dieser Doktorarbeit bedanken. Vielen Dank für den regen Austausch, die Brainstorming-Sessions, die hilfreiche Kritik, die Unterstützung und Förderung in allen Bereichen und das motivierende Umfeld, das du deinen Doktoranden bietest und das so essentiell für unsere persönliche Weiterentwicklung ist.

Ich bedanke mich außerdem herzlich bei Frau Prof. Dr. Anette-Gabriele Ziegler für die Möglichkeit, die Doktorarbeit an ihrem Institut durchzuführen. Vielen Dank für die Diskussionen bei den Thesis Committee Meetings, die Patientenproben und für dein Interesse.

Vielen Dank auch an Frau Prof. Dr. Hannelore Daniel für die Zweitbetreuung der Doktorarbeit, das Interesse an meiner Arbeit und die kritischen Fragen und Kommentare während der Thesis Committee Meetings.

Ein besonderer Dank gilt auch Herrn Prof. Dr. Matthias H. Tschöp für die wertvollen Ideen, Visionen, Hilfestellungen und Kommentare zu allen Projekten.

Ein herzliches Dankeschön auch an alle Kollaborationspartner, die Probandenmaterial, Reagenzien, Mäuse oder Protokolle bereitgestellt und somit einen wichtigen Beitrag geleistet haben. Hier sind insbesondere Benno Weigmann und sein Labor zu nennen. Außerdem vielen Dank an die Arbeitsgruppen von Ingo Bechmann (insb. Dr. Martin Krüger) und Ari Waisman (insb. Alexei Nikolaev und Alma Mohebiany), wo ich während der Gastbesuche viele neue Techniken lernen konnte. Vielen herzlichen Dank auch an Prof. Dr. Hans Hauner, Laura Mengel und das FREECE study team für die spannende und fruchtbare Zusammenarbeit.

Mein ganz spezieller Dank gilt neben dem gesamten IDF dem IDO, IDR und IDC für die vielen spannenden Kollaborationen. Außerdem selbstverständlich der AG Daniel mit allen ehemaligen und derzeitigen Mitarbeitern. Isabelle, danke, dass du so viele Jahre meine lab wife warst, immer parat, immer ein offenes Ohr und immer eine helfende Hand - mit deiner gewissen Vorliebe für verrückte Ideen und riesen Experimente. Danke Verena für deinen permanenten Einsatz, die gemeinsamen Wahnsinnsexperimente und deine Art. Es hat mir wahnsinnig viel Spaß gemacht, mit euch zu arbeiten.

Zuletzt möchte ich mich bei Andy und meiner Familie für die bedingungslose Unterstützung bedanken.

7 Appendix

7.1 Published manuscript: Kälin*, Becker* et al., Cell Metabolism 2017

Cell Metabolism

A Stat6/Pten Axis Links Regulatory T Cells with Adipose Tissue Function

Graphical Abstract

Highlights

- Cold exposure or beta3-adrenergic stimuli induce adipose tissue Foxp3^{+} Tregs

- Short-term high-calorie diet induces Foxp3^{+} Tregs in brown adipose tissue

- Stat6 links Foxp3^{+} Tregs with adipose tissue function

- Cold exposure or beta3-adrenergic stimulation increases C17orf59 expression

Authors

Stefanie Kälin, Maike Becker, Verena B. Ott, ..., Matthias Mann, Matthias H. Tschöp, Carolin Daniel

Correspondence

tschoep@helmholtz-muenchen.de (M.H.T.), carolin.daniel@helmholtz-muenchen.de (C.D.)

In Brief

Obesity and type 2 diabetes are associated with metabolic defects and adipose tissue inflammation. Kälin et al. report that a T cell-specific Stat6/Pten signaling axis links cold exposure or adrenergic stimuli with immunosuppressive regulatory T cell activity and adipose tissue function, offering novel molecular targets for improvement of adipose tissue function.

Data Resources

PXD004671

Article

CellPress

A Stat6/Pten Axis Links Regulatory
T Cells with Adipose Tissue Function

Stefanie Kälin,[1,2,17] Maike Becker,[2,3,17] Verena B. Ott,[1,2,4] Isabelle Serr,[2,3] Fabian Hosp,[5] Mohammad M.H. Mollah,[2,3]
Susanne Keipert,[1,2] Daniel Lamp,[1,2] Francoise Rohner-Jeanrenaud,[6] Victoria K. Flynn,[2,3] Martin G. Scherm,[2,3]
Lucas F.R. Nascimento,[2,3] Katharina Gerlach,[7] Vanessa Popp,[7] Sarah Dietzen,[8] Tobias Bopp,[8] Purna Krishnamurthy,[9]
Mark H. Kaplan,[9] Manuel Serrano,[10] Stephen C. Woods,[11] Philipp Tripal,[12] Ralf Palmisano,[12] Martin Jastroch,[1,2]
Matthias Blüher,[13] Christian Wolfrum,[14] Benno Weigmann,[7] Anette-Gabriele Ziegler,[2,15,16] Matthias Mann,[5]
Matthias H. Tschöp,[1,2,18,*] and Carolin Daniel[3,2,*]

[1]Institute for Diabetes and Obesity, Helmholtz Diabetes Center at Helmholtz Zentrum München and Division of Metabolic Diseases,
Department of Medicine, Technische Universität München, 85748 Munich, Germany
[2]German Center for Diabetes Research (DZD), 85764 Munich-Neuherberg, Germany
[3]Institute for Diabetes Research, Research Group Immune Tolerance in Diabetes, Helmholtz Diabetes Center at Helmholtz Zentrum München,
80939 Munich, Germany
[4]Institute for Advanced Study, Technische Universität München, 85748 Garching, Germany
[5]Max Planck Institute of Biochemistry, 82152 Martinsried, Germany
[6]Laboratory of Metabolism, Division of Endocrinology, Diabetology, Hypertension, and Nutrition, Department of Internal Medicine Specialties,
Faculty of Medicine, University of Geneva, Geneva, Switzerland
[7]Department of Medicine 1, University of Erlangen-Nuremberg, 91052 Erlangen, Germany
[8]Institute of Immunology, University Medical Center of the Johannes Gutenberg University, 55131 Mainz, Germany
[9]Department of Pediatrics and HB Wells Center for Pediatric Research, Indiana University School of Medicine, Indianapolis, IN 46202, USA
[10]Tumour Suppression Group, Spanish National Cancer Research Centre (CNIO), 28029 Madrid, Spain
[11]Department of Psychiatry and Behavioral Neuroscience, University of Cincinnati, Cincinnati, OH, USA
[12]OICE (Optical Imaging Centre Erlangen), University Erlangen, 91052 Erlangen, Germany
[13]Department of Medicine, Research Group Molecular Endocrinology, University of Leipzig, 04103 Leipzig, Germany
[14]Swiss Federal Institute of Technology, Institute of Food Nutrition and Health, Laboratory of Translational Nutrition Biology, ETH Zurich,
8603 Schwerzenbach, Switzerland
[15]Institute for Diabetes Research, Helmholtz Diabetes Center at Helmholtz Zentrum München, 80939 Munich, Germany
[16]Klinikum rechts der Isar, Technische Universität München, 80333 Munich, Germany
[17]These authors contributed equally
[18]Lead Contact
*Correspondence: tschoep@helmholtz-muenchen.de (M.H.T.), carolin.daniel@helmholtz-muenchen.de (C.D.)
http://dx.doi.org/10.1016/j.cmet.2017.08.008

SUMMARY

Obesity and type 2 diabetes are associated with metabolic defects and adipose tissue inflammation. Foxp3^{+} regulatory T cells (Tregs) control tissue homeostasis by counteracting local inflammation. However, if and how T cells interlink environmental influences with adipocyte function remains unknown. Here, we report that enhancing sympathetic tone by cold exposure, beta3-adrenergic receptor (ADRB3) stimulation or a short-term high-calorie diet enhances Treg induction in vitro and in vivo. CD4^{+} T cell proteomes revealed higher expression of Foxp3 regulatory networks in response to cold or ADRB3 stimulation in vivo reflecting Treg induction. Specifically, Ragulator-interacting protein C17orf59, which limits mTORC1 activity, was upregulated in CD4^{+} T cells by either ADRB3 stimulation or cold exposure, suggesting contribution to Treg induction. By loss- and gain-of-function studies, including Treg depletion and transfers in vivo, we demonstrated that a T cell-specific Stat6/Pten axis links cold exposure or ADRB3 stimulation with Foxp3^{+} Treg induction and adipose tissue function. Our findings offer a new mechanistic model in which tissue-specific Tregs maintain adipose tissue function.

INTRODUCTION

Obesity and type 2 diabetes (T2D) are among the most severe health threats of modern society. Each of these metabolic disorders is associated with tissue-specific maladaptive alterations, including amplified inflammatory processes in individual fat depots. Based on the currently accepted model, adipocytes can be divided into classes of white, brown, and beige cells (Rosen and Spiegelman, 2014) and are surrounded by several immune cell types. Immune cell type composition, number, and function dramatically change in visceral white adipose tissue (visWAT) in response to overnutrition. Accordingly, visWAT is especially prone to obesity-associated inflammation (Rosen and Spiegelman, 2014).

CD4^{+}CD25^{+}Foxp3^{+} regulatory T cells (Tregs) critically contribute to tissue homeostasis by interfering with local inflammation. Tregs can be induced in the peripheral immune system,
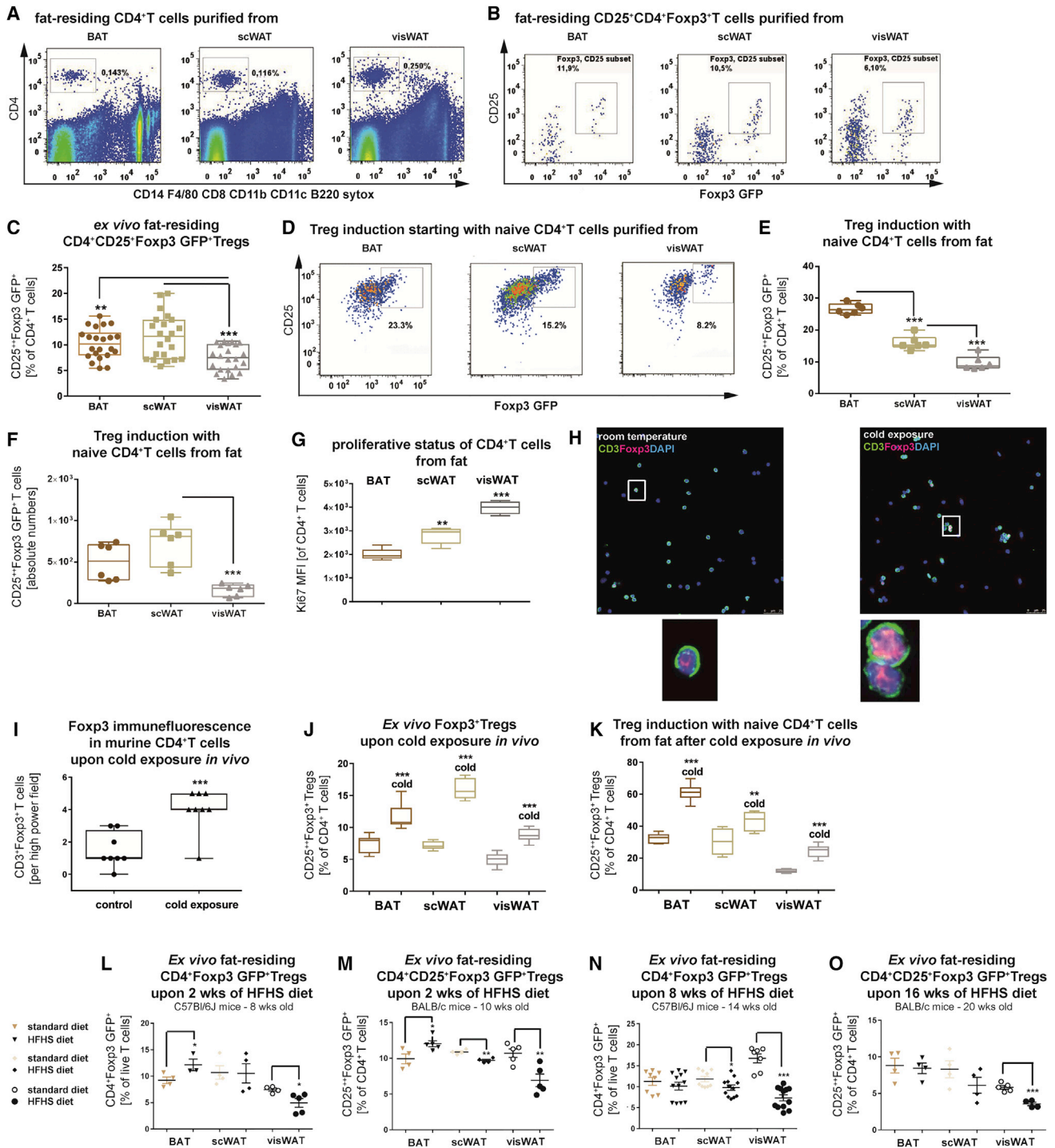
Figure 1. Treg Accumulation in Brown and White Adipose Tissue

(A) Representative fluorescence-activated cell sorting (FACS) plots for identification of fat-residing CD4$^+$ T cells from BAT, scWAT, or visWAT of young lean female BALB/c Foxp3GFP reporter mice. CD4$^+$ T cells were gated on CD14$^-$, F4/80$^-$, CD8a$^-$, CD11b$^-$, CD11c$^-$, B220, and sytox$^-$.

(B) Representative FACS plots for identification of fat-residing CD4$^+$CD25^{++}Foxp3GFP$^+$ Tregs in BAT, scWAT, or visWAT. Plots are pre-gated as shown in (A).

(C) Box-and-whisker plots for frequencies of CD25$^+$Foxp3GFP$^+$ Tregs residing in fat depots as indicated in (B). n = 22 per group from five independent experiments.

(D) Representative FACS plots for *in vitro* Treg induction assays using limited TCR stimulation and naive CD4$^+$ T cells purified from fat depots.

(E and F) *In vitro* Treg induction assays of fat-residing CD4$^+$ T cells (E) and absolute Treg numbers (F) obtained starting with identical numbers of naive CD4$^+$ T cells. n = 6 per group.

(G) Summary graph for proliferating CD4$^+$ T cells from fat depots as assessed by Ki67 mean fluorescence intensity (MFI). n = 5 per group.

(legend continued on next page)

a process referred to as Treg induction (von Boehmer and Daniel, 2013).

Recently, a critical function of fat-residing CD4^{+} T effector and Tregs in adipose-immune crosstalk was reported (Bapat et al., 2015; Cipolletta et al., 2012; Feuerer et al., 2009). Specifically, a subcategory of Tregs was identified as functionally participating in maintenance of visWAT energy homeostasis (Cipolletta et al., 2012; Feuerer et al., 2009; Mathis, 2013). Functional orchestration of Treg populations in visWAT is influenced by PPAR-γ signaling (Cipolletta et al., 2012; Panduro et al., 2016); i.e., PPAR-γ collaborates with Foxp3 to impose the transcriptional profile characteristic of visWAT Tregs onto naive CD4^{+} T cells (Cipolletta et al., 2012). Fat-residing Tregs control local inflammatory processes.

However, despite these insights in adipose-immune crosstalk in visWAT, including the contribution of Treg cells, our understanding of Treg function and the subsequent interaction with subcutaneous white adipose tissue (scWAT) and brown adipose tissue (BAT) remains in its infancy. One relevant study reported that Tregs in BAT of female C57BL/6 mice have a different transcriptome than that of their splenic counterparts (Medrikova et al., 2015).

In addition, the molecular underpinnings of the functional interplay between adipose tissue (AT) and Treg cells, especially in scWAT and BAT, remain largely unknown, and we hypothesized that this Treg-adipose crosstalk is at least partially regulated by environmental influences. However, if and how T cells and Tregs interlink environmental challenges with adipocyte function are still unclear. Specific insights into the mutual crosstalk between local Tregs and AT, especially in BAT and scWAT, are critical for the development of precision interventions to improve and maintain AT function.

To mechanistically dissect Treg induction in adipose function, we focused on three environmental influences to increase sympathetic tone *in vivo*: cold exposure and enhancement of sympathetic tone (beta3-adrenergic signaling) as well as on short-term exposure to a high-caloric challenge as a means of inducing diet-induced thermogenesis. Cold exposure was chosen based on its major role in the regulation of energy expenditure and consequent significant impact on diverse metabolic processes of AT, especially as recent studies uncovered cold-inducible BAT in adult humans (Cypess et al., 2013; Saito et al., 2009). Accordingly, cold exposure or short-term cryostimulation was used to activate beta3-adrenergic receptors (ADRB3s) in clinical situations; e.g., in rheumatoid arthritis or multiple sclerosis (Guillot et al., 2014). Further, increased anti-inflammatory cytokine production has been reported upon short-term cryostimulation (Klimek et al., 2011; Lubkowska et al., 2011), and short-term

high-calorie exposure supports BAT thermogenesis (Rothwell and Stock, 1979).

Here, we report that cold exposure or ADRB3 stimulation induces Tregs *in vitro* as well as *in vivo*. Diet-induced thermogenesis likewise increased Foxp3^{+} Treg numbers and their induction in BAT. Mechanistically, using CD4^{+} T cell proteomes, we uncovered Treg induction and higher protein expression of Foxp3 regulatory networks. Specifically, the Ragulator-interacting protein C17orf59, which limits mTORC1 activity, was upregulated by both ADRB3 stimulation and cold exposure, likely supporting enhanced Treg induction. Using a series of T cell-specific and adipose-related loss- and gain-of-function studies, including depletion, transfers, and expansion of Tregs *in vivo*, we demonstrated that a T cell-specific Stat6/Pten axis adjusts Foxp3^{+} Treg induction and AT function according to the degree of sympathetic tone and environmental temperature.

RESULTS

BAT and scWAT Harbor Higher Foxp3^{+} Treg Percentages than visWAT

To dissect the interplay between the induction of Tregs and adipose function, we first investigated their frequency, functional characteristics, and induction in different fat depots using young lean BALB/c Foxp3 GFP reporter mice (3–6 weeks of age). A set of exclusion markers permitted the direct identification of a CD4^{+} T cell subset purified from three fat depots (Figure 1A). Locally residing CD4^{+}CD25^{+}Foxp3GFP^{+} Treg percentages were higher in BAT and scWAT than in visWAT (Tregs in BAT versus visWAT, p = 0.0015; Tregs in scWAT versus visWAT, p = 0.0003; Figures 1B and 1C).

Treg Induction Is More Efficient in T Cells from BAT and scWAT than from visWAT

To determine Foxp3^{+} Treg induction capacities in different fat depots, we purified naive CD4^{+}CD25^{−}Foxp3GFP^{−}CD44^{low} T cells from BAT, scWAT, and visWAT of BALB/c Foxp3-GFP reporter mice. We based our approach on recently emerging evidence that naive CD4^{+}CD25^{−} T cells are present in various non-lymphoid tissues (Kim, 2007; Lewis et al., 2008). Efficient Foxp3^{+} Treg induction requires subimmunogenic stimulation of naive CD4^{+} T cells (Daniel and von Boehmer, 2011; Daniel et al., 2011; Gottschalk et al., 2010), while a lower proliferative capacity of T cells results in more efficient Treg induction (Kretschmer et al., 2005). To mimic such subimmunogenic T cell receptor (TCR) stimulation *in vitro*, we used premature withdrawal of TCR stimulation in the absence of transforming growth factor β (Sauer et al., 2008; Serr et al., 2016).

(H) Representative confocal microscopy images of CD4^{+} T cells purified from mice upon *in vivo* cold exposure (4 days, 8°C). Scale bar, 25 μm.

(I) Foxp3^{+}CD3^{+} T cells per high power field in samples from (G). n = 8 per group from SEM from two independent experiments.

(J) *Ex vivo* Treg frequencies purified from AT of young BALB/c mice upon *in vivo* cold exposure (24 hr, 4°C). n = 9 per group.

(K) *In vitro* Treg induction assays of fat-residing naive T cells after *in vivo* cold exposure (24 hr, 4°C). n = 6 per group.

(L and M) *Ex vivo* CD4^{+}CD25^{++}Foxp3^{+} Treg frequencies in fat depots of 8-week-old C57BL/6J mice (L) or 10-week-old BALB/c mice (M) that were subjected to 2 weeks of HFHS diet. n = 4 per group in (L), n > 4 per group in (M).

(N) Summary graphs for *ex vivo* CD4^{+}CD25^{++}Foxp3^{+} Treg frequencies in BAT, scWAT, and visWAT of 14-week-old C57BL/6J mice upon 8 weeks of HFHS diet. n = 12 for HFHS diet group, n = 8 for standard diet group.

(O) Depicted are *ex vivo* fat-residing CD4^{+}CD25^{++}Foxp3^{+} Tregs of 20-week-old BALB/c animals that were on an HFHS diet for 16 weeks. n = 4–5 per group. See also Figure S1. Data are presented as box-and-whisker plots with min and max values for data distribution or as means ± SEM. *p < 0.05, **p < 0.01, ***p < 0.001.

Specifically, we compared Treg induction between naive CD4+CD25−Foxp3GFP−CD44low T cells from different fat depots. Treg induction was most efficient using naive T cells purified from BAT and scWAT (induced CD4+CD25++Foxp3+ Tregs [% of CD4+ T cells] BAT 26.5 ± 0.6 versus scWAT 16.0 ± 0.9; Figures 1D–1F). Significantly lower induced Treg frequencies were obtained with naive CD4+ T cells from visWAT (induced CD4+CD25++Foxp3+ Tregs [% of CD4+ T cells] visWAT 9.6 ± 0.9, p < 0.01; Figures 1D–1F).

Consistent with the increased Treg induction capacity, there was a lower proliferative potential in T cells from BAT and scWAT when compared with visWAT (CD4+Ki67+ T cells mean fluorescence intensity [MFI]: BAT 2,050 ± 50 versus scWAT CD4+Ki67+ T cells 3,025 ± 75 versus visWAT CD4+Ki67+ T cells 4,235 ± 45, p < 0.01; Figure 1G).

Cold Exposure Enhances Treg Induction of Adipose Tissue T Cells

Brown/beige fat thermogenesis is stimulated by environmental cold as a means to enhance sympathetic tone. To dissect if and how Tregs interlink thermal challenges with adipocyte function, we first investigated the effects of cold exposure. Cold acclimation (1 week at 8°C) significantly increased Foxp3+ Treg percentages purified from inguinal lymph nodes (inLNs) of mice (Figures 1H and 1I). Short-term cold acclimation (24 hr at 4°C) likewise enhanced Foxp3+ Treg percentages in T cells from BAT, scWAT, and visWAT (CD4+CD25++Foxp3+ T cells [% of CD4+ T cells]: BAT 7.4 ± 0.6 versus BAT after cold 11.6 ± 0.8, p < 0.001; scWAT 7.2 ± 0.2 versus scWAT after cold 15.9 ± 0.6, p < 0.001; visWAT 4.9 ± 0.3 versus visWAT after cold 8.8 ± 0.4, p < 0.001; Figure 1J).

In addition, Treg induction of naive CD4+ T cells from the respective fat depots after 24 hr of cold was significantly enhanced (Figure 1K).

Short-Term Exposure to a High-Calorie Environment Increases Foxp3+ Tregs in BAT

Short-term high-caloric diets promote BAT thermogenesis (Rothwell and Stock, 1979), which depends on uncoupling protein 1 (UCP1 function; Feldmann et al., 2009).

A 2-week high-fat/high-sugar (HFHS) diet environment to 6-week-old Bl6 Foxp3-GFP reporter mice or 8-week-old BALB/c Foxp3-GFP reporter mice significantly enhanced Foxp3+ Treg accumulation in BAT (Figures 1L and 1M). Mild changes in Tregs were seen in scWAT, whereas the 2-week HFHS diet resulted in a significant decline in visWAT Treg percentages (Figures 1L and 1M). HFHS diet exposure for 8 weeks did not alter Treg ratios in BAT or scWAT of B6 Foxp3-GFP reporter mice. In accordance with earlier reports (Cipolletta et al., 2012, 2015) indicating local Treg expansion in visWAT in this age group (∼14 weeks of age), we found higher Treg ratios on the standard diet. In contrast to higher Treg percentages residing in BAT and scWAT, Treg percentages in visWAT were severely reduced by HFHS diet exposure (Figure 1N). An HFHS diet for 16 weeks left Foxp3+ Tregs in BAT unaltered and only mildly reduced them in scWAT of BALB/c mice, while percentages of Foxp3+ Tregs in visWAT were significantly reduced by high-caloric challenge (Figure 1O).

In accordance with the increase of BAT-residing Tregs after 2 weeks on the HFHS diet, the Treg induction potential of naive

CD4+ T cells was likewise significantly enhanced (Figures S1A and S1B).

Beta-Adrenergic Stimulation Increases Foxp3+ Treg Induction In Vivo

Given the results on cold exposure or a short-term high-calorie environment to enhance sympathetic tone and support BAT thermogenesis, we next directly increased sympathetic tone and assessed local Treg induction using ADRB3 agonists. Previous studies as well as in silico analyses (Heng et al., 2008) suggested Adrb3 expression, which encodes for the ADRB3 in human and murine lymphocytes (Yu et al., 2007).

ADRB3 stimulation to young BALB/c Foxp3 GFP reporter mice in vivo (2 days, 1 mg/kg intraperitoneally [i.p.]) with the beta3 receptor agonist CL-316243 (CL) enhanced Foxp3 abundance in CD4+ T cells from inLNs as well as from fat (Figures 2A–2D; negative staining controls in Figure S1C). Treg induction with naive CD4+ T cells was most prominently increased in T cells from BAT and scWAT compared with visWAT (Figure 2E).

Treg Induction Is Impaired in the Absence of Beta-Adrenergic Receptors In Vivo

To mechanistically dissect the link among beta3-adrenergic signaling, Treg induction, and AT function, we next analyzed betaless mice, which lack all three beta-adrenergic receptors (Bachman et al., 2002). This loss-of-function model had significantly decreased Treg percentages in inLNs and scWAT depots (Figures 2F–2H). Likewise, Treg induction using naive CD4+ T cells from fat depots of betaless mice was reduced when compared with wild-type (WT) animals (Figure 2I).

Treg Induction by Sympathetic Drive Is Required for Normal Adipose Tissue Function

To determine if and how Tregs interconnect an enhanced sympathetic tone with changes in AT function, we next performed loss-of-function experiments. Specifically, ADRB3 stimulation in vivo (CL for 3 days, 1 mg/kg, i.p.) induces genes relevant for BAT function (Figure S1D). In a first set of loss-of-function studies, Tregs were depleted in BALB/c Foxp3-GFP reporter mice prior to the start of ADRB3 stimulation by the use of established procedures involving anti-CD25 antibody application (Setiady et al., 2010) (Figures 3A and S1E). Treg-depleted mice (control stainings for Treg depletion efficacy in AT; Figure S1E) and control animals were injected with CL. In control mice without Treg depletion, canonical thermogenic gene programs (Ucp1, Ppargc1a, Prdm16, and Cidea) were induced in BAT following ADRB3 stimulation. In contrast, this induction by ADRB3 stimulation was blunted in mice with Treg depletion (Figure 3C). Accordingly, upon ADRB3 stimulation, we found surrogate markers of β-oxidation (Acox1 and Ascl1 gene expression) as well as lipolysis (Lpl, Lipe gene expression) to be upregulated in BAT, and again, this induction did not occur in mice with depleted Tregs (Figure 3C). Moreover, in contrast to control mice treated with ADRB3 stimuli in vivo, BAT tissue of Treg-depleted CL-treated mice had significantly increased Il6 gene expression (Figure 3C). Analyses of BAT tissue revealed a significant decline of Plin1, Cycs, P2rx5, Glut1, and Adipoq gene expression in Treg-depleted CL-treated mice (Figure S1F),
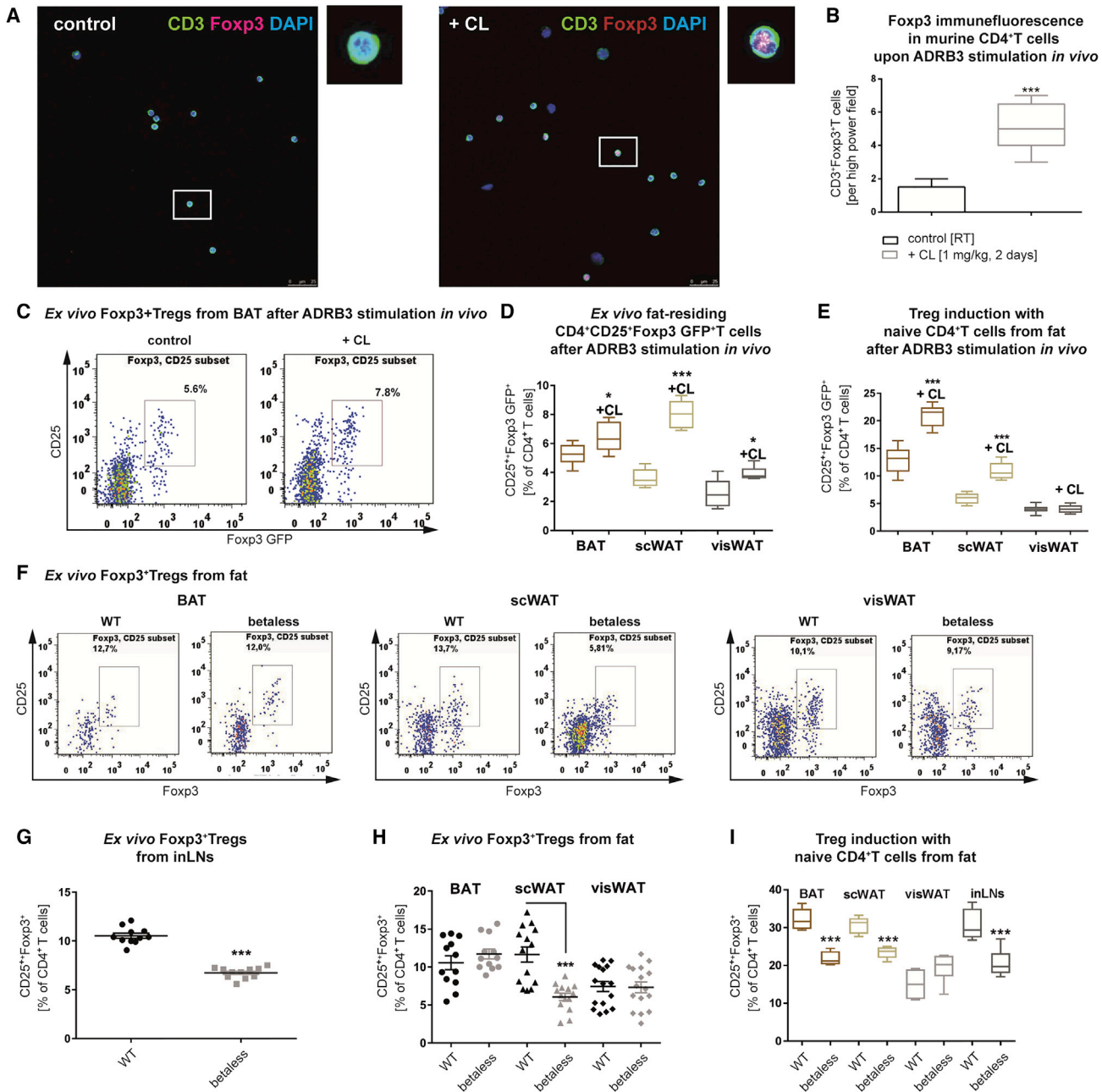
Figure 2. The Role of Beta-Adrenergic Signaling for Foxp3+ Tregs

(A) Representative confocal microscopy images of CD4+ T cells purified from BALB/c Foxp3GFP reporter mice after *in vivo* CL treatment (2 days, 1 mg/kg i.p.). Scale bar, 25 μm.

(B) Foxp3+CD3+ T cells per high power field in samples from (A). n = 5 per group, p = 0.0003.

(C) Representative FACS plots for the identification of *ex vivo* CD4+CD25+Foxp3GFP+ Tregs from BAT upon *in vivo* CL treatment (3 days, 1 mg/kg i.p.). Plots are pre-gated as shown in Figure 1A.

(D) Summary graph for *ex vivo* Treg frequencies purified from AT of young BALB/c mice as in (C). n = 6 per group.

(E) Summary graph for *in vitro* Treg induction assays with naive CD4+ T cells from ATs after *in vivo* treatment with CL (3 days, 1 mg/kg i.p.). n = 6 per group.

(F) Representative FACS plots for the identification of *ex vivo* CD4+CD25++Foxp3+ Tregs from fat depots of WT or betaless mice.

(G and H) Summary graph for *ex vivo* Treg frequencies purified from inLNs (G; n = 11) or fat depots (H; n > 12 per group) of WT or beta-less mice. n = 11 per group.

(I) Summary graph for *in vitro* Treg induction assays of naive CD4+ T cells purified from fat depots or inLNs of WT or betaless mice. n = 6 per group.

See also Figure S1. Data are presented as box-and-whisker plots with min and max values for data distribution or as mean ± SEM. *p < 0.05, ***p < 0.001.

A CD4+CD25++Foxp3+Tregs in inguinal lymph nodes
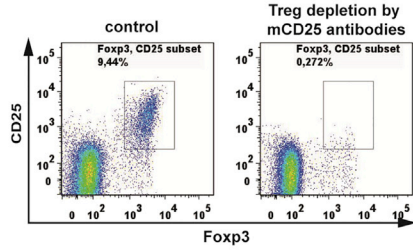
control | Treg depletion by mCD25 antibodies

B mRNA abundance of BAT after ADRB3 stimulation *in vivo*

☐ ADRB3 stimulation
☐ ADRB3 stimulation + Treg depletion

C CD4+CD25++Foxp3+Tregs in inguinal lymph nodes

control | Foxp3 DTR + diphtheria toxin
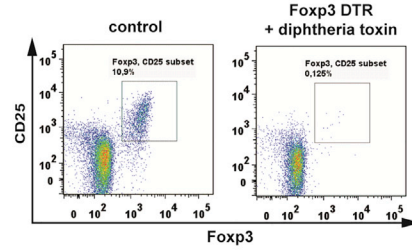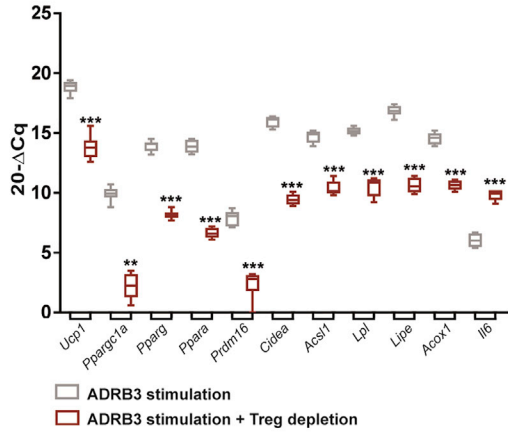
D mRNA abundance of BAT after cold exposure *in vivo*

☐ cold exposure [4°C, 24h]
☐ cold exposure [4°C, 24h] + Treg depletion
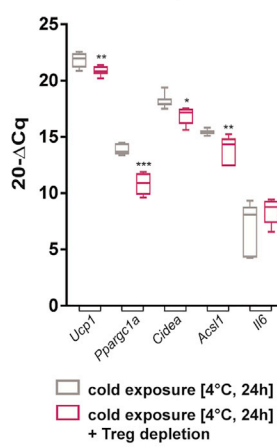
E mRNA abundance of scWAT after cold exposure *in vivo*

☐ cold exposure [4°C, 24h]
☐ cold exposure [4°C, 24h] + Treg depletion
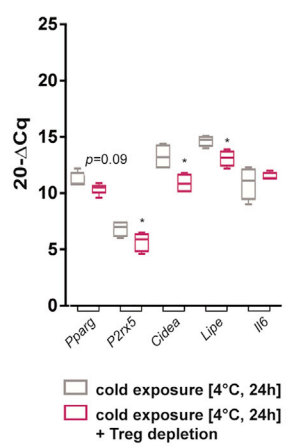
F mRNA abundance of visWAT after cold exposure *in vivo*

☐ cold exposure [4°C, 24h]
☐ cold exposure [4°C, 24h] + Treg depletion
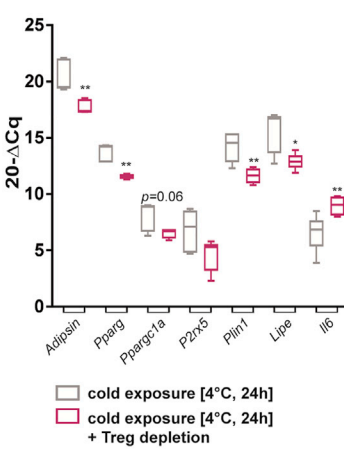
G mRNA abundance of BAT after Treg transfer *in vivo*

☐ control
☐ Treg transfer
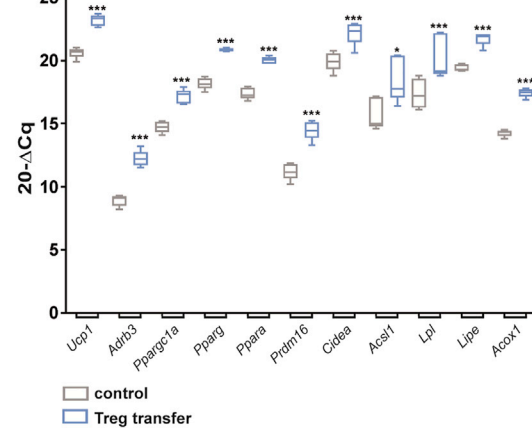
H *Ex vivo* Foxp3+Tregs from fat

I Treg induction with naive CD4+T cells from fat
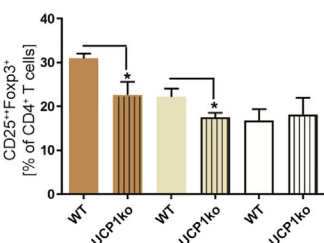
J *Ex vivo* proliferative status of CD4+T cells from fat
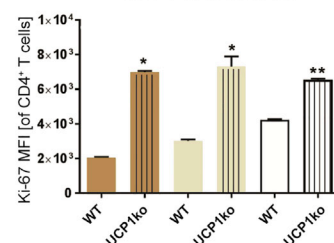
K Proliferative status of CD4+T cells during Treg induction with naive CD4+T cells from fat
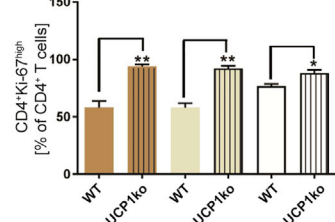
(legend on next page)

thereby revealing a role of Foxp3^{+} Tregs in regulating lipolysis and thermogenesis in BAT.

To further dissect the mutual crosstalk between Tregs and AT during diet-induced thermogenesis, Tregs were likewise depleted prior to exposure to a 1-week HFHS diet challenge. Such loss of function by anti-CD25 antibodies significantly reduced thermogenic BAT gene programs including *Ucp1*, *Ppargc1a*, *Pparg*, *Ppara*, and *Prdm16* (Figure S2A). In addition, β-oxidation- (*Ascl1*) as well as lipolysis-related genes (*Lipe*) were reduced in Treg-depleted mice. Furthermore, expression of *Cycs*, *P2rx5*, and *Adipsin* was also decreased in BAT of Treg-depleted mice (Figure S2A). The responses in scWAT were more heterogeneous; Treg depletion promoted a significant decline in *Pparg*, *Prdm16*, and *Acsl1* (Figure S2B).

In a second set of loss-of-function studies, we used C57BL/6 Foxp3-DTR mice (Kim et al., 2007) and diphtheria toxin (DT)-mediated Treg depletion to confirm the results seen in Treg-depleted animals using anti-CD25 antibodies. Accordingly, upon ADRB3 stimulation, Treg-depleted Foxp3-DTR mice (Figures 3C and 3D) exposed to cold (4°C for 24 hr) had a significant reduction in thermogenic gene expression, including *Ucp1*, *Ppargc1a*, and *Cidea* and in β-oxidation genes such as *Acsl1* in BAT, while *Il6* levels mildly increased (Figure 3D; control stainings for Treg depletion in fat; Figure S2C). Treg loss of function mildly reduced scWAT function as indicated by a decline in *Pparg*, *P2rx5*, *Cidea*, and *Lipe* expression (Figure 3E). Moreover, upon DT-mediated Treg depletion and cold exposure, we found expression levels of *Adipsin*, *Pparg*, *Ppargc1a*, *P2rx5*, *Plin1*, and *Lipe* to be decreased in visWAT, while *Il6* were significantly upregulated (Figure 3F).

Foxp3[+] Tregs Control Adipose Tissue Function

To directly assess the role of Foxp3^{+} Tregs in regulating AT function, we performed gain-of-function experiments by *in vivo* transfers of CD25^{+}Foxp3GFP^{+} Tregs into respective BALB/c recipient mice (intravenous or intraperitoneal transfer). Analyses of BAT function 1 week after transfer revealed a significant enhancement of thermogenic genes (*Ucp1*, *Adrb3*, *Ppargc1a*, *Prdm16*, and *Cidea*) in BAT (Figure 3G). Consistent with this, there were increased levels of mRNA of β-oxidation-related genes (*Acox1* and *Ascl1*) as well as of lipolysis-related genes (*Lpl* and *Lipe*) in BAT after the Treg transfer (Figure 3G). In addition, *Plin1*, *Cycs*, *P2rx5*, *Glut1*, and *Adipoq* were all enhanced in BAT after Treg

transfer (Figure S3A). Mild changes were also seen after Treg transfer in scWAT, with *Ppara*, *Prdm16*, *Cpt1b*, and *Glut1* being upregulated (Figure S3B). The Treg-mediated improvement of BAT function (thermogenic capacity and lipolytic function) upon Treg transfer (Figure 3G) was equal, or partially superior to, that which occurred with ADRB3 agonist treatment *in vivo*.

We next employed *in situ* expansion of Foxp3^{+} Treg cells using subcutaneous injections of interleukin (IL)-2/mAb complexes (3 days, 6 μg/day) as a second gain-of-function model. These complexes cause a selective expansion of Foxp3^{+} Tregs (Daniel et al., 2010; Webster et al., 2009). Following Foxp3^{+} Treg expansion, there was a significant enhancement of thermogenic genes (*Ucp1*, *Ppargc1a*, *Prdm16*, and *Cidea*) in scWAT, accompanied by increased levels of β-oxidation- (*Acox1* and *Acsl1*) and lipolysis-related genes (e.g., *Lipe* and *Plin1*; Figures S3C and S3D) and increased *P2rx5*, *Pparg*, *Ppara*, and *Adipsin* expression.

Gain of function by Treg expansion also had a mild impact on visWAT metabolic function. Specifically, genes related to differentiation (*Pparg*), adipogenesis (*Adipsin*), browning (*Cd137*), and lipolysis (*Acox1*, *Lipe*, *Lpl*, and *Plin1*) (Figure S3E) were all upregulated.

Treg Induction in BAT Is Impaired in the Absence of UCP1

To determine whether Treg-adipose crosstalk in BAT also includes a functional programming of BAT-residing T cells, we next investigated a BAT loss-of-function model. Specifically, the thermogenic activity of brown fat cells relies, to a great extent, on UCP1, which is localized on the inner membrane of BAT mitochondria. Upon activation, UCP1 catalyzes the leak of protons across the mitochondrial membrane (Fedorenko et al., 2012), uncoupling oxidative respiration from ATP synthesis, while the resulting energy derived from substrate oxidation is dissipated as heat.

Therefore, we used UCP1-ablated (UCP1ko) mice to dissect whether the fat thermogenic response causes Treg activation or whether Treg activity is required for thermogenic responses. The percentages of locally residing CD4^{+}CD25^{++}Foxp3^{+} Tregs purified from fat depots of young UCP1ko mice were reduced in BAT and scWAT, whereas marginal or no changes occurred in visWAT (Figures 3H and S4A). Likewise, Treg induction was lower in naive CD4^{+}CD25^{−} T cells purified from BAT and scWAT of UCP1ko mice when compared with WT T cells (Figures 3I

Figure 3. Foxp3^{+} Tregs Regulate Adipose Tissue Function and Vice Versa

(A and C) Representative FACS plots demonstrating Treg depletion efficacy in inLNs after (A) 3 days of mCD25 antibody treatment of WT mice or (C) 48 hr after diphtheria toxin administration to Foxp3 DTR mice.

(B) mRNA expression of genes involved in BAT function upon treatment with CL *in vivo* in the presence or absence of Tregs. Tregs were depleted using anti-CD25 antibodies. n = 6 per group.

(D–F) mRNA expression of genes involved in BAT (D), scWAT (E), and visWAT (F) function after cold exposure (4°C, 24 hr) in the presence or absence of Tregs. Tregs were depleted in Foxp3 DTR mice by administration of DT. n = 6 per group.

(G) In gain-of-function experiments, CD4^{+}CD25^{+}Foxp3GFP^{+} Tregs were adoptively transferred into congenic recipients. Analyses of BAT function by qPCR were performed 1 week after transfer. n = 6 per group.

(H) Summary graph for *ex vivo* Treg frequencies purified from BAT, scWAT, and visWAT of WT or UCP1ko animals. n = 5–6 for WT mice and n = 4–6 for UCP1ko animals.

(I) Summary graph for *in vitro* Treg induction assays of naive CD4^{+} T cells purified from fat depots of WT or UCP1ko animals. n = 5 per group.

(J) Summary graph for the *ex vivo* proliferative status of CD4^{+} T cells from fat depots of WT and UCP1ko mice as assessed by analysis of Ki67 mean fluorescence intensity (MFI). n = 5 per group.

(K) Shown is the proliferative status of CD4^{+} T cells during Treg induction assays from fat depots of WT and UCP1ko mice as assessed by analysis of Ki67^{high}.

See also Figures S1–S4. Data are presented as box-and-whisker plots with min and max values for data distribution. *p < 0.05, **p < 0.01, ***p < 0.001.
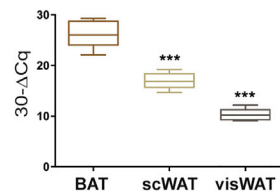
A RNA-Seq data of CD4⁺T cells from fat tissue
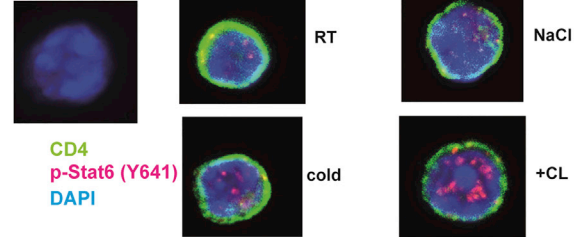
B control / + CL — CD4 Stat6 DAPI
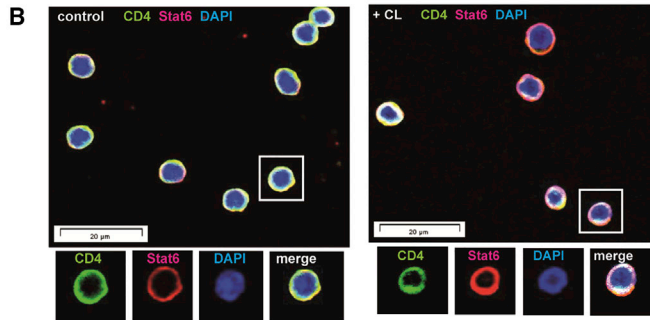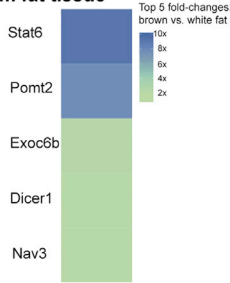
C *Stat6* mRNA abundance in CD4⁺T cells upon cold exposure *in vivo*
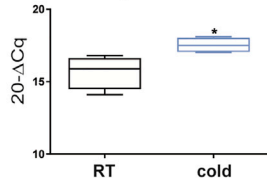
D *Stat6* mRNA abundance in CD4⁺T cells from fat
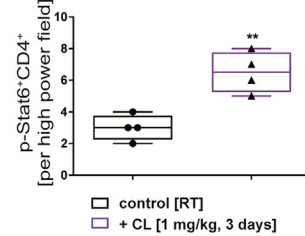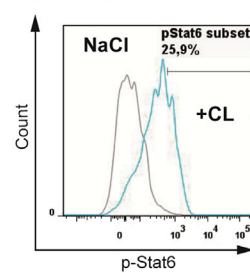
E neg.control — CD4 / p-Stat6 (Y641) / DAPI

F p-Stat6 (Y641) immunefluorescence in murine CD4⁺T cells upon upon cold exposure *in vivo*
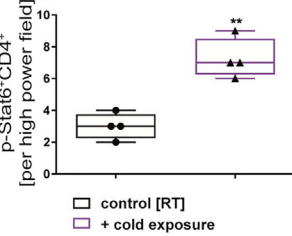
G p-Stat6 (Y641) immunefluorescence in murine CD4⁺T cells upon upon ADRB3 stimulation *in vivo*
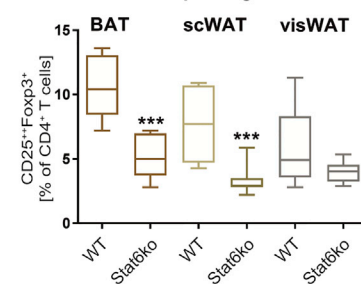
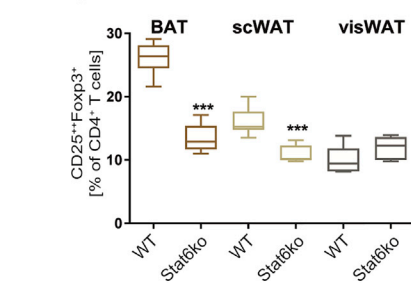**H** p-Stat6 (Y641) after ADRB3 stimulation *in vitro*
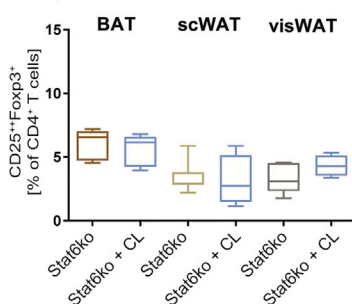
I *Ex vivo* Foxp3⁺Tregs from BAT
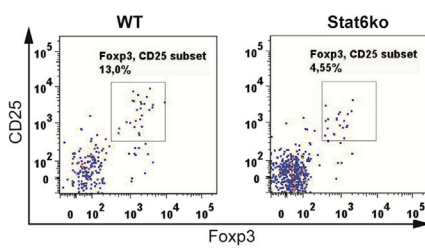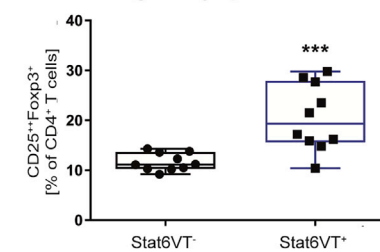
J *Ex vivo* Foxp3⁺Tregs from fat
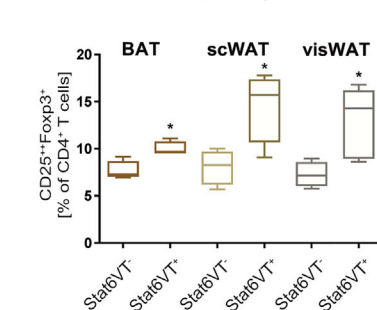
K Treg induction with naive CD4⁺T cells from fat

L *Ex vivo* Foxp3⁺Tregs from fat upon ADRB3 stimulation *in vivo*

M *Ex vivo* Foxp3⁺Tregs from inguinal lymph nodes

N *Ex vivo* Foxp3⁺Tregs from fat

(legend on next page)

and S4B). The reduced Treg percentages and their lower Treg induction potential were accompanied by a higher proliferative potential in local CD4$^+$CD25$^-$ T cells from UCP1ko mice when compared with littermate controls, both *ex vivo* and upon TCR stimulation *in vitro* (Figures 3J, 3K, and S4C). These data imply the existence of a mutual crosstalk between Treg cells and AT in that the local tissue environment affects T cell differentiation and function, which in turn can influence tissue function and organismal homeostasis.

CD4$^+$ T Cells from BAT Show Higher *Stat6* Abundance than WAT

We next aimed to identify molecular underpinnings of the functional interplay between Treg cells and AT that are linked with cold exposure and beta3-adrenergic stimulation in scWAT and BAT. When comparing the gene expression patterns of murine CD4$^+$ T cells from young BALB/c Foxp3-GFP reporter mice at room temperature (RT) in a pilot experiment, we observed higher levels of transcripts encoding the transcription factor *Stat6* in BAT compared to WAT (Figure 4A).

In vivo application of an ADRB3 agonist (2 days CL, 1 mg/kg i.p.) resulted in increased *Stat6* expression in CD4$^+$ T cells (Figure 4B; see quantification in Figure S5A). Moreover, *in vivo* cold exposure (1 week, 8°C) induced *Stat6* mRNA expression in CD4$^+$ T cells (Figure 4C). When *Stat6* expression levels in fat-residing CD4$^+$ T cells of BALB/c Foxp3-GFP reporter mice were verified, there was higher *Stat6* expression in CD4$^+$ T cells from BAT than in scWAT or visWAT (Figure 4D).

Short-term cold exposure (4°C, 24 hr) and ADRB3 stimulation (3 days CL, 1 mg/kg i.p.) likewise induced phosphorylation of Stat6 at position pY641 in CD4$^+$ T cells (Figures 4E–4G). Moreover, the percentage of cells that are p-Stat6 positive (and the MFI of the entire population) was increased in pre-activated CD4$^+$ T cells after ADRB3 stimulation for 15 min *in vitro* (100 nM CL; Figure 4H).

Stat6 has been implicated in promoting cold-induced remodeling of fat. For instance, cold-induced expression of *Ucp1* in scWAT was reported to be severely decreased in *Stat6*$^{-/-}$

(Stat6ko) mice (Qiu et al., 2014). From an immunological perspective, Stat6 promotes Th2 and Th9 immunity (Goenka and Kaplan, 2011). However, recent studies pointed to a positive role for Stat6 as a second required signal in antigen-specific Treg induction (Chapoval et al., 2010; Pillemer et al., 2009; Sanchez-Guajardo et al., 2007), while in Stat6VT transgenic mice, the constitutive activation of Stat6 in CD4$^+$ T cells increased the percentages of peripheral Tregs (Sanchez-Guajardo et al., 2007).

Treg Induction in Adipose Tissue Requires Stat6

Local Treg ratios (CD4$^+$CD25^{++}Foxp3$^+$ T cells [% of CD4$^+$ T cells] BAT, WT 10.5 ± 0.7 versus Stat6ko 5.2 ± 0.5, p < 0.001; scWAT, WT 7.7 ± 0.9 versus Stat6ko 3.2 ± 0.3, p = 0.0003; Figures 4I and 4J) and Treg induction of naive T cells purified from fat depots of BALB/c Stat6ko (Gessner et al., 2005; Kaplan et al., 1996) were significantly blunted in the absence of Stat6 (CD4$^+$CD25$^+$Foxp3$^+$ T cells [% of CD4$^+$ T cells] BAT, WT 26.1 ± 1.0 versus Stat6ko 13.4 ± 0.9, p < 0.001; scWAT, WT 16.0 ± 0.9 versus Stat6ko 10.8 ± 0.5, p < 0.001; Figure 4K). In a second approach, a pharmacological Stat6 inhibitor significantly reduced Treg induction using naive CD4$^+$ T cells from inguinal lymph nodes of BALB/c Foxp3-GFP reporter mice (Figure S5B). ADRB3 stimulation/blockade *in vitro* (Figures S5C and S5D) or *in vivo* (CL 1 mg/kg, i.p., 3 days; Figure 4L) did not affect Treg induction in the absence of Stat6.

Since T cell-specific Stat6ko mice are not available for loss-of-function studies, we used *in vivo* T cell transfer experiments to assess T cell-intrinsic effects of Stat6 relevant for Treg induction upon beta3-adrenergic stimulation. We purified naive CD4$^+$ T cells from WT and Stat6ko animals and transferred them into congenic CD90.1 BALB/c hosts to permit re-identification of transferred cells. In addition, mice were treated for 3 days with CL at 1 mg/kg, i.p., *in vivo*. Re-analysis of transferred cells revealed that in accordance with previous studies, Treg induction capacities *in vivo* in polyclonal TCR repertoires were low, although we found the percentages of induced Tregs to be significantly reduced in T cells transferred from Stat6ko mice

Figure 4. Stat6 Regulates Treg Accumulation in Adipose Tissue

(A) Depicted are the top five fold changes for upregulated genes in CD4$^+$ T cells purified from brown versus white fat by mRNA expression profiling. The cutoff for reading counts was set to 30 and pseudogenes have been manually removed.

(B) Representative confocal microscopy images of CD4$^+$ T cells purified from BALB/c control mice or BALB/c mice after *in vivo* treatment with CL (3 days, 1 mg/kg i.p.). Scale bar, 20 μm.

(C) qRT-PCR analyses of *Stat6* mRNA abundance in CD4$^+$ T cells purified from BALB/c mice upon cold exposure (1 week, 8°C). n = 4 mice per group from two independent experiments.

(D) *Stat6* mRNA expression in CD4$^+$ T cells purified from BAT, scWAT, or visWAT of young lean BALB/c mice. n = 5 mice per group.

(E) Representative confocal microscopy images for p-Stat6 induction in CD4$^+$ T cells from inLNs after CL treatment (3 days at 1 mg/kg i.p.) and *in vivo* cold exposure (24 hr, 4°C).

(F) Quantification of p-Stat6$^+$CD4$^+$ T cells per high power field in samples from (E) after cold exposure. n = 4 per group.

(G) Quantification of p-Stat6$^+$CD4$^+$ T cells per high power field in samples from (E) after CL treatment. n = 4 per group.

(H) Histogram of p-Stat6 detection in pre-activated CD4$^+$ T cells after 10 nM CL stimulation for 15 min *in vitro*.

(I) Representative FACS plots for the identification of *ex vivo* CD4$^+$CD25^{++}Foxp3$^+$ Tregs from BAT of WT or Stat6ko mice.

(J) Summary graph for *ex vivo* Treg frequencies purified from fat depots of WT mice or Stat6ko mice. n = 10 per group.

(K) Summary graph for *in vitro* Treg induction assays of naive CD4$^+$ T cells purified from fat depots of WT or Stat6ko mice. n = 6 per group.

(L) Summary graph for *in vitro* Treg induction assays of naive CD4$^+$ T cells purified from BAT, scWAT, and visWAT Stat6ko mice that were treated with vehicle or CL (3 days, 1 mg/kg) *in vivo*.

(M) Representative FACS blots for *ex vivo* Treg frequencies purified from inLNs of WT mice or mice with constitutively active Stat6 (Stat6VT mice). n = 10 per group.

(N) Summary graph for *ex vivo* CD4$^+$CD25^{++}Foxp3$^+$ Treg frequencies purified from fat depots of Stat6VT$^+$ or Stat6VT$^-$ mice. n = 4 per group.

See also Figure S5. Data are presented as box-and-whisker plots with min and max values for data distribution. *p < 0.05, **p < 0.01, ***p < 0.001.
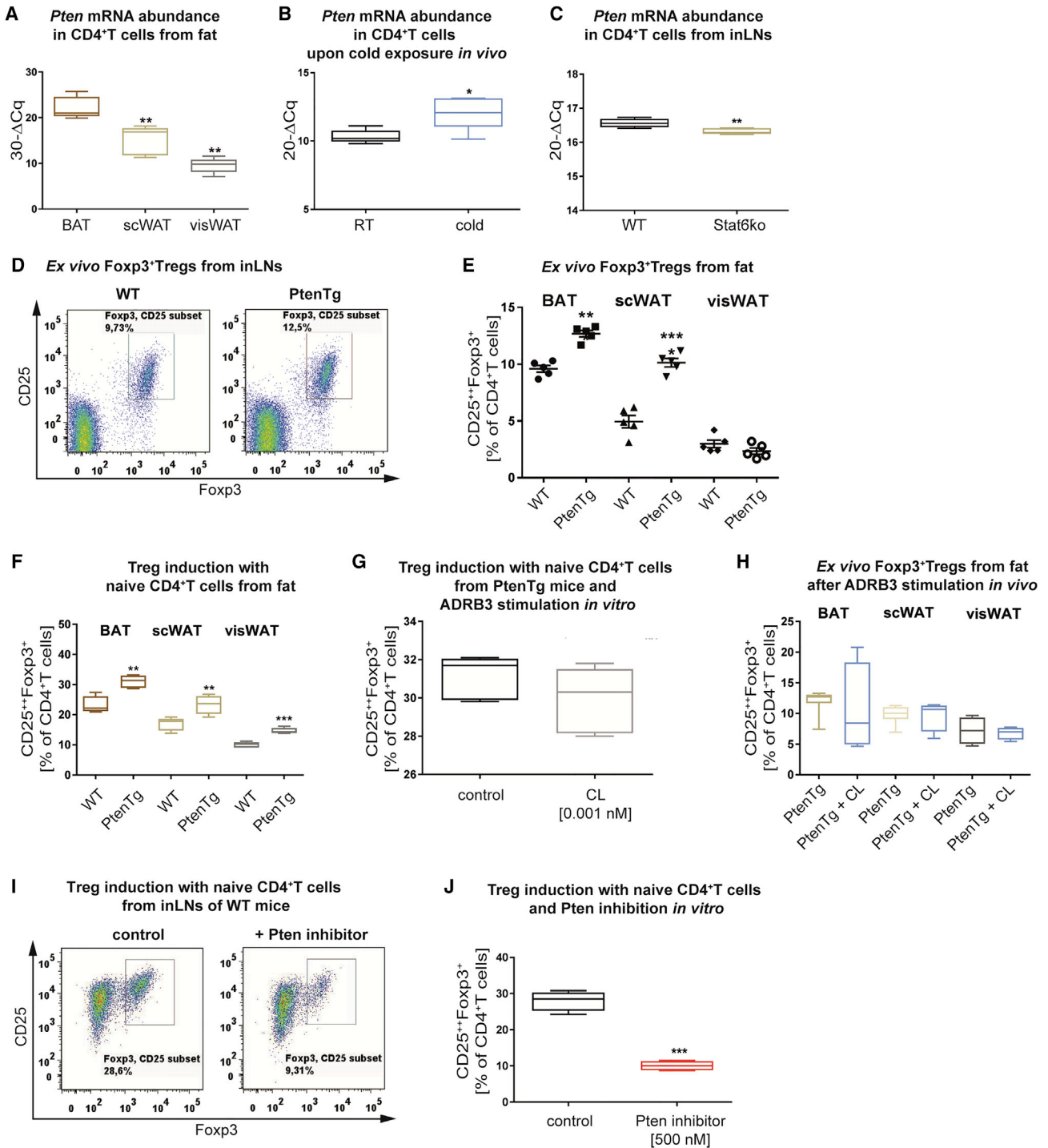
Figure 5. Role of Pten in Treg Accumulation of Fat-Residing CD4^{+} T Cells

(A–C) qRT-PCR analyses of *Pten* mRNA abundance in CD4^{+} T cells purified from (A) BAT, scWAT, or visWAT of young lean BALB/c animals (n = 5 per group), (B) inLNs after *in vivo* cold exposure of BALB/c animals (n = 5 per group), and (C) in CD4^{+} T cells purified from inLNs of Stat6ko animals (n = 4 per group).

(D) Representative FACS plots identifying *ex vivo* CD4^{+}CD25^{++}Foxp3^{+} Tregs from inLNs of WT or mice transgenetically overexpressing *Pten* (PtenTg animals).

(E) Summary graph for the identification of *ex vivo* CD4^{+}CD25^{++}Foxp3^{+} Tregs purified from BAT, scWAT, or visWAT of WT or PtenTg mice. n = 5 per group.

(F) Summary graph for *in vitro* Treg induction assays using limited TCR stimulation of naive CD4^{+} T cells purified from fat depots of WT or PtenTg animals. n = 6 per group.

(G) Summary graph for *in vitro* Treg induction assays using limited TCR stimulation of naive CD4^{+} T cells of PtenTg animals in the presence or absence of ADRB3 stimulation (0.001 nM CL). n = 5 per group.

(legend continued on next page)

(CD4⁺CD25⁺⁺Foxp3⁺ T cells [% of CD4⁺ T cells]: WT 3.8 ± 0.9 versus Stat6ko 1.5 ± 0.3, p = 0.0200; Figure S5E).

Treg-Adipose Crosstalk Induced by ADRB3 Stimulation Requires Stat6 *In Vivo*

To determine whether the impaired Treg induction in fat depots of Stat6ko mice is associated with altered AT function, we examined AT function of Stat6ko mice upon ADRB3 stimulation *in vivo*. In contrast to WT mice (Figure S5F), ADRB3 stimulation of Stat6ko mice *in vivo* did not increase genes important for BAT function (no upregulation was seen for *Ucp1*, *Ppargc1a*, *Cidea*, *Ascl1*, *Plin1*, *Lipe*, or *P2rx5*), while ADRB3 stimulation in the absence of Stat6 significantly reduced *Pparg* abundance (p = 0.0117) and *Adipsin* (p = 0.0388) (Figure S5F). Genes related to thermogenesis, lipolysis, and adipose differentiation were likewise unaffected by ADRB3 stimulation in scWAT from Stat6ko animals, while ADRB3 stimulation significantly reduced *Ucp1*, *Pparg*, *Lipe*, *Adipsin*, and *P2rx5* in visWAT of Stat6ko mice (Figures S5G and S5H).

Treg Induction Is Enhanced by a Constitutively Active Stat6

To address the relevance of Stat6 in mediating a functional interplay of Tregs and AT in gain-of-function experiments, we used mice with a constitutively active Stat6 expression in lymphoid cells (Bruns et al., 2003; Sehra et al., 2008) (Stat6VT⁺ versus Stat6VT^{−} littermates). We identified increased Foxp3⁺ Treg frequencies in inLNs (CD4⁺CD25⁺⁺Foxp3⁺ T cells [% of CD4⁺ T cells]: Stat6VT^{−} 11.7 ± 0.5 versus Stat6VT⁺ 20.6 ± 2.1, p = 0.0007; Figure 4M). *Ex vivo* Treg frequencies from AT of Stat6VT⁺ mice had higher variability but were increased when compared with Stat6VT^{−} littermates (Figure 4N). In the steady state, without ADRB3 stimulation or cold exposure, Stat6VT⁺ mice had increased *Pparg*, *Adipsin*, and *P2rx5* abundance in fat (Figures S5I–S5K).

Treg Induction in BAT Is Driven by Pten Signaling

Phosphatase and tensin homolog (Pten) has been implicated in positively regulating BAT tissue function; e.g., by promoting *Ucp1* expression (Ortega-Molina et al., 2012). We therefore studied Pten as a second potential signaling intermediate linking the interplay between Tregs and AT function given the impaired Treg induction in UCP1ko animals. Animals with overexpression of *Pten* presented with a hyperactive BAT and harbored increased *Ucp1* levels in BAT (Ortega-Molina et al., 2012). Pten also regulates Treg induction (Sauer et al., 2008; Shrestha et al., 2015). We observed increased *Pten* expression in CD4⁺ T cells from BAT and scWAT of BALB/c mice (Figure 5A). In accordance with the results for *Stat6* expression, *in vivo* cold exposure significantly increased *Pten* expression in CD4⁺ T cells (Figure 5B). In CD4⁺ T cells from inLNs of Stat6ko mice, *Pten* expression levels

were mildly diminished when compared with WT animals (Figure 5C). For a gain-of-function approach, we used *Pten*-overexpressing mice (PtenTg) and found them to have significantly increased Foxp3⁺ Treg percentages in inLNs, BAT, and scWAT when compared with WT animals (CD4⁺CD25⁺⁺Foxp3⁺ T cells [% of CD4⁺ T cells] BAT, WT 9.6 ± 0.2 versus PtenTg 12.7 ± 0.2, p < 0.001; scWAT, WT 4.9 ± 0.5 versus PtenTg 10.1 ± 0.3, p < 0.001; Figures 5D and 5E). In addition, Treg induction was significantly enhanced in naive CD4⁺ T cells of PtenTg animals (Figure 5F). Levels of *Pten* overexpression varied in CD4⁺ T cells from PtenTg animals (∼4- to ∼40-fold). Mice with higher levels of *Pten* overexpression (∼40-fold over WT) harbored significantly more Foxp3⁺ Tregs in all ATs, including visWAT (Figure S5L). No further increase in Treg induction was observed *in vitro* upon ADRB3 stimulation using naive CD4⁺ T cells from PtenTg animals (Figure 5G). In addition, ADRB3 stimulation *in vivo* did not alter Treg percentages in AT of PtenTg mice (Figure 5H). A Pten inhibitor significantly reduced Treg induction *in vitro* using naive CD4⁺ T cells from WT mice (Figures 5I and 5J).

Cold Exposure or ADRB3 Stimulation Induces a Treg-Inducing Proteome Signature

For an unbiased approach, we performed quantitative mass spectrometry-based proteomics (Meissner and Mann, 2014) to evaluate proteome compositions in CD4⁺ T cells upon *in vivo* cold acclimation of mice (1 week, 8°C) or treatment with an ADRB3 agonist (3 days CL, 1 mg/kg, i.p.). We identified 5,031 proteins in sorted CD4⁺ T cell proteomes of mice that were either exposed to cold or treated with CL *in vivo*, compared with control animals housed at room temperature (RT) or treated with NaCl, respectively. To verify Treg induction upon cold exposure or ADRB3 stimulation *in vivo* at the protein level, we focused on proteins associated with selected Gene Ontology terms Biological Function (GOBP) related to negative regulation of immune responses/effector responses, as well as Treg induction and Foxp3 regulatory networks. Unsupervised hierarchical clustering conditions revealed upregulation of several GO terms related to Treg induction, among them Stat6 and Foxp3 (Figures 6A and 6B). Similarly, several proteins of the Foxp3 regulatory network were found to be mildly upregulated upon cold exposure or ADRB3 stimulation (Figures 6C and 6D).

Next, to integrate the relevance of Stat6 for linking ADRB3 stimulation with Treg induction in an unbiased setting, we examined proteome compositions in CD4⁺ T cells from Stat6ko mice with or without ADRB3 stimulation *in vivo*. We identified 2,827 proteins in sorted CD4⁺ T cell proteomes of Stat6ko mice that were treated with CL *in vivo*, compared with control mice given NaCl, respectively. Unsupervised hierarchical clustering revealed that in the absence of Stat6 upon ADRB3 stimulation *in vivo*, several GO terms related to Treg induction were downregulated, among them Foxp3 (Figure 6G). Overall, these data

(H) *Ex vivo* Treg frequencies purified from fat depots of PtenTg mice upon *in vivo* ADRB3 stimulation (3 days, 1 mg/kg CL). n = 8 for PtenTg control group and n = 4 for PtenTg + CL group.

(I) Representative FACS plots for *in vitro* Treg induction assays with or without Pten inhibitor (500 nM) using naive CD4⁺ T cells purified from inLNs of WT mice.

(J) Summary graph of Pten inhibition for *in vitro* Treg induction assays of naive CD4⁺ T cells purified from inLNs of WT animals. n = 4 per group from two independent experiments.

See also Figure S5. Data are presented as box-and-whisker plots with min and max values for data distribution or as mean ± SEM. *p < 0.05, **p < 0.01, ***p < 0.001.
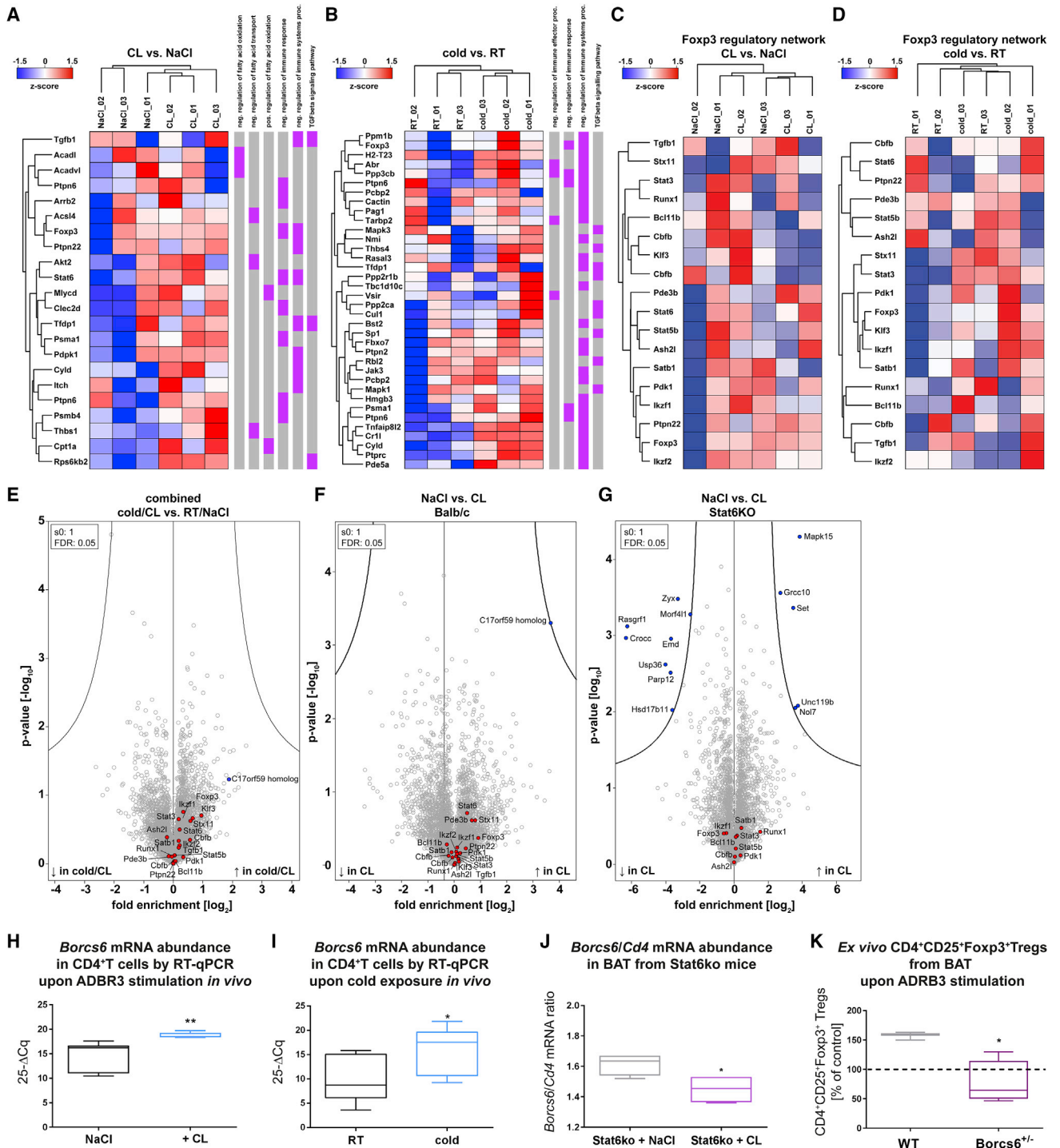
Figure 6. Cold Exposure or ADRB3 Stimulation Induces a Treg-Proneproteome Signature

(A and B) Proteins associated with selected Gene Ontology terms Biological Function (GOBP) were grouped using unsupervised hierarchical clustering of the *Z* scored MaxLFQ-intensities across the indicated experimental groups; CL versus NaCl (A) and cold versus RT (B). GOBP annotations are depicted in purple.

(C and D) Proteins associated with the Foxp3 regulatory network were grouped as in (A) and (B) with groups: CL versus NaCl (C) and cold versus RT (D).

(E–G) Combined volcano plot of the pairwise comparison between CD4^{+} T cell proteomes purified from cold/CL- versus RT/NaCl-treated mice (E), NaCl- versus CL-treated mice (F) and NaCl- versus CL-treated Stat6ko mice (G). Expression fold changes (t test difference, log$_2$) were calculated and plotted against the t test p value (–log$_{10}$). Proteins associated with Foxp3 regulatory networks (red) and the C17orf59 homolog (blue) are highlighted. Their position on the right side of the plot indicates a higher abundance upon cold/CL (E) or CL treatment (F and G).

(legend continued on next page)

highlight that in Stat6-competent animals, either cold exposure or ADRB3 stimulation *in vivo* supports a tolerogenic proteome signature in CD4^{+} T cells in accordance with identified increased Treg percentages and the induction of Foxp3 regulatory networks (Figures 6A–6D).

Importantly, CD4^{+} T cells purified from mice subjected to cold exposure or else treated with CL *in vivo* had upregulated proteins involved in enhancing fatty acid oxidation (FAO), including Acsl4 and Cpt1a, as well as downregulation of proteins involved in negatively regulating FAO, including Acadvl and Acadl (Figures 6A, 6B, and 6E), thereby further supporting Treg induction and function (Chang and Pearce, 2016; MacIver et al., 2013).

Treg Induction in Adipose Tissue by Cold Exposure or ADRB3 Stimulation Involves C17orf59/Borcs6

Next, we combined both the cold/RT and the CL/NaCl datasets and performed pairwise comparison of the CD4^{+} T cells. Besides the mild upregulation of the Foxp3 regulatory network, we identified C17orf59 as one of the most prominently upregulated proteins in CD4^{+} T cells (Figure 6E for combined datasets; Figure 6F for CL treatment only). C17orf59 was reported to function as a Ragulator-interacting protein that inhibits mTORC1 activity through its interaction with Ragulator at the lysosome (Schweitzer et al., 2015). In accordance with previous studies (Daniel and von Boehmer, 2011; Sauer et al., 2008), inhibition of mTORC1 can directly enhance Foxp3^{+} Treg induction (Daniel et al., 2010). C17orf59 was recently assigned a gene name, *BLOC-1-related complex subunit 6 (Borcs6)*. *Borcs6* mRNA levels were significantly increased in CD4^{+} T cells from mice stimulated with ADRB3 (Figure 6F), and *Borcs6* mRNA levels were enhanced following ADRB3 stimulation and cold exposure *in vivo* (Figures 6H and 6I). We next aimed to link the increased *Borcs6* mRNA expression caused by ADRB3 stimulation with the observed mechanistic role of Stat6 for adjusting Treg induction and BAT function. In the absence of Stat6 ADRB3 stimulation, BAT of Stat6ko mice in fact had lowered *Borcs6/Cd4* mRNA ratios (Figure 6J).

In *Borcs6*^{+/−} mice, the induction of Foxp3^{+} Tregs in BAT following ADRB3 stimulation was significantly reduced when compared with WT mice (Figure 6K).

To validate the results by mass spectrometry, we first used immunofluorescence for C17orf59 in CD4^{+} T cells together with confocal microscopy. C17orf59 protein expression was upregulated following cold exposure or ADRB3 stimulation *in vivo* (Figures 7A–7D). We also employed stimulated emission depletion (STED) microscopy for creating super-resolution images to analyze C17orf59 expression changes in cytoplasm of CD4^{+} T cells purified from inguinal lymph nodes of mice upon cold exposure in further detail (Figure 7E). C17orf59 expression was enhanced in CD4^{+} T cells from mice exposed to cold (24 hr, 4°C) when compared with animals at RT (Figure 7E). In line with the increased protein abundance of C17orf59 upon ADRB3 stimulation or cold exposure *in vivo*, we determined

the intracellular localization of mTOR in CD4^{+} T cells (Figures 7F–7H). While mTOR localizes more prominently to lysosomes in control CD4^{+} T cells, it remained more diffuse in T cells from mice that had received ADRB3 stimulation *in vivo* or were exposed to cold (Figures 7F–7H). Both ADRB3 stimulation and cold exposure resulted in significantly reduced numbers of mTOR^{+}Lamp2^{+}CD4^{+} T cells (Figures 7I and 7J). Finally, to integrate the findings on the role of Stat6 for Treg induction and AT function, we provide the first evidence that in the absence of Stat6, C17orf59 expression was reduced in the steady state when compared with WT mice (Figures 7K–7M). Consistent with this observation, CD4^{+} T cells from Stat6VT^{+} animals, which harbor a constitutively active Stat6 in CD4^{+} T cells, had increased C17orf59 expression when compared with CD4^{+} T cells from Stat6VT^{−} littermates (Figures 7N and 7O).

DISCUSSION

Here, we report the discovery of an important role of Tregs in maintaining AT function in response to environmental or systemic challenges. Specifically, we demonstrate that cold exposure, physiological levels of beta-adrenergic stimulation, or short-term exposure to a high-caloric challenge each enhances Foxp3^{+} Tregs and their induction in BAT.

To determine whether the observed Treg-adipose crosstalk in BAT includes a functional programming of BAT-residing T cells, we utilized UCP1ko mice as a BAT loss-of-function model and found that local Treg induction was reduced. Specifically, these findings document that the local AT environment can co-opt local T cell differentiation programs and thereby influence tissue function and organismal homeostasis.

We used loss- and gain-of-function studies, including Treg depletion, transfer, and *in vivo* expansion, to demonstrate an important role of Foxp3^{+} Tregs for AT function including efficient thermogenesis and lipolysis. Further, the Treg-expansion data implicate a critical function of Foxp3^{+} Tregs in beiging/browning of white fat.
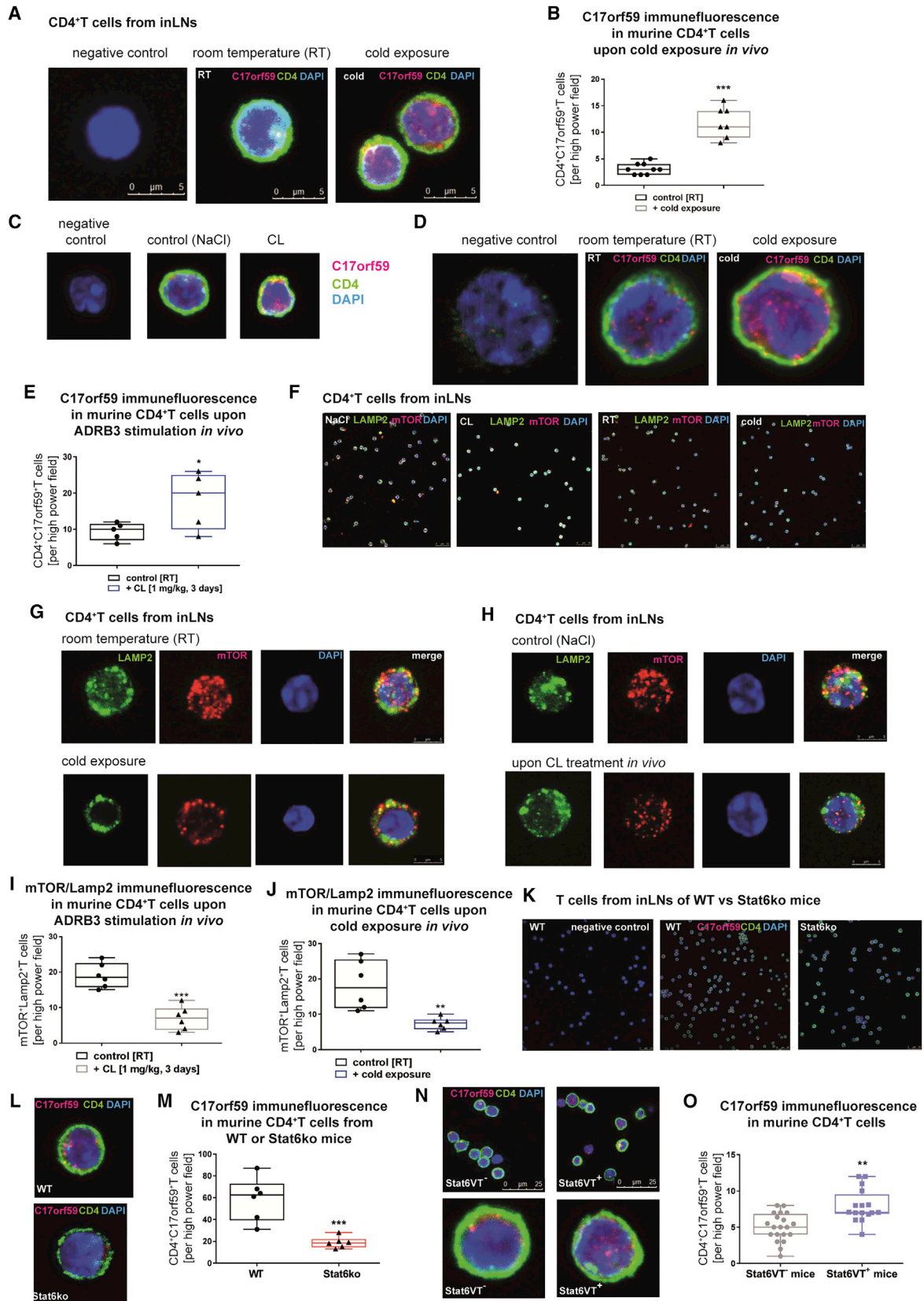
We further found that a T cell-specific Stat6/Pten axis is a key mechanistic link between environmental challenges, induction of Foxp3^{+} Treg cells, and AT function. The involvement of Stat6 in Foxp3^{+} Treg induction has been linked with the IL-2-Stat5 signaling pathway. IL-2R signals can induce IL-4 production through Stat5 (Zhu et al., 2003) or c-Maf activation (Hwang et al., 2002). The IL-4/Stat6/c-Maf/CD25 and IL-2/CD25/c-Maf/IL-4 pathways may converge to act on CD4^{+}CD25^{++}Foxp3^{+} Tregs (Sanchez-Guajardo et al., 2007). One possibility to explain the increase in peripheral Foxp3^{+} Tregs in mice with constitutively active Stat6 in T cells (Stat6VT^{+} mice) might be improved Treg cell survival by using common downstream elements of the IL-2 pathways (Sanchez-Guajardo et al., 2007). In addition, IL-4, which promotes Stat6 activation (Quelle et al., 1995), can prevent apoptosis of CD25^{++}Foxp3^{+} Tregs (Maerten et al., 2005). It has been hypothesized that in the periphery, Stat6

(H and I) qRT-PCR analyses of *Borcs6* mRNA abundance in CD4^{+} T cells purified from mice after (H) *in vivo* ADRB3 stimulation or (I) cold exposure. n = 5 mice per group.
(J) Ratios of *Borcs6/Cd4* mRNA abundance in BAT from Stat6ko mice upon NaCl versus CL treatment. n = 4 per group.
(K) *Ex vivo* Treg frequencies purified from BAT of young WT or *Borcs6*^{+/−} mice upon stimulation with CL (2 days, 1 mg/kg i.p.). n = 3–4 per group.
Data are presented as box-and-whisker plots with min and max values for data distribution. *p < 0.05, **p < 0.01.

A CD4⁺T cells from inLNs

negative control | room temperature (RT) | cold exposure

B C17orf59 immunefluorescence in murine CD4⁺T cells upon cold exposure *in vivo*

C negative control | control (NaCl) | CL

C17orf59 CD4 DAPI

D negative control | room temperature (RT) | cold exposure

E C17orf59 immunefluorescence in murine CD4⁺T cells upon ADRB3 stimulation *in vivo*

F CD4⁺T cells from inLNs

G CD4⁺T cells from inLNs
room temperature (RT)
LAMP2 | mTOR | DAPI | merge
cold exposure

H CD4⁺T cells from inLNs
control (NaCl)
LAMP2 | mTOR | DAPI | merge
upon CL treatment *in vivo*

I mTOR/Lamp2 immunefluorescence in murine CD4⁺T cells upon ADRB3 stimulation *in vivo*

J mTOR/Lamp2 immunefluorescence in murine CD4⁺T cells upon cold exposure *in vivo*

K T cells from inLNs of WT vs Stat6ko mice

L WT / Stat6ko

M C17orf59 immunefluorescence in murine CD4⁺T cells from WT or Stat6ko mice

N Stat6VT⁻ / Stat6VT⁺ / Stat6VT⁻ / Stat6VT⁺

O C17orf59 immunefluorescence in murine CD4⁺T cells

(legend on next page)

does not replace IL-2 signals but rather acts in synergy to enhance Treg survival (Sanchez-Guajardo et al., 2007).

We found that cold exposure or beta3-adrenergic stimulation induces Stat6 phosphorylation in CD4^{+} T cells, thereby further integrating these environmental stimuli with induction of Stat6 signaling and Foxp3^{+} Treg induction. Treg abundance and induction, especially in BAT and scWAT, were impaired in the absence of Stat6. These results further integrate with *in vivo* T cell transfer experiments using Stat6-deficient T cells with or without beta3 adrenergic stimulation. These data indicate that Treg induction is impaired intrinsically in the absence of Stat6 and that beta3-adrenergic stimulation does not favor Treg induction in T cells deficient for Stat6.

The role of Stat6 in Treg induction upon cold exposure or beta3-adrenergic stimulation was confirmed in an unbiased T cell proteomics setting. Specifically, in the absence of Stat6 upon ADRB3 stimulation *in vivo*, we observed a downregulation of tolerogenic protein signatures including Foxp3. These immunological data on the reduction of Treg induction in Stat6-deficient animals integrate with metabolic analyses of fat depots from Stat6ko mice. In contrast to what occurs in WT mice upon ADRB3 stimulation *in vivo*, Stat6ko mice have a reduced expression of markers relevant for adipogenesis such as *Adipsin*, and for adipocyte differentiation such as *Pparg* and *P2rx5*. Together with the results from Treg gain- and loss-of-function studies, these findings support a role of Foxp3^{+} Tregs in affecting AT function.

As one possible means to further interlink Stat6-relevant signaling intermediates, Pten-overexpressing mice had decreased phosphorylated Akt as well as phosphorylated Foxo1 levels together with a significant enhancement of UCP1 expression in BAT (Ortega-Molina et al., 2012). Molecular analyses, including PI3K inhibitors, underscored that the effects of Pten on BAT are mediated by the PI3K/Akt/Foxo signaling pathway that results in the activation of UCP1 and its transcriptional regulator, Ppargc1a (Ortega-Molina et al., 2012).

Our findings linking BAT function with Treg induction are consistent with reports that inhibition of the PI3K/Akt pathway enhances Foxp3^{+} Treg induction (Daniel and von Boehmer,

2011; Sauer et al., 2008). Regulation of Foxo transcriptional activity is mainly dependent on the phosphorylation of Foxo proteins via the PI3K/Akt pathway. Furthermore, using our unbiased proteomic approach, we identified a series of proteins involved in negative regulation of immune responses as well as Treg induction, frequency, and function. Accordingly, we observed regulation of networks that have an impact on Foxp3 itself as well as its interacting partners. Previous analyses indicated that Foxp3 forms large transcriptional complexes comprising several hundred partners (Rudra et al., 2012). Moreover, upon cold exposure or ADRB3 stimulation, we observed upregulation of Foxp3-associated factors implicated in transcription regulation including Bc11b, CBFβ, and Runx1. Besides being controlled by Foxp3, some of these Foxp3-bound transcription factors also regulate Foxp3 gene expression by binding to its promoter and intronic enhancers (Rudra et al., 2012).

Consistent with these observations, we found C17orf59 to be one of the more prominently enhanced proteins identified in CD4^{+} T cell proteomes of mice subjected to cold or ADRB3 stimulation. C17orf59 was recently demonstrated to function as a Ragulator-interacting protein that regulates mTORC1 activity through its interaction with Ragulator at the lysosome (Schweitzer et al., 2015). Overexpression of C17orf59 disrupts the Rag-Ragulator complex, prevents Rag lysosomal localization, and thereby inhibits mTORC1 activity (Schweitzer et al., 2015). Inhibition of mTORC1 activity, as demonstrated by established drugs such as rapamycin or everolimus, directly induces Foxp3^{+} Tregs (Daniel et al., 2010; Sauer et al., 2008; von Boehmer and Daniel, 2013). The increased C17orf59 protein abundance in CD4^{+} T cells of mice subjected to cold or ADRB3 stimulation supports a concept in which physiological levels of ADRB3 stimulation can exert mTORC1-inhibiting activity, thereby directly contributing to the induction of Foxp3^{+} Tregs. To integrate the findings on the role of Stat6 for T cell tolerance induction, C17orf59 protein expression in CD4^{+} T cells from Stat6ko animals was not identified under steady-state conditions or following beta3-adrenergic stimulation.

In sum, we demonstrate that local Foxp3^{+} Treg induction in AT in response to environmental stimuli such as cold or a

Figure 7. Treg Accumulation in Adipose Tissue by Cold Exposure or ADRB3 Stimulation Involves C17orf59/Borcs6

(A) Representative confocal microscopy images for C17orf59 expression of CD4^{+} T cells purified from inLNs of mice exposed to cold *in vivo* (24 hr, 4°C). Scale bar, 5 μm.

(B) C17orf59^{+}CD4^{+} T cells per high power field in samples from CD4^{+} T cells from (A). n = 9 for control group at room temperature and n = 6 for group at 4°C.

(C) Representative high-magnification confocal images for C17orf59 expression of CD4^{+} T cells purified from inLNs of mice subjected to ADRB3 stimulation (3 days, 1 mg/kg CL).

(D) C17orf59^{+}CD4^{+} T cells per high power field in samples from (C). n = 5 per group.

(E) Stimulated emission depletion microscopy of cytoplasmic C17orf59 expression in CD4^{+} T cells purified from inLNs of mice upon cold exposure.

(F) Representative confocal microscopy images for Lamp2 and mTOR expression in CD4^{+} T cells purified from inLNs of mice subjected to ADRB3 stimulation or cold exposure *in vivo*. Scale bar, 25 μm.

(G and H) Single-cell magnifications and depiction of single stainings of samples from (F) after cold exposure (G) or ADRB3 stimulation (H). Scale bar, 5 μm.

(I) mTOR^{+}Lamp2^{+} T cells per high power field in samples from CD4^{+} T cells purified from inLNs of mice subjected to CL (3 days, 1 mg/kg CL). n = 6 per group.

(J) mTOR^{+}Lamp2^{+} T cells per high power field from CD4^{+} T cells purified from inLNs of mice subjected to cold exposure (24 hr, 4°C) *in vivo*. n = 6 per group.

(K) Left: negative staining control of C17orf59. Shown are stainings with secondary antibody in the absence of primary antibodies using CD4^{+} T cells from WT mice. Middle and right: representative confocal microscopy overview images for C17orf59 expression in CD4^{+} T cells purified from inLNs of WT or BALB/c Stat6ko mice. Scale bar, 25 μm.

(L) Representative confocal microscopy images for C17orf59 expression in CD4^{+} T cells purified from inLNs of WT or BALB/c Stat6ko mice.

(M) Quantification of C17orf59 immunofluorescence of murine CD4^{+} T cells from WT or Stat6ko mice.

(N and O) Representative confocal microscopy images for C17orf59 abundance in CD4^{+} T cells from Stat6VT^{−} versus Stat6VT^{+} mice (N) and the corresponding quantification (O). Scale bar, 25 μm.

Data are presented as box-and-whisker plots with min and max values for data distribution. *p < 0.05, **p < 0.01, ***p < 0.001.

high-caloric challenge, or direct beta3-adrenergic stimulation, involves Stat6/Pten signaling. These findings are consistent with recently emerging hypotheses that local metabolic changes can link gene regulation, signaling, differentiation, and function in order to drive tissue-specific T cell differentiation and fate (Panduro et al., 2016). These novel insights into the molecular underpinnings of tissue-specific Treg induction uncover their role in linking environmental influences with adipose function and metabolic diseases. Our discoveries suggest the potential for tailored anti-inflammatory interventions aimed toward restoring AT homeostasis.

STAR★METHODS

Detailed methods are provided in the online version of this paper and include the following:

- KEY RESOURCES TABLE
- CONTACT FOR REAGENT AND RESOURCE SHARING
- EXPERIMENTAL MODEL AND SUBJECT DETAILS
  - Mice
  - *In Vitro* Studies with Primary Murine T Cells
- METHOD DETAILS
  - Isolation of CD4$^+$T Cells from Lymphoid Organs
  - Isolation of CD4$^+$T Cells from Adipose Tissues
  - Cell Staining for Flow Cytometry
  - *In vitro* Treg-Induction Assay
  - Chemicals and Enzymes Used for Experiments
  - Quantitative Analysis of mRNA Abundance
  - Proteomics
  - Immunefluorescence by Confocal Microscopy
  - Immunofluorescence by STED Microscopy
- QUANTIFICATION AND STATISTICAL ANALYSIS
- DATA AND SOFTWARE AVAILABILITY
  - Data Resources

SUPPLEMENTAL INFORMATION

Supplemental Information includes five figures and one table and can be found with this article online at http://dx.doi.org/10.1016/j.cmet.2017.08.008.

AUTHOR CONTRIBUTIONS

S. Kälin and M. Becker performed experiments, analyzed data, and wrote the manuscript. V.B.O. performed analyses of AT function. I.S. performed *in vivo* experiments. L.F.R.N. performed *in vitro* experiments. M.M.H.M. and V.K.F. performed *in vitro* experiments. M.G.S. performed Treg induction analyses. S. Keipert supported BAT analyses. D.L. supported T cell analyses. F.R.-J. provided beta-less mice and supported analyses of animals. K.G. and V.P. analyzed T cells. M.H.K. and P.K. provided Stat6VT mice and supported analyses of mice. M.J. supported analyses of BAT tissues. F.H. performed proteomic profiling of CD4$^+$ T cells. M.S. provided PtenTg mice and supported analyses of animals. M. Blüher supported analyses of AT function. S.D. supported experiments with Foxp3 DTR mice. T.B. provided Foxp3 DTR mice. C.W. performed experiments with *in vivo* cold exposure. P.T. and R.P. performed STED microscopy and related analyses. B.W. performed gain- and loss-of-function experiments for Treg analyses, immunofluorescence, and confocal microscopy. S.C.W. contributed to the writing of the manuscript. A.-G.Z. contributed to conceptualization and discussion of the project. M.M. supervised proteomic analyses. M.H.T. provided substantial conceptualization and contributed to writing of the manuscript. C.D. conceptualized, designed, and performed *in vivo* experiments; analyzed and interpreted data; and wrote the manuscript.

REFERENCES

Anders, S., Pyl, P.T., and Huber, W. (2015). HTSeq–a Python framework to work with high-throughput sequencing data. Bioinformatics *31*, 166–169.

Andrews, S. (2010). FastQC: a quality control tool for high throughput sequence data. (Babraham Bioinformatics). http://www.bioinformatics. babraham.ac.uk/projects/fastqc.

Bachman, E.S., Dhillon, H., Zhang, C.-Y., Cinti, S., Bianco, A.C., Kobilka, B.K., and Lowell, B.B. (2002). βAR signaling required for diet-induced thermogenesis and obesity resistance. Science *297*, 843–845.

Bapat, S.P., Myoung Suh, J., Fang, S., Liu, S., Zhang, Y., Cheng, A., Zhou, C., Liang, Y., LeBlanc, M., Liddle, C., et al. (2015). Depletion of fat-resident Treg cells prevents age-associated insulin resistance. Nature *528*, 137–141.

Bruns, H.A., Schindler, U., and Kaplan, M.H. (2003). Expression of a constitutively active stat6 in vivo alters lymphocyte homeostasis with distinct effects in T and B cells. J. Immunol. *170*, 3478–3487.

Chang, C.H., and Pearce, E.L. (2016). Emerging concepts of T cell metabolism as a target of immunotherapy. Nat. Immunol. *17*, 364–368.

Chapoval, S., Dasgupta, P., Dorsey, N.J., and Keegan, A.D. (2010). Regulation of the T helper cell type 2 (Th2)/T regulatory cell (Treg) balance by IL-4 and STAT6. J. Leukoc. Biol. *87*, 1011–1018.

Cipolletta, D., Feuerer, M., Li, A., Kamei, N., Lee, J., Shoelson, S.E., Benoist, C., and Mathis, D. (2012). PPAR-gamma is a major driver of the accumulation and phenotype of adipose tissue Treg cells. Nature *486*, 549–553.

Cipolletta, D., Cohen, P., Spiegelman, B.M., Benoist, C., and Mathis, D. (2015). Appearance and disappearance of the mRNA signature characteristic of Treg cells in visceral adipose tissue: age, diet, and PPARgamma effects. Proc. Natl. Acad. Sci. USA *112*, 482–487.

Cox, J., Hein, M.Y., Luber, C.A., Paron, I., Nagaraj, N., and Mann, M. (2014). Accurate proteome-wide label-free quantification by delayed normalization and maximal peptide ratio extraction, termed MaxLFQ. Mol. Cell. Proteomics *13*, 2513–2526.

Cox, J., and Mann, M. (2008). MaxQuant enables high peptide identification rates, individualized p.p.b.-range mass accuracies and proteome-wide protein quantification. Nat. Biotechnol. *26*, 1367–1372.

Cox, J., Neuhauser, N., Michalski, A., Scheltema, R.A., Olsen, J.V., and Mann, M. (2011). Andromeda: a peptide search engine integrated into the MaxQuant environment. J. Proteome Res. *10*, 1794–1805.

Cypess, A.M., White, A.P., Vernochet, C., Schulz, T.J., Xue, R., Sass, C.A., Huang, T.L., Roberts-Toler, C., Weiner, L.S., Sze, C., et al. (2013). Anatomical localization, gene expression profiling and functional characterization of adult human neck brown fat. Nat. Med. 19, 635–639.

Daniel, C., and von Boehmer, H. (2011). Extrathymic generation of regulatory T cells–chances and challenges for prevention of autoimmune disease. Adv. Immunol. 112, 177–213.

Daniel, C., Wennhold, K., Kim, H.J., and von Boehmer, H. (2010). Enhancement of antigen-specific Treg vaccination in vivo. Proc. Natl. Acad. Sci. USA 107, 16246–16251.

Daniel, C., Weigmann, B., Bronson, R., and von Boehmer, H. (2011). Prevention of type 1 diabetes in mice by tolerogenic vaccination with a strong agonist insulin mimetope. J. Exp. Med. 208, 1501–1510.

Fedorenko, A., Lishko, P.V., and Kirichok, Y. (2012). Mechanism of fatty-acid-dependent UCP1 uncoupling in brown fat mitochondria. Cell 151, 400–413.

Feldmann, H.M., Golozoubova, V., Cannon, B., and Nedergaard, J. (2009). UCP1 ablation induces obesity and abolishes diet-induced thermogenesis in mice exempt from thermal stress by living at thermoneutrality. Cell Metab. 9, 203–209.

Feuerer, M., Herrero, L., Cipolletta, D., Naaz, A., Wong, J., Nayer, A., Lee, J., Goldfine, A.B., Benoist, C., Shoelson, S., et al. (2009). Lean, but not obese, fat is enriched for a unique population of regulatory T cells that affect metabolic parameters. Nat. Med. 15, 930–939.

Gessner, A., Mohrs, K., and Mohrs, M. (2005). Mast cells, basophils, and eosinophils acquire constitutive IL-4 and IL-13 transcripts during lineage differentiation that are sufficient for rapid cytokine production. J. Immunol. 174, 1063–1072.

Goenka, S., and Kaplan, M.H. (2011). Transcriptional regulation by STAT6. Immunol. Res. 50, 87–96.

Gottschalk, R.A., Corse, E., and Allison, J.P. (2010). TCR ligand density and affinity determine peripheral induction of Foxp3 in vivo. J. Exp. Med. 207, 1701–1711.

Guillot, X., Tordi, N., Mourot, L., Demougeot, C., Dugue, B., Prati, C., and Wendling, D. (2014). Cryotherapy in inflammatory rheumatic diseases: a systematic review. Expert Rev. Clin. Immunol. 10, 281–294.

Heng, T.S., and Painter, M.W.; Immunological Genome Project Consortium (2008). The immunological genome project: networks of gene expression in immune cells. Nat. Immunol. 9, 1091–1094.

Hwang, E.S., White, I.A., and Ho, I.C. (2002). An IL-4-independent and CD25-mediated function of c-maf in promoting the production of Th2 cytokines. Proc. Natl. Acad. Sci. USA 99, 13026–13030.

Kaplan, M.H., Schindler, U., Smiley, S.T., and Grusby, M.J. (1996). Stat6 is required for mediating responses to IL-4 and for the development of Th2 cells. Immunity 4, 313–319.

Kim, C.H. (2007). Molecular targets of FoxP3+ regulatory T cells. Mini Rev. Med. Chem. 7, 1136–1143.

Kim, J.M., Rasmussen, J.P., and Rudensky, A.Y. (2007). Regulatory T cells prevent catastrophic autoimmunity throughout the lifespan of mice. Nat. Immunol. 8, 191–197.

Klimek, A.T., Lubkowska, A., Szygula, Z., Fraczek, B., and Chudecka, M. (2011). The influence of single whole body cryostimulation treatment on the dynamics and the level of maximal anaerobic power. Int. J. Occup. Med. Environ. Health 24, 184–191.

Kretschmer, K., Apostolou, I., Hawiger, D., Khazaie, K., Nussenzweig, M.C., and von Boehmer, H. (2005). Inducing and expanding regulatory T cell populations by foreign antigen. Nat. Immunol. 6, 1219–1227.

Kulak, N.A., Pichler, G., Paron, I., Nagaraj, N., and Mann, M. (2014). Minimal, encapsulated proteomic-sample processing applied to copy-number estimation in eukaryotic cells. Nat. Methods 11, 319–324.

Lewis, M., Tarlton, J.F., and Cose, S. (2008). Memory versus naive T-cell migration. Immunol. Cell Biol. 86, 226–231.

Li, H., Handsaker, B., Wysoker, A., Fennell, T., Ruan, J., Homer, N., Marth, G., Abecasis, G., and Durbin, R.; 1000 Genome Project Data Processing Subgroup (2009). The sequence Alignment/Map format and SAMtools. Bioinformatics 25, 2078–2079.

Love, M.I., Huber, W., and Anders, S. (2014). Moderated estimation of fold change and dispersion for RNA-seq data with DESeq2. Genome Biol. 15, 550.

Lubkowska, A., Szygula, Z., Chlubek, D., and Banfi, G. (2011). The effect of prolonged whole-body cryostimulation treatment with different amounts of sessions on chosen pro- and anti-inflammatory cytokines levels in healthy men. Scand. J. Clin. Lab. Invest. 71, 419–425.

MacIver, N.J., Michalek, R.D., and Rathmell, J.C. (2013). Metabolic regulation of T lymphocytes. Annu. Rev. Immunol. 31, 259–283.

Maerten, P., Shen, C., Bullens, D.M., Van Assche, G., Van Gool, S., Geboes, K., Rutgeerts, P., and Ceuppens, J.L. (2005). Effects of interleukin 4 on CD25+CD4+ regulatory T cell function. J. Autoimmun. 25, 112–120.

Mathis, D. (2013). Immunological goings-on in visceral adipose tissue. Cell Metab. 17, 851–859.

Medrikova, D., Sijmonsma, T.P., Sowodniok, K., Richards, D.M., Delacher, M., Sticht, C., Gretz, N., Schafmeier, T., Feuerer, M., and Herzig, S. (2015). Brown adipose tissue harbors a distinct sub-population of regulatory T cells. PLoS One 10, e0118534.

Meissner, F., and Mann, M. (2014). Quantitative shotgun proteomics: considerations for a high-quality workflow in immunology. Nat. Immunol. 15, 112–117.

Ortega-Molina, A., Efeyan, A., Lopez-Guadamillas, E., Munoz-Martin, M., Gomez-Lopez, G., Canamero, M., Mulero, F., Pastor, J., Martinez, S., Romanos, E., et al. (2012). Pten positively regulates brown adipose function, energy expenditure, and longevity. Cell Metab. 15, 382–394.

Panduro, M., Benoist, C., and Mathis, D. (2016). Tissue Tregs. Annu. Rev. Immunol. 34, 609–633.

Pillemer, B.B., Qi, Z., Melgert, B., Oriss, T.B., Ray, P., and Ray, A. (2009). STAT6 activation confers upon T helper cells resistance to suppression by regulatory T cells. J. Immunol. 183, 155–163.

Qiu, Y., Nguyen, K.D., Odegaard, J.I., Cui, X., Tian, X., Locksley, R.M., Palmiter, R.D., and Chawla, A. (2014). Eosinophils and type 2 cytokine signaling in macrophages orchestrate development of functional beige fat. Cell 157, 1292–1308.

Quelle, F.W., Shimoda, K., Thierfelder, W., Fischer, C., Kim, A., Ruben, S.M., Cleveland, J.L., Pierce, J.H., Keegan, A.D., Nelms, K., et al. (1995). Cloning of murine Stat6 and human Stat6, Stat proteins that are tyrosine phosphorylated in responses to IL-4 and IL-3 but are not required for mitogenesis. Mol. Cell. Biol. 15, 3336–3343.

Rosen, E.D., and Spiegelman, B.M. (2014). What we talk about when we talk about fat. Cell 156, 20–44.

Rothwell, N.J., and Stock, M.J. (1979). A role for brown adipose tissue in diet-induced thermogenesis. Nature 281, 31–35.

Rudra, D., deRoos, P., Chaudhry, A., Niec, R.E., Arvey, A., Samstein, R.M., Leslie, C., Shaffer, S.A., Goodlett, D.R., and Rudensky, A.Y. (2012). Transcription factor Foxp3 and its protein partners form a complex regulatory network. Nat. Immunol. 13, 1010–1019.

Saito, M., Okamatsu-Ogura, Y., Matsushita, M., Watanabe, K., Yoneshiro, T., Nio-Kobayashi, J., Iwanaga, T., Miyagawa, M., Kameya, T., Nakada, K., et al. (2009). High incidence of metabolically active brown adipose tissue in healthy adult humans: effects of cold exposure and adiposity. Diabetes 58, 1526–1531.

Sanchez-Guajardo, V., Tanchot, C., O'Malley, J.T., Kaplan, M.H., Garcia, S., and Freitas, A.A. (2007). Agonist-driven development of CD4+CD25+Foxp3+ regulatory T cells requires a second signal mediated by Stat6. J. Immunol. 178, 7550–7556.

Sauer, S., Bruno, L., Hertweck, A., Finlay, D., Leleu, M., Spivakov, M., Knight, Z.A., Cobb, B.S., Cantrell, D., O'Connor, E., et al. (2008). T cell receptor signaling controls Foxp3 expression via PI3K, Akt, and mTOR. Proc. Natl. Acad. Sci. USA 105, 7797–7802.

Scheltema, R.A., and Mann, M. (2012). SprayQc: a real-time LC-MS/MS quality monitoring system to maximize uptime using off the shelf components. J. Proteome Res. 11, 3458–3466.

Schwanhäusser, B., Busse, D., Li, N., Dittmar, G., Schuchhardt, J., Wolf, J., Chen, W., and Selbach, M. (2011). Global quantification of mammalian gene expression control. Nature 473, 337–342.

Schweitzer, L.D., Comb, W.C., Bar-Peled, L., and Sabatini, D.M. (2015). Disruption of the rag-ragulator complex by c17orf59 inhibits mTORC1. Cell Rep. 12, 1445–1455.

Sehra, S., Bruns, H.A., Ahyi, A.N., Nguyen, E.T., Schmidt, N.W., Michels, E.G., von Bulow, G.U., and Kaplan, M.H. (2008). IL-4 is a critical determinant in the generation of allergic inflammation initiated by a constitutively active Stat6. J. Immunol. 180, 3551–3559.

Serr, I., Fürst, R.W., Achenbach, P., Scherm, M.G., Gökmen, F., Haupt, F., Sedlmeier, E.-M., Knopff, A., Shultz, L., Willis, R.A., et al. (2016). Type 1 diabetes vaccine candidates promote human Foxp3+Treg induction in humanized mice. Nat. Commun. 7, 10991.

Setiady, Y.Y., Coccia, J.A., and Park, P.U. (2010). In vivo depletion of CD4+FOXP3+ Treg cells by the PC61 anti-CD25 monoclonal antibody is mediated by FcgammaRIII+ phagocytes. Eur. J. Immunol. 40, 780–786.

Shrestha, S., Yang, K., Guy, C., Vogel, P., Neale, G., and Chi, H. (2015). Treg cells require the phosphatase PTEN to restrain TH1 and TFH cell responses. Nat. Immunol. 16, 178–187.

Tyanova, S. (2016). The Perseus computational platform for comprehensive analysis of (prote)omics data. Nat. Methods 13, 731–740.

UniProt, C. (2015). UniProt: a hub for protein information. Nucleic Acids Res. 43, D204–D212.

Vizcaino, J.A., Deutsch, E.W., Wang, R., Csordas, A., Reisinger, F., Rios, D., Dianes, J.A., Sun, Z., Farrah, T., Bandeira, N., et al. (2014). ProteomeXchange provides globally coordinated proteomics data submission and dissemination. Nat. Biotechnol. 32, 223–226.

von Boehmer, H., and Daniel, C. (2013). Therapeutic opportunities for manipulating T(Reg) cells in autoimmunity and cancer. Nat. Rev. Drug Discov. 12, 51–63.

Webster, K.E., Walters, S., Kohler, R.E., Mrkvan, T., Boyman, O., Surh, C.D., Grey, S.T., and Sprent, J. (2009). In vivo expansion of T reg cells with IL-2-mAb complexes: induction of resistance to EAE and long-term acceptance of islet allografts without immunosuppression. J. Exp. Med. 206, 751–760.

Yu, X.Y., Lin, S.G., Wang, X.M., Liu, Y., Zhang, B., Lin, Q.X., Yang, M., and Zhou, S.F. (2007). Evidence for coexistence of three beta-adrenoceptor subtypes in human peripheral lymphocytes. Clin. Pharmacol. Ther. 81, 654–658.

Zhu, J., Cote-Sierra, J., Guo, L., and Paul, W.E. (2003). Stat5 activation plays a critical role in Th2 differentiation. Immunity 19, 739–748.

STAR★METHODS

KEY RESOURCES TABLE

REAGENT or RESOURCE	SOURCE	IDENTIFIER
Antibodies		
CD4 Biotin	BioLegend	Clone: GK1.5; Cat# 553728; RRID: AB_395012
CD8a Pacific Blue	BioLegend	Clone: 53-6.7; Cat# 100725; RRID: AB_493425
CD11b Pacific Blue	BioLegend	Clone: M1/70; Cat# 101224; RRID: AB_755986
CD11c Brilliant Violett 421	BioLegend	Clone: N418; Cat# 117330; RRID: AB_11219593
B220 Pacific Blue	BioLegend	Clone: RA3-6B2; Cat# 103227; RRID: AB_492876
F4/80 Pacific Blue	BioLegend	Clone: BM8; Cat# 123124; RRID: AB_893475
CD25 PerCP-Cy5.5	BioLegend	Clone: PC61; Cat# 102030; RRID: AB_893288
CD44 PE	BioLegend	Clone: IM7; Cat# 103008; RRID: AB_312959
Ki67 APC	BioLegend	Clone: 16A8; Cat# 652406; RRID: AB_2561930
Ki67 Brilliant Violett 605	BioLegend	Clone: 16A8; Cat# 652413; RRID: AB_2562664
CD4 Alexa Fluor 700	eBioscience	Clone: RM4-5; Cat# 56-0042-82; RRID: AB_494000
CD62L APC	eBioscience	Clone: MEL-14; Cat# 17-0621-82; RRID: AB_469410
Foxp3 FITC	eBioscience	Clone: FJK-16s; Cat# 11-5773-82; RRID: AB_465243
CD14 V450	BD Biosciences	Clone: rmC5-3; Cat# 560639; RRID: AB_1727429
CD90.1 PerCP-Cy5.5	BioLegend	Clone: OX-7; Cat# 202515; RRID: AB_961438
CD90.2 APC-Cy7	BioLegend	Clone: 30-H12; Cat#105328; RRID: AB_10613293
Anti-mouse CD25 (mCD25)	BioXCell	Clone: PC-61.5.3; Cat# BE0012; RRID: AB_1107619
Fc-Block	BD Pharmingen	Clone: 2.4G2; Cat# 553142; RRID: AB_394657
CD3e	BD Pharmingen	Clone: 145-2C11; Cat# 553057; RRID: AB_394590
CD28	BD Pharmingen	Clone: 37.51; Cat# 553294; RRID: AB_394763
p-Stat6 (pY641) Alexa Fluor 647	BD Phosflow™	Clone: J71-773.58.11; Cat# 558242; RRID: AB_647145
p-Stat6 rabbit anti-mouse	Cell Signaling	Cat# 9361S; RRID: AB_331595
anti-mouse IL-2	eBioscience	Clone: JES6-1A12; Cat# 16-7022-85; RRID: AB_469207
rabbit anti-mouse C17orf59	MyBioSource	polyclonal; Cat# MBS6004199; RRID: N/A
mouse anti-mouse Stat6	Cell Signaling	polyclonal; Cat# 9362; RRID: AB_2271211
rat-anti-mouse LAMP2	BioLegend	Clone: M3/84; Cat# 108502; RRID: AB_313383
Mouse anti-mTOR	Thermo Fisher Scientific	Clone: 215Q18; Cat# AHO1232; RRID: AB_2536329
Hamster anti-mouse CD3	BioLegend	Clone: 145-2C11; Cat# 100302; RRID: AB_312667
Rat anti-mouse CD4	BioLegend	Clone: RM4-5; Cat #100506; RRID: AB_312709
Rat anti-mouse CD4	eBioscience	Clone: GK1.5; Cat# 14-0041-8; RRID: AB_467064
F(ab')₂ donkey anti-rabbit IgG PE	eBioscience	polyclonal; Cat# 12-4739-81; RRID: AB_1210761
goat anti-rat Alexa Fluor 488	Life Technologies	polyclonal; Cat #A11006; RRID: AB_2534074
biotinylated goat-anti- armen. hamster IgG	eBioscience	polyclonal; Cat #13-4113-85; RRID: AB_466651
donkey-anti-mouse AlexaFluor 555	Life Technologies	polyclonal; Cat# A-31570; RRID: AB_2536180
goat-anti-mouse Cy3	Dianova	polyclonal; Cat# 115-165-146; RRID: AB_2491007
goat-anti-rat AlexaFluor 594	Life Technologies	polyclonal; Cat#A11007; RRID: AB_141374
goat anti-rabbit AlexaFluor 594	Life Technologies	polyclonal; Cat# A11012; RRID: AB_141359
rat-anti-mouse biotinylated	Dianova	polyclonal; Cat# 415-065-166; RRID: AB_2340272
horse anti-rabbit biotinylated	Vector Laboratory	Cat# BA-1100; RRID: AB_2336201
goat-anti-rat STAR580	abberior	Cat# 2-0132-005-1; RRID: N/A
goat-anti-rabbit STAR635P	abberior	Cat# 2-0132-005-5; RRID: N/A
Chemicals, Peptides, and Recombinant Proteins		
Foxp3 Staining Buffer Set	eBioscience	Cat# 00-5523-00
Fixable Viability Dye eFluor450	eBioscience	Cat# 65-0863-18

(Continued on next page)

Continued

REAGENT or RESOURCE	SOURCE	IDENTIFIER
Sytox Red	Thermo Fisher Scientific	Cat# S34859
Sytox Blue	Thermo Fisher Scientific	Cat# S34857
Streptavidin Microbeads	Miltenyi	Cat #130-048-101
Dynabeads untouched CD4+ mouse	Invitrogen	Cat# 11415D
Streptavidin Alexa Fluor 488	Dianova	Cat# 016-540-084
Streptavidin Dylight 549	Vector Laboratory	Cat# SA-5549
Streptavidin Pacific Blue	Invitrogen	Cat# S11222
Hoechst 33342 dye	Invitrogen	Cat # H1399; CAS 23491-52-3
high fat high sugar (HFHS) diet	Research Diets	Cat# D12331
Pten Inhibitor SF1670	Abcam	Cat# ab141303; CAS 345630-40-2
Stat6 Inhibitor AS 1517499	Axon Medchem	Cat# Axon 1992 ; CAS 919486-40-1
CL-316243	Sigma Aldrich	Cat# C5976; CAS 138908-40-4
cyanopindolol hemifumarate	Tocris	Cat#0993; CAS 69906-86-1
LysC	Wako Chemicals	Cat# 129-02541; EC# 3.4.21.50
trypsin	Sigma Aldrich	Cat# T6567; EC# 232-650-8
ReproSil-Pur C18-AQ 1.9 μm resin	Dr. Maisch GmbH	Cat# R119.b9
Roti-Histofix 4%	Carl Roth	Cat# P087.5
Ficoll-Paque PLUS	GE Healthcare	Cat# 17-1440-03
recombinant human IL-2	ReproTech	Cat# 200-02
collagenase type II	Sigma Aldrich	Cat#C6885; EC #3.4.24.3
collagenase D	Roche	Cat#11088882001; EC #3.4.24.3
Critical Commercial Assays		
miRNeasy Micro Kit	Qiagen	Cat# 217084
Eva Green SuperMix	BioRad	Cat# 1725202
iScript Advanced cDNA Synthesis Kit	BioRad	Cat# 1725038
SMARTer ultra-low input RNA Kit for sequencing – v4	Takara Clonetech	Cat# 634890
SMARTer Universal Low Input RNA Kit for Sequencing	Takara Clonetech	Cat# 634889
Deposited Data		
mass spectrometry data	This paper	ProteomeXchange Consortium via PRIDE repository; Identifier: ProteomeXchange: PXD004671
Experimental Models: Organisms/Strains		
CD90.1 Balb/c; genotype: CBy.PL(B6)-Thy1ª/ScrJ	Jackson Laboratory	RRID: IMSR_JAX:005443
CD90.2 Balb/c; genotype: Balb/cByJ	Jackson Laboratory	RRID: IMSR_JAX:001026
Foxp3 GFP Balbc; genotype: C.Cg-Foxp3tm2Tch/J	Jackson Laboratory	RRID: IMSR_JAX:006769
Foxp3 GFP Bl6; genotype: B6.Cg-Foxp3tm2Tch/J	Jackson Laboratory	RRID: IMSR_JAX:006772
Stat6VT+ Bl6; genotype: Stat6 VT/AA mutation	Mark H. Kaplan, Indiana University, USA (Bruns et al., 2003)	N/A
Stat6KO Balbc; genotype: C.129S2-Stat6tm1Gru/J	Mark H. Kaplan, Indiana University, USA (Kaplan et al., 1996)	RRID: IMSR_JAX:002828
Stat6KO 4get-GFP, Balbc	Benno Weigmann, University Erlangen, Germany (Gessner et al., 2005)	N/A
PtenTg Bl6	Manuel Serrano, Spanish National Cancer Research Center, Spain (Ortega-Molina et al., 2012)	N/A
Betaless; genotype: Adrb1,2,3TKO	Francoise Rohner-Jeanrenaud, University of Geneva, Switzerland	N/A

(Continued on next page)

Continued

REAGENT or RESOURCE	SOURCE	IDENTIFIER
Borcs6^{+/-}; genotype: B6N(Cg)-*Borcs6[tm1.1(KOMP)Vlcg]*/J	Jackson Laboratory	RRID: IMSR_JAX:028178
Humanized mice; genotype: *NOD.Cg-Prkdc[scid] H2-Ab1[tm1Gru] Il2rg[tm1Wjl]* Tg(HLA-DQA1,HLA-DQB1)1Dv//Sz	Leonard Shultz, Jackson Laboratory	N/A
Foxp3-DTR; genotype: C57BL/6-Tg(Foxp3-DTR/EGFP)23.2Spar/Mmjax	Tobias Bopp, Johannes Gutenberg University Mainz, Germany	RRID: MMRRC_032050-JAX
Sequence-Based Reagents		
Custom primers used for qPCR	This paper	Table S1
Software and Algorithms		
FlowJo software (version 7.6.1)	TreeStar, OR	https://www.flowjo.com/solutions/flowjo/downloads/
FACSDiva software (version 6.1.3)	Beckton Dickinson	N/A
Prism (version 6.0.1)	GraphPad	https://www.graphpad.com/scientific-software/prism/
Statistical Package for the Social Sciences (SPSS) (version 19.0)	IBM	https://www-01.ibm.com/software/de/analytics/spss/download/
SprayQc software	(Scheltema and Mann, 2012)	http://sprayqc.sourceforge.net/
MaxQuant software package (version 1.5.3.29)	(Cox and Mann, 2008)	http://www.coxdocs.org/doku.php?id=maxquant:start
Andromeda search engine	(Cox et al., 2011)	http://www.coxdocs.org/doku.php?id=maxquant:andromeda:start
iBAQ algorithm	(Schwanhäusser et al., 2011)	N/A
Perseus software package	(Tyanova, 2016)	http://www.coxdocs.org/doku.php?id=perseus:common:download_and_installation
DESeq2	(Love et al., 2014)	https://bioconductor.org/packages/release/bioc/html/DESeq2.html
SAMTools	(Li et al., 2009)	N/A
FastQC	(Andrews, 2010)	http://www.bioinformatics.babraham.ac.uk/projects/fastqc
HTSeq-count	(Anders et al., 2015)	http://www-huber.embl.de/users/anders/HTSeq/doc/install.html

CONTACT FOR REAGENT AND RESOURCE SHARING

Further information and requests for resources and reagents should be directed to and will be fulfilled by the Lead Contact, Matthias Tschöp (tschoep@helmholtz-muenchen.de).

EXPERIMENTAL MODEL AND SUBJECT DETAILS

Mice

CBy.PL(B6)-*Thy1[a]*/ScrJ (CD90.1 BALB/c), Balb/cByJ (CD90.2 BALB/c), heterozygous B6N(Cg)-*Borcs6[tm1.1(KOMP)Vlcg]*/J (Borcs6^{+/-}), C.Cg-Foxp3[tm2Tch]/J (Foxp3-GFP BALB/c) and B6.Cg-Foxp3[tm2Tch]/J mice (Foxp3-GFP Bl6) mice were originally obtained from Jackson Laboratories. C.129S2-*Stat6[tm1Gru]*/J (Kaplan et al., 1996), referred to as Stat6ko mice, and Stat6VT mice (Bruns et al., 2003) were previously described. Pten Tg Bl6 mice were kindly provided by Manuel Serrano (Spanish National Cancer Research Center (CNIO), Spain). Adrb1,2,3TKO mice, referred to as betaless mice, were kindly provided by Francoise Rohner-Jeanrenaud (Faculty of Medicine, University of Geneva, Switzerland). Humanized mice, *NOD.Cg-Prkdc[scid] H2-Ab1[tm1Gru] Il2rg[tm1Wjl]* Tg(HLA-DQA1,HLA-DQB1)1Dv//Sz mice, lack murine MHC class II and transgenically express human HLA-DQ8. These mice were developed by Leonard Shultz at the Jackson Laboratory. For the high-caloric challenge, mice were fed *ad libitum* with a high-fat, high-sugar (HFHS) diet composed of 58.0% kcal from fat, 25.5% kcal from carbohydrates (including 8% sucrose) and 16.4% kcal from protein (Research Diets, #D12331, New Brunswick, NJ) or standard diet (Altromin, #1314, Lage, Germany) for 1-16 wk. Mice were maintained group-housed on a 12h/12h light dark cycle at 25°C under specific pathogen free (SPF) conditions. C57BL/6-Tg(Foxp3-DTR/EGFP)23.2Spar/Mmjax mice, referred to as Foxp3 DTR mice, were kindly provided by Tobias Bopp (Institute of Immunology, University Medical Center Mainz, Johannes Gutenberg-University, Mainz, Germany) and Stat6KO 4get-GFP BALB/c mice (Gessner et al., 2005) were

kindly provided by Benno Weigmann (Department of Medicine 1, University of Erlangen-Nuremberg, Erlangen, Germany). All mice had *ad libitum* access to food and water and were maintained in the respective animal facilities according to guidelines established by the relevant Institutional Animal Committees. Mice were randomized to test groups. For *in vivo* ADRB3 stimulation or inhibition mice were injected *i.p.* with 1 mg/kg CL or 0.3 mg/kg Cyanopindolol on three consecutive days, respectively. 0.9% NaCl was used as vehicle control. For Treg depletion, Foxp3-DTR mice were injected *i.p.* with 50 ng diphtheria toxin per g bodyweight on three consecutive days. For a second approach of Treg depletion, 250 μg anti-mCD25 antibodies (BioXCell) were injected *i.p.* on three consecutive days (Setiady et al., 2010). For *in vivo* Treg expansion, 6 μg anti-IL2/IL2 antibody (IL-2-mAb) complexes were injected *s.c.* on three consecutive days (Webster et al., 2009). For *in vivo* cold exposure experiments, mice were acclimated to 8°C for 1 wk or to 4°C for 24 h as indicated in the text. No animals were excluded due to illness or outlier results; therefore, no exclusion determination was required. The investigators were not blinded to group allocation or to the assessment of experimental end points. All animal care was executed according to guidelines established by the Institutional Animal Committees at each institution. Ethical approval for all mouse experimentations has been received by corresponding local animal welfare authorities (District government of upper Bavaria or Veterinary office of Zurich).

In Vitro Studies with Primary Murine T Cells

Freshly isolated murine CD4^{+} T cells were cultured for three days in RPMI media (Gibco by life technologies) supplemented with 10% FCS, 1 mM sodium pyruvate (Sigma Aldrich), 50 mM β-mercaptoethanol (Amimed), 1X non-essential amino acids (Merck Millipore), 100 U/ml human recombinant IL-2 (ReproTech), 100 U/ml penicillin and 100 μg/ml streptomycin (Sigma Aldrich) at 37°C in an humidified CO_2 incubator. Cell culture treated 96-well U bottom plates were used (Bio-Greiner one).

METHOD DETAILS

Isolation of CD4^{+}T Cells from Lymphoid Organs

Lymph nodes and spleens were mashed through 70 μm cell strainers in HBSS^{+} (supplemented with 5% FCS and 10 mM HEPES). After surface antibody staining, CD4^{+}T cells were enriched using biotin-labelled anti-CD4 antibodies and magnetic activated cell sorting (MACS, Miltenyi) with streptavidin microbeads (Miltenyi). Streptavidin-fluorochrome-conjugates (molecular probes by life technologies) were added after 5 min to allow flow cytometric detection. Cells were further processed for FACS sorting as described below. For immunefluorescence experiments, T cells were isolated from lymph nodes using Dynabeads untouched Mouse CD4 Kit (Invitrogen) according to manufacturer's instructions.

Isolation of CD4^{+}T Cells from Adipose Tissues

White adipose tissue was collected in PBS supplemented with 0.5% BSA and digested with Collagenase II solution [3-4 mg/ml Collagenase II, 10 mM CaCl₂] for 10 minutes at 37°C on a rotator. The cell suspension was passed through a 200 μm nylon mesh and centrifuged (380xg, 5 min., 4°C) to separate the stromal vascular fraction from adipocytes. Pelleted cells were re-suspended in HBSS[+] (HBSS supplemented with 5% FCS and 10 mM HEPES) and stained for flow cytometric analysis. *Brown AT* was digested in three digestion rounds with 1 mg/ml Collagenase D in HBSS[+] at 37°C for 20 min on a rotator. Cell suspensions were passed through a 200 μm nylon mesh and stained for flow cytometric analysis.

Cell Staining for Flow Cytometry
Murine FACS Stainings
The following monoclonal antibodies were used for murine FACS stainings: From BioLegend (San Diego, CA): anti-CD4 Biotin (GK1.5, 1:400), anti-CD8a Pacific Blue (53-6.7; 1:300), anti-CD11b Pacific Blue (M1/70, 1:300), anti-CD11c Brilliant Violet 421 (N418, 1:400), anti-B220 Pacific Blue (RA3-6B2, 1:300), anti-F4/80 Pacific Blue (BM8, 1:400), anti-CD25 PerCP-Cy5.5 (PC61, 1:200), anti-CD44 PE (IM7, 1:800, 1:3000 for analysis with ≤1,000 cells per well), anti-Ki67 APC (16A8, 1:400); anti-Ki67 Brilliant Violet 605 (16A8, 1:400), anti-CD90.1 PerCP-Cy5.5 (OX-7, 1:500), anti-CD90.2 APC-Cy7 (30-H12, 1:500); from eBioscience (San Diego, CA): anti-CD4 Alexa Fluor 700 (RM4-5; 1:200; 1:600 for analysis with ≤1,000 cells), anti-CD62L APC (MEL-14, 1:400), anti-Foxp3 FITC (FJK-16s, 1:200), polyclonal donkey anti-rabbit IgG PE (1:2000); from BD Biosciences: anti-CD14 V450 (rmC5-3, 1:400). Unspecific binding of antibodies was prevented by incubation of cell suspensions with Fc-Block (BD Pharmingen, 2.4G2, 1:100) for 10 min on ice, followed by flow cytometric staining for 30 min on ice in the dark. Cells were passed through a 40 μm cell strainer (NeoLab) to remove large debris. Enumeration of cells and acquisition were performed by using FACSAriaIII and FACSDiva software (BD version 6.1.3). Single-cell data analyses were performed by the use of the FlowJo software 7.6.1 (Tree Star, OR).
Intracellular Staining
To detect intracellular protein expression, T cells were fixed and permeabilized using the Foxp3 Staining Buffer Set (eBioscience) after surface staining. For phospho-Stat6 stainings, MACS-enriched CD4^{+} T cells were cultured over night with 5 μg/ml plate-bound anti-CD3 and anti-CD28 in RPMI media with supplements and 100 U/ml IL-2. Cells were washed and re-stimulated with CL (100 nM) for 15 min. Surface staining was performed as described above with Fc Block supplemented with sodium vanadate (New England Biolabs). Cells were fixed with PFA (4.5% Histofix, Carl Roth) and permeabilized with 100% methanol. Anti-phospho Stat6-AlexaFluor 647 was stained as recommended by the manufacturer.

Sample Acquisition

Cells were acquired on BD FACSAriaIII flow cytometer using FACSDiva software with optimal compensation and gain settings determined for each experiment based on unstained and single-color stained samples. Doublets were excluded based on SSC-A vs. SSC-W plots and FSC-A vs. FSC-W plots. Live cell populations were gated on the basis of cell side and forward scatter and the exclusion of cells positive for Sytox Blue (Life Technologies) or Fixable Viability Dye eFluor450 (eBioscience). Samples were analyzed using FlowJo software version 7.6.1 (TreeStar, OR).

In vitro Treg-Induction Assay

Murine naive $CD4^+$T cells were defined as $CD4^+CD25^-Foxp3^-GFP^-CD44^{low}$ for Foxp3-GFP reporter mice and as $CD4^+CD25^-CD44^{low}$ for non-reporter mice. Cells were sorted with a FACSAriaIII (BD) cell sorter for purity. Murine naive $CD4^+$T cells were cultured for 18 hours in RPMI media (Gibco by life technologies) supplemented with 10% FCS, 1 mM sodium pyruvate (Sigma Aldrich), 50 mM β-mercaptoethanol (Amimed), 1X non-essential amino acids (Merck Millipore), 100 U/ml human recombinant IL-2 (ReproTech), 100 U/ml penicillin and 100 μg/ml streptomycin (Sigma Aldrich) in 96-well plates pre-coated with 5 μg/ml anti-CD3e (145-2C11, BD Pharmingen) and 5 μg/ml anti-CD28 (37.51, BD Pharmingen). TCR stimulation was limited to 18 hours by transferring cells into uncoated wells. Cells were cultured for additional 36 hours without further TCR stimulation.

Chemicals and Enzymes Used for Experiments

To test the influence of adrenergic receptor stimulation or inhibition on Treg induction capacities, chemicals were added to *in vitro* cultures in the concentrations given in the text: CL-316243 (Sigma Aldrich, CAS 138908-40-4) and Cyanopindolol hemifumarate (Tocris, CAS 69906-86-1). To evaluate the influence of specific signaling pathways on Treg induction we used a specific PTEN inhibitor SF1670 (Abcam, CAS 345630-40-2) and a specific Stat6 inhibitor AS 1517499 (Axon Medchem, CAS 919486-40-1). Collagenase type II (Sigma Aldrich, EC #3.4.24.3) and Collagenase D (Roche, EC #3.4.24.3) were used for T cell isolation from ATs.

Quantitative Analysis of mRNA Abundance

RNA Extraction and cDNA Synthesis

Total RNA was extracted from sort-purified T cell populations using QIAzol Lysis Reagent/ miRNeasy Micro Kit and from snap-frozen total tissue samples (BAT, scWAT, visWAT), which were previously homogenized using QIAshredder (Qiagen) according to the manufacturer's instructions. 1 μg total RNA was converted to first strand cDNA using iScript Advanced cDNA Synthesis Kit (Bio-Rad). For cell numbers < 2000 and/or RNA amounts < 200 ng, cDNA synthesis and subsequent amplification was performed using the SMARTer ultra-low input RNA Kit for sequencing – v4 or SMARTer Universal Low Input RNA Kit for Sequencing (Takara Clonetech) according to the manufacturer's instructions. cDNA was generated in the Thermal Cycler peqStar 2X (Peqlab). Real-time PCR quantification was performed using SsoFast Evagreen Supermix (Bio-Rad) or SYBR Premix Ex Taq (Takara Clonetech) and gene-specific primer sets on a CFX96 real time system (Bio-Rad). *Histone* and *18S* RNA levels were used for normalization of target gene expression levels. Analysis of candidate genes involved in thermogenesis, browning, lipolysis, glycolysis and inflammation was performed. *Primers* used for Quantitative Real-Time PCR analyses are listed in Table S1.

Gel Electrophoresis

2% (w/v) peqGOLD Universal Agarose (Peqlab) was dissolved in 1X TAE Buffer (Applichem) and 3 μL/100 mL Midori Green Advance (Biozym Scientific) were added. Products from RT-qPCR were mixed with Gel Loading Dye Blue (BioLabs). 100 bp Ladder (New England Biolabs) was used as reference. Gel electrophoresis was performed with 130 V for 40-120 min using the power supply unit peqPOWER E250 (Peqlab). DNA fragments were detected using FUSION-FX7 Spectra (Vilber).

mRNA Expression Profiling

cDNA Synthesis: cDNA was generated directly from cells in the Thermal Cycler peqStar 2X (Peqlab) using the SMARTer ultra-low input RNA Kit for sequencing – v4 or SMARTer Universal Low Input RNA Kit for Sequencing (Takara Clonetech) according to the manufacturer's instructions. mRNA expression profiling using next generation sequencing (NGS). For NGS, cDNA concentration and integrity (quality) of the samples were assessed using Agilent High Sensitivity DNA Chips (Agilent Technologies) and Agilent 2100 Bioanalyzer. We employed NGS for expression profiling in pooled sample-sets of $CD4^+$T cells purified from white and brown fat. mRNA library preparation was conducted with Nextera reagents (Illumina), according to the manufacturer's instructions. NGS was performed on a NextSeq (Illumina) with 75bp single end reads for mRNA using Illumina reagents and following the manufacturer's instructions.

NGS Data Processing and Statistical Analysis

Quality was assessed by FastQC (Andrews, 2010). Reads were mapped to the mouse genome (mm10) using BWA-mem with default configuration. Read counts lists were created using SAMTools (Li et al., 2009) and HTSeq-count (Anders et al., 2015). Reads were normalized using DESeq2 (Love et al., 2014). Normalized read counts were further processed for descriptive visualization of expression trends for this preliminary experiment. The cut-off for reading counts was set to 30 and pseudogenes were manually removed. The top 5 upregulated genes are shown.

Proteomics

Mice were treated for three days with 1 mg/kg CL316243 or 0.9% NaCl as vehicle control *in vivo*. Additionally, mice were subjected to cold exposure (8°C) vs. room temperature for 1 week CD4$^+$T cells were isolated by MACS enrichment using CD4-biotin antibodies and streptavidin microbeads as described above.

Sample Preparation for LC-MS/MS Analysis

Cell lysis of isolated cells was performed in LB buffer (50% (v/v) 2-2-2-trifluoroethanol (TFE) plus 2 mM dithiothreitol, 50% (v/v) 50 mM ammonium bicarbonate (ABC) buffer) at 99°C for 10 min followed by sonication for 10 min (10 cycles high intensity, Bioruptor, Diagenode). Cell debris was removed after 10 min centrifugation (16,000 g at 4°C) and proteins in the lysate were alkylated for 30 min with 10 mM iodoacetamide in the dark. Next, the solution was centrifuged in a vacuum evaporator for about three hours at 45°C. Proteins were resolubilized in 10% (v/v) TFE in 50 mM ABC and sonicated in a water bath for 5 min. Proteins were digested by adding 0.2 μg of LysC and 0.2 μg of Trypsin and incubation at 37°C overnight. The next day, the digest was stopped by adding 1% (v/v) TFE and the solution volume was reduced in a vacuum evaporator for about one hour at 45°C. Samples were finally desalted on SDB-RPS StageTips (3M, Empore, Neuss, Germany) and eluted as described (Kulak et al., 2014).

LC-MS/MS Analysis

MS analysis was performed using Q-Exactive HF mass spectrometers (Thermo Fisher Scientific, Bremen, Germany) coupled on-line to a nanoflow UHPLC instrument (Easy nLC, Thermo Fisher Scientific). Peptides were separated on a 50 cm long (75 μm inner diameter) column packed in-house with ReproSil-Pur C18-AQ 1.9 μm resin (Dr. Maisch GmbH, Ammerbuch, Germany). Column temperature was kept at 50 °C by an in-house designed oven with a Peltier element and operational parameters were monitored in real time by the SprayQc software (Scheltema and Mann, 2012). Peptides were loaded with buffer A (0.1% (v/v) formic acid) and eluted with a nonlinear gradient of 5–60% buffer B (0.1% (v/v) formic acid, 80% (v/v) acetonitrile) at a flow rate of 300 nl/min. Peptide separation was achieved by 120 min gradients. The survey scans (300–1650 m/z, target value = 3E6, maximum ion injection times = 20ms) were acquired at a resolution of 60,000 followed by higher-energy collisional dissociation (HCD) based fragmentation (normalized collision energy = 27) of up to 15 dynamically chosen, most abundant precursor ions (isolation window = 1.4 m/z). The MS/MS scans were acquired at a resolution of 15,000 (target value = 1E5, maximum ion injection times = 60 ms). Repeated sequencing of peptides was minimized by excluding the selected peptide candidates for 20 s.

Computational MS Data Analysis

All data was analyzed using the MaxQuant software package 1.5.3.29 (Cox and Mann, 2008). The false discovery rate (FDR) cut-off was set to 1% for protein and peptide spectrum matches. Peptides were required to have a minimum length of 7 amino acids and a maximum mass of 4600 Da. MaxQuant was used to score fragmentation scans for identification based on a search with an initial allowed mass deviation of the precursor ion of a maximum of 4.5 ppm after time-dependent mass calibration. The allowed fragment mass deviation was 20 ppm. Fragmentation spectra were identified using the UniprotKB *Mus musculus* database (UniProt, 2015), based on the 2014_07 release, combined with 262 common contaminants by the integrated Andromeda search engine (Cox et al., 2011). Enzyme specificity was set as C-terminal to arginine and lysine, also allowing cleavage before proline, and a maximum of two missed cleavages. Carbamidomethylation of cysteine was set as fixed modification and N-terminal protein acetylation as well as methionine oxidation as variable modifications. Both 'label-free quantification (MaxLFQ)' and 'match between runs' with standard settings were enabled (Cox et al., 2014). Protein copy number estimates were calculated using the iBAQ algorithm (Schwanhäusser et al., 2011).

Statistics and Data Visualization

Basic data handling, normalization, statistics and annotation enrichment analysis was performed with the Perseus software package (Tyanova, 2016). We filtered for protein groups that were quantified with at least two valid values in at least one group of triplicates. Missing values were imputed with values representing a normal distribution (generated at 1.8 standard deviations of the total intensity distribution, subtracted from the mean, and a width of 0.3 standard deviations). Differentially expressed proteins were identified by one-way ANOVA test at a permutation-based FDR cutoff of 0.05. Enrichment for annotation categories was evaluated by 1D annotation enrichment or Fisher exact test to obtain a p-value. The mass spectrometry proteomics data have been deposited to the ProteomeXchange Consortium (Vizcaino et al., 2014) via the PRIDE partner repository with the dataset identifier ProteomeX change: PXD004671.

Immunefluorescence by Confocal Microscopy

T cells were isolated from thymus and lymph nodes with Dynabeads untouched CD4$^+$ mouse kit (Invitrogen) according to the manufacturer's instructions. Isolated cells were fixed with PFA (Histofix 4.5%, Carl Roth) for 10 min at RT. Immunefluorescence staining was done using rat-anti-mCD4 antibodies (RM4-5; BioLegend) and goat-anti-rat antibodies conjugated with AlexaFluor488 dye (Life Technologies). For CD3 staining armenian hamster-anti-mouse antibodies (145-2C11; BioLegend) were used together with biotinylated goat-anti-hamster antibodies followed by streptavidin-AlexaFluor488 (Life Technologies). For mTOR immunefluorescence analyses, mouse-anti-mTOR antibodies (215Q18; Thermo) and donkey-anti-mouse antibodies conjugated with AlexaFluor555 (Life Technologies) were used. For CD107b staining rat-anti-mouse LAMP2 (M3/84; BioLegend) antibodies were used followed by goat-anti-rat antibodies conjugated with AlexaFluor488 dye (Life Technologies). STAT6 was stained using mouse-anti-mSTAT6 antibodies followed by goat-anti-mouse antibodies conjugated with Cy3 dye. Negative control slides were incubated with secondary antibodies only. In most experiments the cells were PFA-fixed and prepared with cytospin centrifuge (Shandon). For Foxp3 staining, T cells were aceton-fixed, incubated with rat-anti-mouse antibodies (eBioscience) and goat-anti-rat antibodies conjugated with AlexaFluor594

dye (BioLegend). Nuclei were counterstained with DAPI (Vector). Finally, cells were analyzed by confocal microscopy (Leica DMI6000CS).

Immunofluorescence by STED Microscopy

Untouched CD4^{+}T cells from inLNs were fixed with PFA for 10 min at RT. After permeabilization with TritonX100 for 5 min and protein block for 10 min with 2% BSA, staining of rat anti-CD4 antibody (BD) and rabbit anti-C17orf59 antibody (MyBioSource) was performed. Goat-anti-rat-STAR580 (abberior) and goat-anti-rabbit STAR635P (abberior) were used as secondary antibodies. Finally, nuclei were counterstained with DAPI. Negative control slides were incubated with secondary antibodies only. Cells were analyzed by Abberior 3D STED 2-Channel Super Resolution Microscope (Abberior, Göttingen). The dye STAR580 was excited with a 594 nm pulsed laser, STAR635p with a 640 nm pulsed laser and DAPI with a 405 nm CW laser and depletion of STAR580 + STAR635p was done with a 775 nm pulsed STED laser.

QUANTIFICATION AND STATISTICAL ANALYSIS

Results are presented as means±SEM, as percentage, where appropriate or as summary box-and-whisker plots indicating minimum to maximum values to demonstrate data distribution. For normally distributed data, Student's t-test for unpaired values was used to compare independent groups. Group size estimations were based upon a power calculation to minimally yield an 80% chance to detect a significant difference in the respective parameter of $p<0.05$ between the relevant groups. For all tests, a two-tailed p value of <0.05 was considered to be significant. Statistical significance is shown as $* = p<0.05$; $** = p<0.01$; $*** = p<0.001$. N numbers can be found within the text and/or within the figure legends. Analyses were performed using GraphPad Prism 6.0.1 (La Jolla, CA) and the Statistical Package for the Social Sciences (SPSS 19.0; SPSS, Chicago, IL).

DATA AND SOFTWARE AVAILABILITY

Data Resources

The mass spectrometry proteomics data have been deposited to the ProteomeXchange Consortium (Vizcaino et al., 2014) via the PRIDE partner repository with the dataset identifier ProteomeXchange: PXD004671.

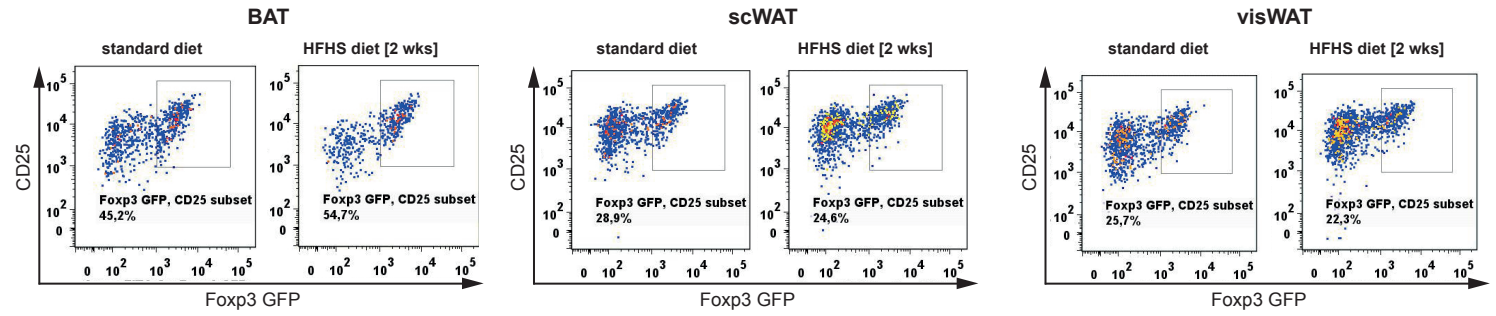**Supplemental Information**

A Stat6/Pten Axis Links Regulatory

T Cells with Adipose Tissue Function

Stefanie Kälin, Maike Becker, Verena B. Ott, Isabelle Serr, Fabian Hosp, Mohammad M.H. Mollah, Susanne Keipert, Daniel Lamp, Francoise Rohner-Jeanrenaud, Victoria K. Flynn, Martin G. Scherm, Lucas F.R. Nascimento, Katharina Gerlach, Vanessa Popp, Sarah Dietzen, Tobias Bopp, Purna Krishnamurthy, Mark H. Kaplan, Manuel Serrano, Stephen C. Woods, Philipp Tripal, Ralf Palmisano, Martin Jastroch, Matthias Blüher, Christian Wolfrum, Benno Weigmann, Anette-Gabriele Ziegler, Matthias Mann, Matthias H. Tschöp, and Carolin Daniel

Figure S1

A
Treg induction with naive CD4⁺T cells from fat after HFHS diet [2 wks]

BAT

standard diet · HFHS diet [2 wks]
Foxp3 GFP, CD25 subset 45,2% · Foxp3 GFP, CD25 subset 54,7%

scWAT

standard diet · HFHS diet [2 wks]
Foxp3 GFP, CD25 subset 28,9% · Foxp3 GFP, CD25 subset 24,6%

visWAT

standard diet · HFHS diet [2 wks]
Foxp3 GFP, CD25 subset 25,7% · Foxp3 GFP, CD25 subset 22,3%

B
Treg induction with naive CD4⁺T cells from fat

CD25⁺⁺Foxp3 GFP⁺ [% of CD4⁺ T cells]

- standard diet / HFHS diet [2 wks]
- standard diet / HFHS diet [2 wks]
- standard diet / HFHS diet [2 wks]

C
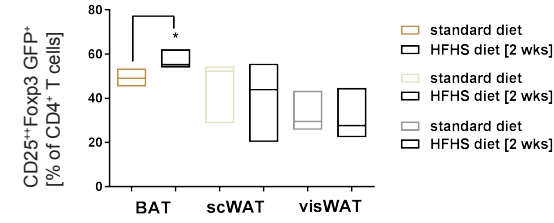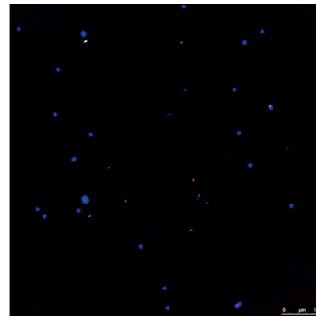
negative control NaCl · **negative control** CL [1 mg/kg, *i.p.*]
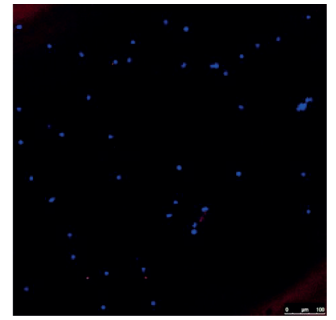
D
mRNA abundance of BAT after ADRB3 stimulation *in vivo*

$20 - \Delta Cq$

Ucp1, Adrb3, Ppargc1a, Pparg, Ppara, Prdm16, Cidea, Acsl1, Lpl, Lipe, Acox1

□ control
■ ADRB3 stimulation

E
control · **Treg depletion by mCD25 antibodies**

Tregs residing in BAT
Foxp3, CD25 subset 12,0% · Foxp3, CD25 subset 0,00%

Tregs residing in scWAT
Foxp3, CD25 subset 16,9% · Foxp3, CD25 subset 1,92%

Tregs residing in visWAT
Foxp3, CD25 subset 11,5% · Foxp3, CD25 subset 2,36%

CD25 / Foxp3
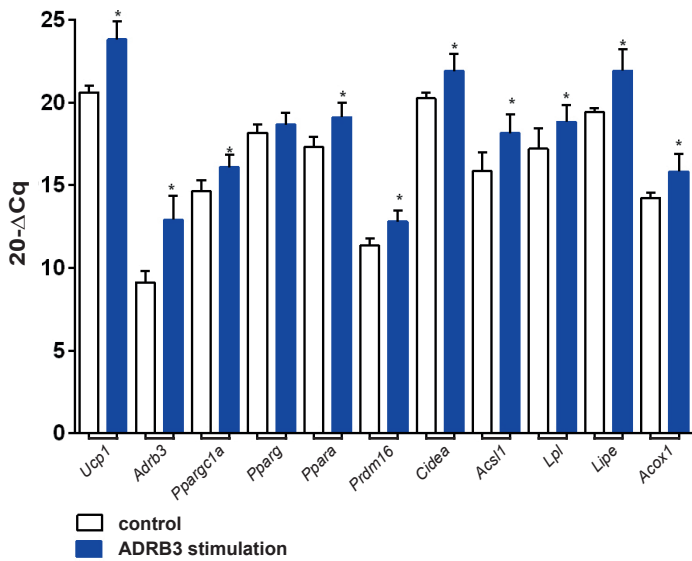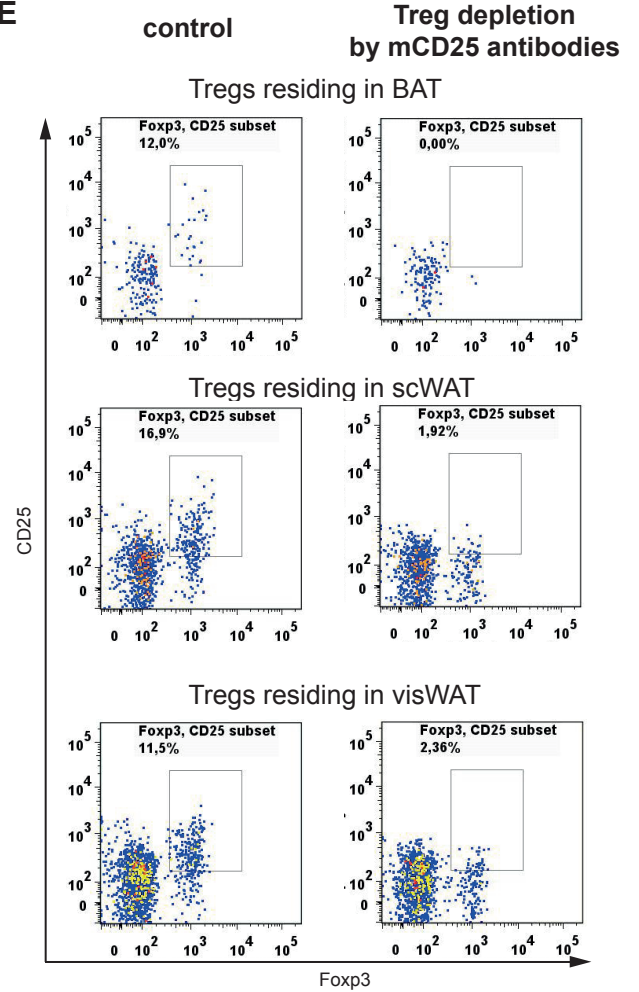
F
mRNA abundance of BAT after ADRB3 stimulation *in vivo* in the presence or absence of Tregs

$20 - \Delta Cq$

Plin, Cycs, P2rx5, Glut1, Adipoq

□ ADRB3 stimulation
□ ADRB3 stimulation + Treg depletion
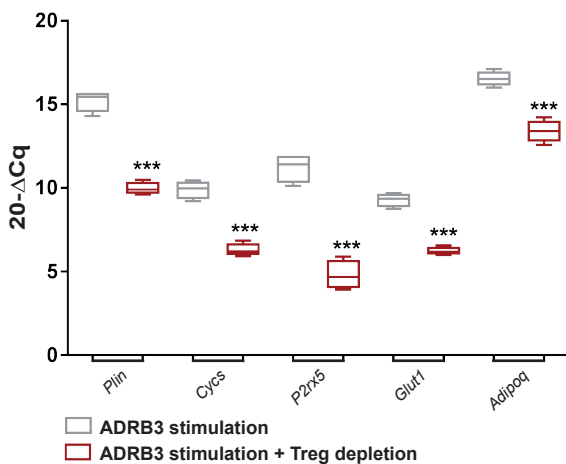
Figure S1 related to Figures 1-3: Treg enhancement by ADRB3 stimulation is required for adipose tissue function.

(**A+B**) (A) Representative FACS plots for *in vitro* Treg induction assays using limited TCR stimulation and naïve CD4$^+$T cells purified from BAT, scWAT and visWAT of BALB/c mice on standard diet or upon 2 wk of HFHS diet. (B) Quantification of (A). n=4.

(**C**) Confocal microscopy images for negative control stainings of CD3 and Foxp3. Shown are stainings with secondary antibodies in the absence of primary antibodies using CD4$^+$T cells from mice kept at room temperature or subjected to 3 d of 1mg/kg CL. Scale bar = 100 μm.

(**D**) mRNA expression of genes involved in BAT tissue function upon treatment of BALB/c mice with CL [2 d, 1 mg/kg, *i.p.*] *in vivo*. n=6 per group.

(**E**) Representative FACS plots demonstrating Treg depletion efficacy in fat depots after 3 d of anti-CD25 antibody treatment.

(**F**) mRNA expression of genes involved in BAT function after ADRB3 stimulation (3 d, 1 mg/kg CL, *i.p.*) in the presence or absence of Tregs. Tregs were depleted using anti-CD25 antibodies. n=4 per group.

Data are presented as box-and-whisker plots with min and max values for data distribution. * = $p<0.05$, *** = $p<0.001$.
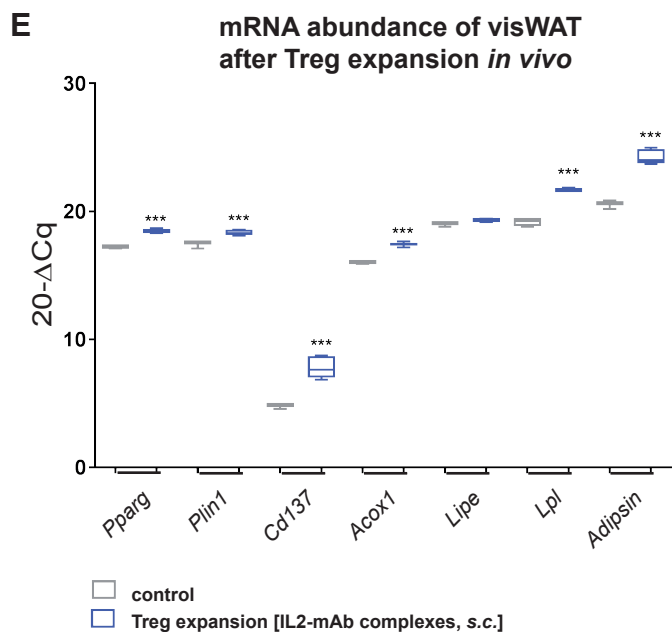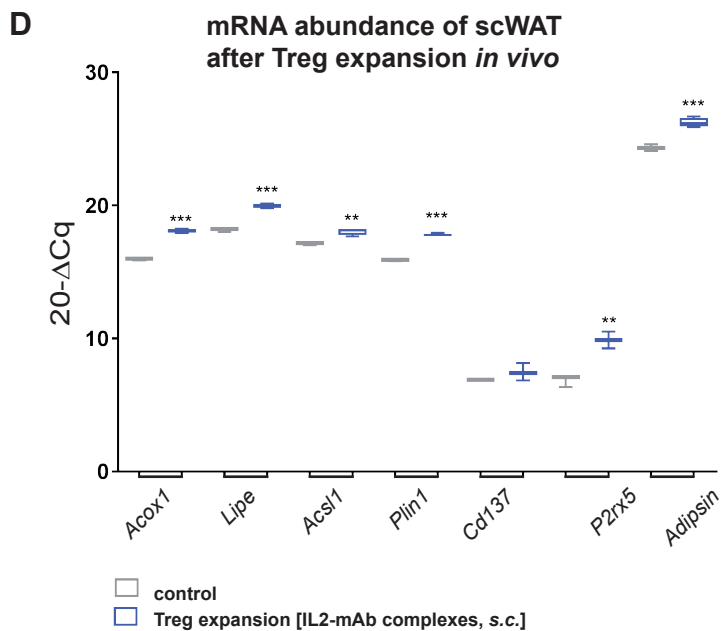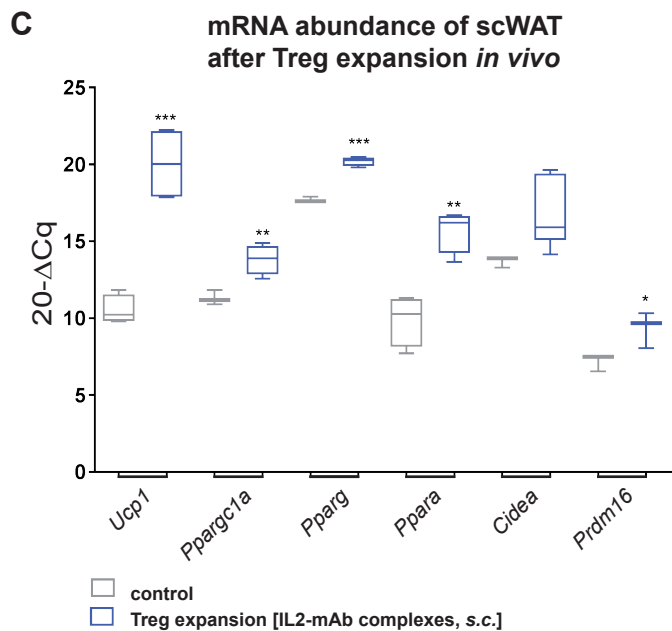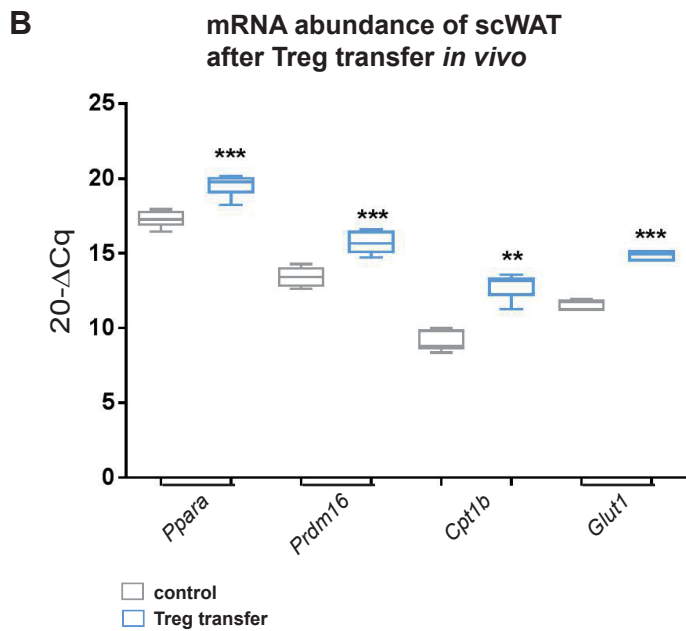
Figure S2

A mRNA abundance of BAT after HFHS diet [1 wk] in the presence or absence of Tregs

□ HFHS diet [1 wk]
□ HFHS diet [1 wk] + prior Treg depletion

B mRNA abundance of scWAT after HFHS diet [1 wk] in the presence or absence of Tregs

□ HFHS diet [1 wk]
□ HFHS diet [1 wk] + prior Treg depletion

C

Tregs residing in BAT | Tregs residing in scWAT | Tregs residing in visWAT
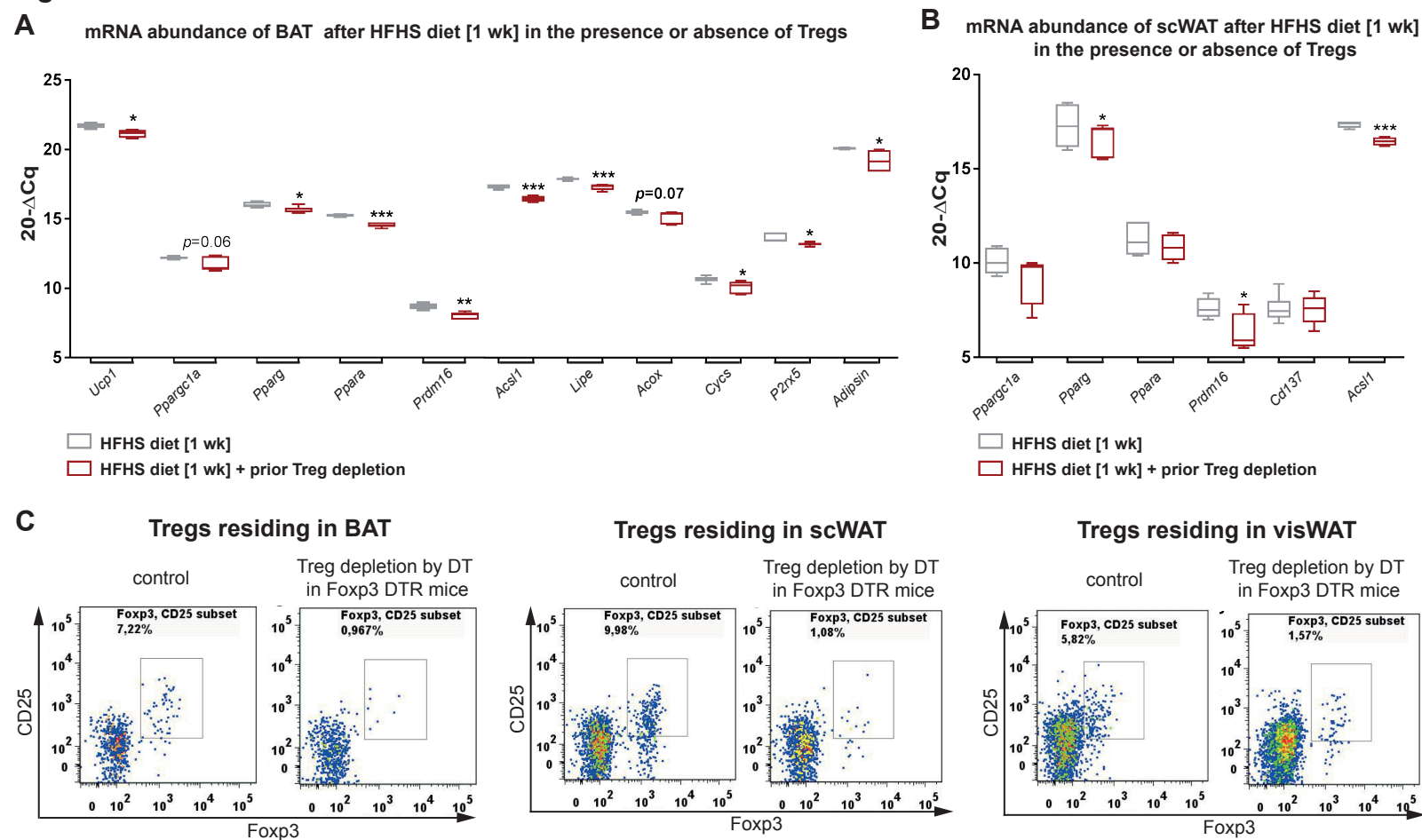
Figure S2 related to Figure 3: Diet-induced thermogenesis in adipose tissue is impaired in the absence of Tregs.

(**A**+**B**) Analysis of mRNA abundance of genes involved in BAT (A) and scWAT (B) function after 1 wk HFHS diet with or without additional Treg depletion. Treg depletion was achieved by using anti-CD25 antibodies. n=6 per Treg-complete group, n=4 for Treg-depleted group.

(**C**) Representative FACS plots demonstrating Treg depletion efficacy in BAT, scWAT and visWAT 48 h after administration of DT.

Data are presented as box-and-whisker plots with min and max values for data distribution. * = $p<0.05$, ** = $p<0.01$, *** = $p<0.001$.

Figure S3

A mRNA abundance of BAT after Treg transfer *in vivo*

B mRNA abundance of scWAT after Treg transfer *in vivo*

C mRNA abundance of scWAT after Treg expansion *in vivo*

D mRNA abundance of scWAT after Treg expansion *in vivo*

E mRNA abundance of visWAT after Treg expansion *in vivo*
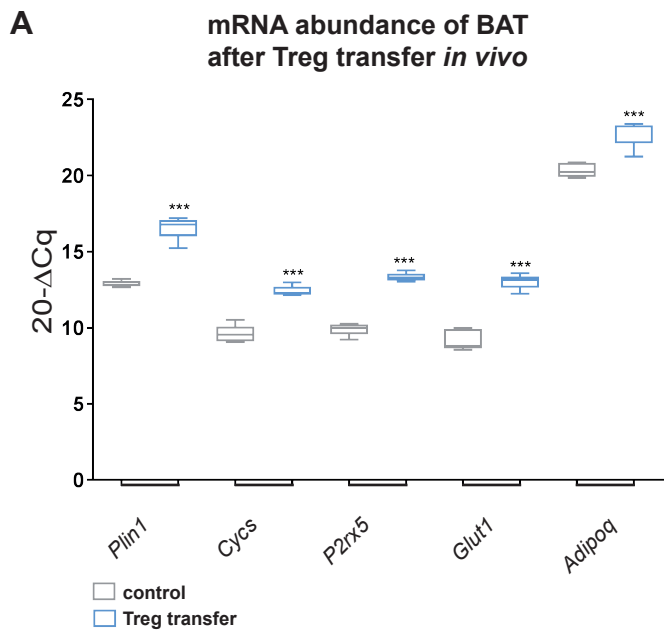
**Figure S3 related to Figure 3: Role of transferred or expanded Tregs for adipose tissue function.**

(**A+B**) In gain-of-function experiments, $CD4^+CD25^{++}Foxp3GFP^+$Tregs were adoptively transferred into congenic recipients. Analysis of BAT (A) and scWAT (B) function by RT-qPCR was performed 1 wk after transfer. n=5 per group.

(**C-E**) A selective expansion of $Foxp3^+$Tregs was assessed using IL-2-mAb complexes [3 d, 6 µg per injection, *s.c.*]. Analysis of scWAT (C+D) and visWAT (E) function was analyzed by RT-qPCR. n=4 per group.

Data are presented as box-and-whisker plots with min and max values for data distribution. * = $p<0.05$, ** = $p<0.01$, *** = $p<0.001$.

Figure S4

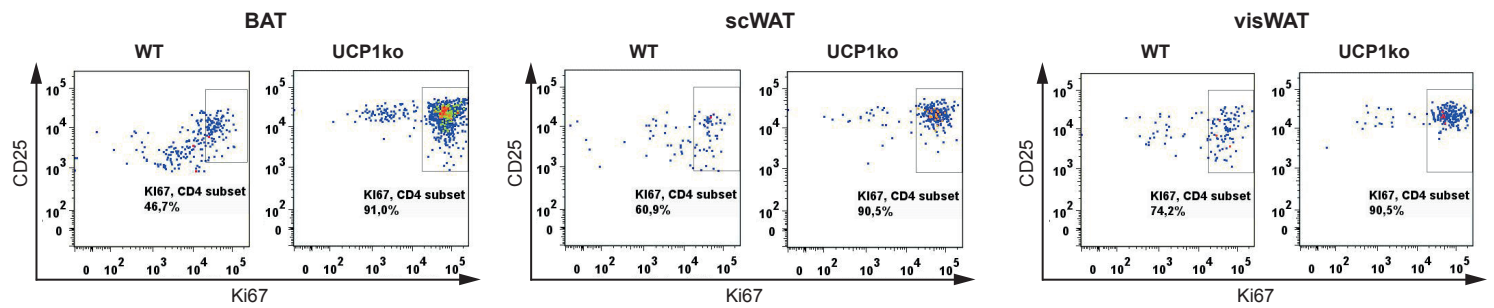**A** Fat-residing CD4$^+$CD25^{++}Foxp3$^+$Tregs purified from
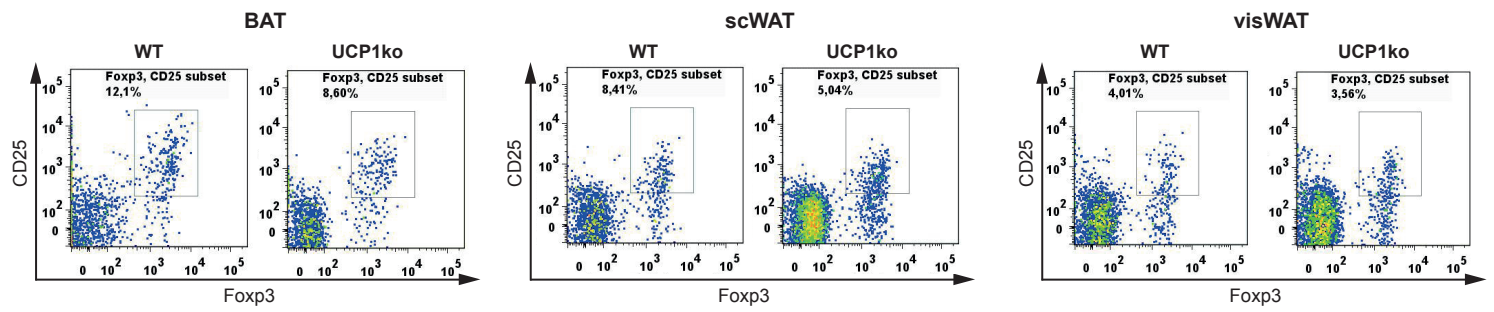
B Treg induction with naive CD4$^+$CD25$^-$CD44^{low}T cells from fat
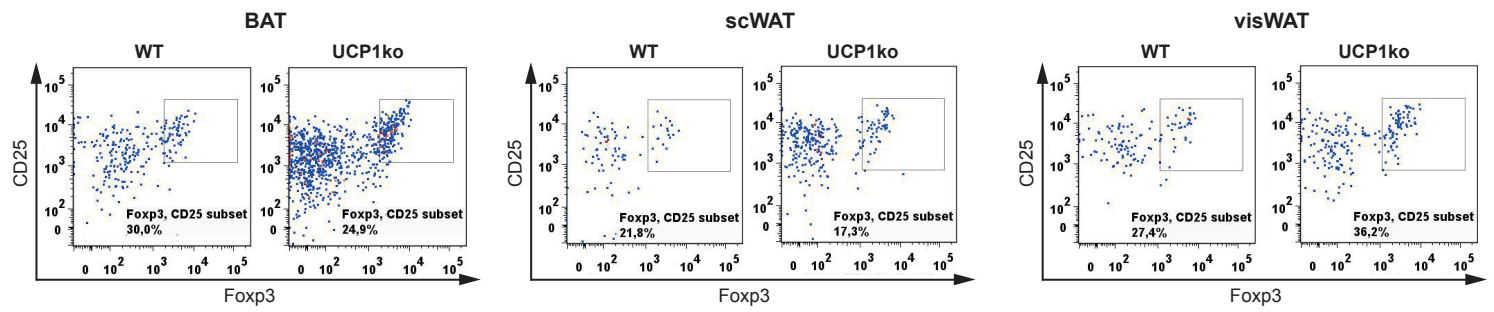
C Proliferative status of CD4$^+$T cells during Treg induction with naive CD4$^+$CD25$^-$CD44^{low} from fat
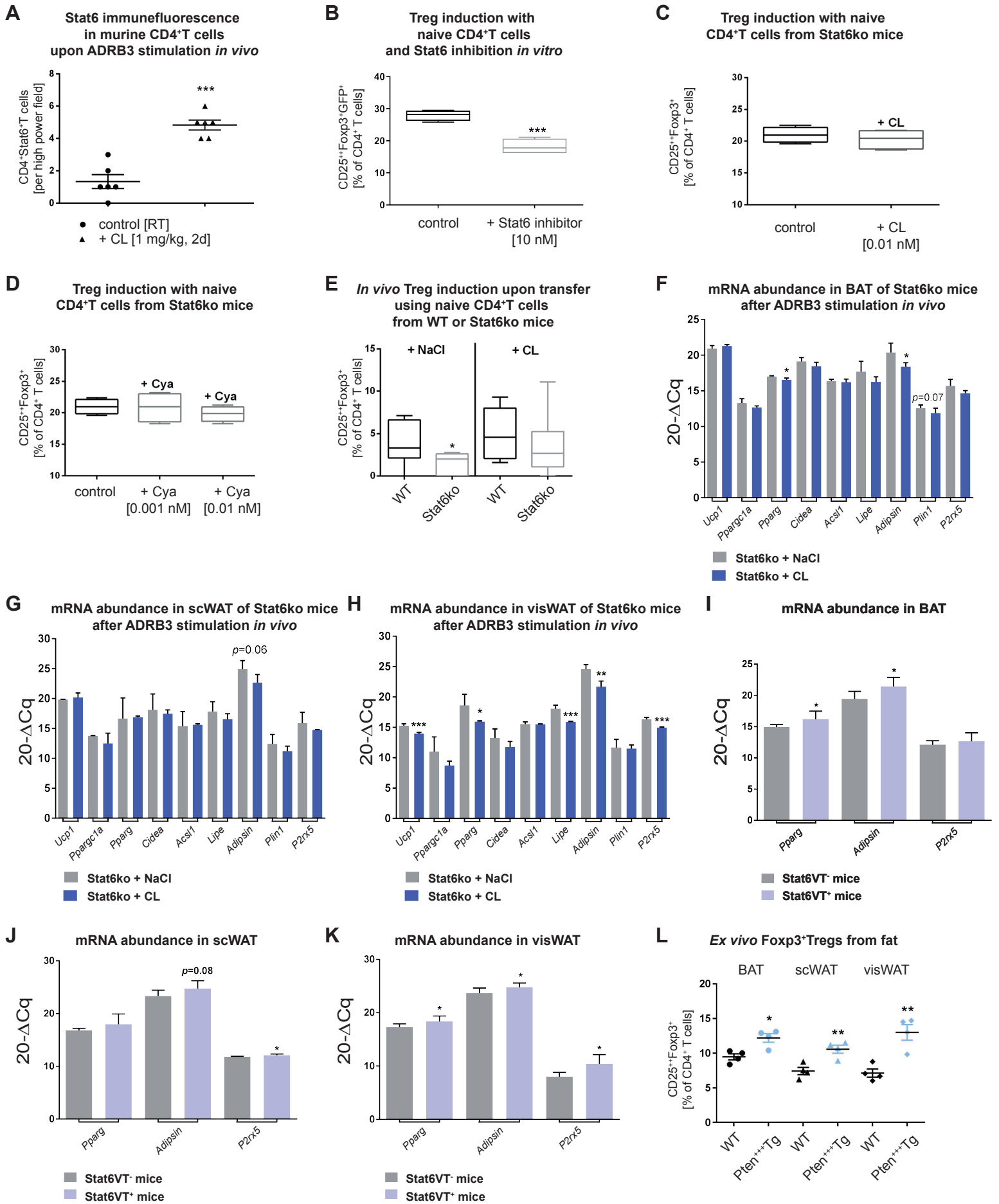
Figure S4 related to Figure 3: Impaired Treg enhancement in the absence of UCP1.

(**A**) Representative FACS plots for the identification of *ex vivo* CD4$^+$CD25^{++}Foxp3$^+$Tregs from fat depots of WT or UCP1ko mice.

(**B**) Representative FACS plots for *in vitro* Treg induction assays using limited TCR stimulation and naïve CD4$^+$T cells purified from BAT, scWAT and visWAT of WT or UCP1ko animals.

(**C**) Representative FACS plots depicting the proliferative status of CD4$^+$T cells during Treg induction assays from (B).

Figure S5

A Stat6 immunefluorescence in murine CD4⁺T cells upon ADRB3 stimulation *in vivo*

B Treg induction with naive CD4⁺T cells and Stat6 inhibition *in vitro*

C Treg induction with naive CD4⁺T cells from Stat6ko mice

D Treg induction with naive CD4⁺T cells from Stat6ko mice

E *In vivo* Treg induction upon transfer using naive CD4⁺T cells from WT or Stat6ko mice

F mRNA abundance in BAT of Stat6ko mice after ADRB3 stimulation *in vivo*

G mRNA abundance in scWAT of Stat6ko mice after ADRB3 stimulation *in vivo*

H mRNA abundance in visWAT of Stat6ko mice after ADRB3 stimulation *in vivo*

I mRNA abundance in BAT

J mRNA abundance in scWAT

K mRNA abundance in visWAT

L *Ex vivo* Foxp3⁺Tregs from fat

Figure S5 related to Figures 4+5: Role of Stat6 in Treg accumulation of fat-residing CD4$^+$T cells.

(**A**) Summary graph for the enumeration of CD4$^+$Stat6$^+$T cells per high power field as assessed by immunefluorescence using CD4$^+$T cells from mice treated with CL [2 d, 1 mg/kg] or NaCl. n=6 per group.

(**B**) Summary graph of Stat6 inhibition for *in vitro* Treg induction assays of naïve CD4$^+$T cells purified from inLNs of BALB/c Foxp3 GFP reporter mice. n=4 per condition.

(**C+D**) *In vitro* Treg induction assay of naïve CD4$^+$T cells from inLNs of Stat6ko mice using limited TCR stimulation after *in vitro* stimulation with CL [0.01 nM] (C) or a titration of Cya [0.001 nM and 0.01 nM] (D). n=4 per condition.

(**E**) Summary graph for analysis of CD25^{++}Foxp3$^+$Tregs after *in vivo* Treg induction using adoptive T cell transfer of naïve CD4$^+$T cells from WT or Stat6ko mice in congenic CD90.1 BALB/c recipients with or without stimulation with CL (3 d, 1 mg/kg, *i.p.*). n=8 per group.

(**F-H**) mRNA expression of genes involved in BAT (F), scWAT (G) and visWAT (H) function after *in vivo* ADRB3 stimulation (3 d, 1 mg/kg CL) in Stat6ko animals. n=4 per group.

(**I-K**) mRNA expression in BAT (I), scWAT (J) and visWAT (K) of Stat6VT+ vs. Stat6VT- animals. n= 6 per group.

(**L**) Identification of *ex vivo* CD4$^+$CD25^{++}Foxp3$^+$Tregs purified from BAT, scWAT and visWAT of WT or PtenTg mice that had ~40-fold higher *Pten* expression compared to WT mice. n= 4 per group.

Data are presented as box-and-whisker plots with min and max values for data distribution or as mean±SEM. * = $p<0.05$, ** = $p<0.01$, *** = $p<0.001$.

Table S1 related to STAR Methods.

gene	forward	reverse	source
Histone	5'-ACTGGCTACAAAAGCCG-3'	5'-ACTTGCCTCCTGCAAAGCAC-3'	Sigma Aldrich
Ucp1	5'-GGCCTCTACGACTCAGTCCA-3'	5'-TAAGCCGGCTGAGATCTTGT-3'	Sigma Aldrich
Adrb3	5'-AACTGAAACAGCAGACAGGGAC-3'	5'-CCCCCATGTACACCCTAGTT-3'	Sigma Aldrich
Ppargc1a	5'-GCAACATGCTCAAGCCAAAC-3'	5'-TGCAGTTCCAGAGAGTTCCA-3'	Sigma Aldrich
Pparg	5'-GCCCTTTGGTGACTTTATGGA-3'	5'-CAGCAGGTTGTCTTGGATG-3'	Sigma Aldrich
Ppara	5'-GCCTGTCTGTCGGGATGT-3'	5'-GGCTTCGTGGATTCTCTTG-3'	Sigma Aldrich
Prdm16	5'-CAAGTGCCATCTGTGCAACC-3'	5'-TTCGAGTGGATGCCTGGTTC-3'	Sigma Aldrich
Cidea	5'-TCAGACCTTAAGGGACAACACGCA-3'	5'-TTCTTTGGTTGCTTGCAGACTGGG-3'	Sigma Aldrich
Lipe	5'-GGCTCACAGTTACCATCTCACC-3'	5'-GAGTACCTTGCTGTCCTGTCC-3'	Sigma Aldrich
Lpl	5'-CCCCAGTCGCCTTTCTCCTGAT-3'	5'-CTCTTGGCTCTGACCTTGTTGAT-3'	Sigma Aldrich
Acsl1	5'-ACCACCTTCTGGTATGCCAC-3'	5'-TGACATCGTCGTAGTAGTACACC-3'	Sigma Aldrich
Acox1	5'-CAGGAAGAGCAAGGAAGTGG-3'	5'-CCTTTCTGGCTGATCCCATA-3'	Sigma Aldrich
Il6	5'-AGCCCACCAAGAACGATAGTC-3'	5'-GCATCAGTCCCAAGAAGGCA-3'	Sigma Aldrich
Stat6	5'-ACCTGTCCATTCGCTCACTG-3'	5'- ATCTGGGGCTCTGGAGTAGG-3'	Sigma Aldrich
Borcs6	5'-AAGCCGTGGACATGAGCATT-3'	5'-CAGCAAGCAGTTTCCACCAG-3'	Sigma Aldrich
18s	N/A	N/A	Quantitect Primer Assay (Qiagen)
Pten	N/A	N/A	Quantitect Primer Assay (Qiagen)
Adipsin	5'-AACCGGACAACCTGCAATCT-3'	5'-GAGTCTCCCCTGCAAGTGTC-3'	Sigma Aldrich
Cd137	5'-GGTGGACAGCCGAACTGTAA-3'	5'-AACCCTGCTTCGTTAGCTCC-3'	Sigma Aldrich
P2rx5	5'-CTGCAGCTCACCATCCTGT-3'	5'-CACTCTGCAGGGAAGTGTCA-3'	Sigma Aldrich
Cycs	5'-GAACAAGTGTGGTTGCACCG-3'	5'-ATGCTTGCCTCCCTTTTCCA-3'	Sigma Aldrich
Plin1	5'-AGATCCCGGCTCTTCAATACC-3'	5'-AGAACCTTGTCAGAGGTGCTT-3'	Sigma Aldrich

Primer sequences used for qPCR analyses.

7.2 Published manuscript: Becker et al., Molecular Metabolism 2019

MOLECULAR
METABOLISM

Short-term cold exposure supports human Treg induction *in vivo*

Maike Becker [1,2], Isabelle Serr [1,2], Victoria K. Salb [1,2], Verena B. Ott [1,2,3], Laura Mengel [4], Matthias Blüher [5], Benno Weigmann [6], Hans Hauner [2,4,7], Matthias H. Tschöp [2,3,8], Carolin Daniel [1,2,9,*]

ABSTRACT

Objective: Obesity and type-2 diabetes (T2D) are metabolic diseases that represent a critical health problem worldwide. Metabolic disease is differentially associated with fat distribution, while visceral white adipose tissue (VAT) is particularly prone to obesity-associated inflammation. Next to their canonical function of immune suppression, regulatory T cells (Tregs) are key in controlling adipose tissue homeostasis. Towards understanding the molecular underpinnings of metabolic disease, we focus on how environmental-metabolic stimuli impinge on the functional interplay between Tregs and adipose tissue. Here, cold exposure or beta3-adrenergic signaling are a promising tool to increase energy expenditure by activating brown adipose tissue, as well as by reducing local inflammation within fat depots by supporting immunosuppressive Tregs. However, in humans, the underlying mechanisms that enable the environmental-immune crosstalk in the periphery and in the respective tissue remain currently unknown.

Methods: We used combinatorial approaches of next generation humanized mouse models and *in vitro* and *in vivo* experiments together with beta3-adrenergic stimulation to dissect the underlying mechanisms of human Treg induction exposed to environmental stimuli such as cold. To test the translational relevance of our findings, we analyzed samples from the FREECE study in which human subjects were exposed to individualized cooling protocols. Samples were analyzed *ex vivo* and after *in vitro* Treg induction using qRT-PCR, immunofluorescence, as well as with multicolor flow cytometry and cell sorting.

Results: *In vivo* application of the beta3-adrenergic receptor agonist mirabegron in humanized mice induced thermogenesis and improved the Treg induction capacity of naïve T cells isolated from these animals. Using samples from the human FREECE study, we demonstrate that a short-term cold stimulus supports human Treg induction *in vitro* and *in vivo*. Mechanistically, we identify *BORCS6* encoding the Ragulator-interacting protein C17orf59 to be significantly induced in human CD4^{+} T cells upon short-term cold exposure. Strong mTOR signaling is known to limit successful Treg induction and thus likely by interfering with mTOR activation at lysosomal surfaces, C17orf59 improves the Treg induction capacity of human naïve T cells upon cold exposure.

Conclusions: These novel insights into the molecular underpinnings of human Treg induction suggest an important role of Tregs in linking environmental stimuli with adipose tissue function and metabolic diseases. Moreover, these discoveries shed new light on potential approaches towards tailored anti-inflammatory concepts that support human adipose tissue homeostasis by enabling Tregs.

1. INTRODUCTION

Obesity and Type 2 diabetes (T2D) are metabolic diseases that represent critical health threats to modern societies. Metabolic disease is differentially associated with local fat depots, with visceral white adipose tissue (VAT) being especially prone to obesity-associated inflammation [1].

In addition to their critical role of immune suppression, regulatory T cells (Tregs) are key in controlling tissue homeostasis and function

including local fat depots. Tregs are characterized by the expression of CD4, CD25, and the transcription factor FOXP3, which functions as the master regulator for their function and development [2,3]. Mutations in the *Foxp3* gene have deleterious consequences, leading to autoimmune and severe inflammatory phenotypes in both mice (*scurfy* mice) and humans (IPEX — immunodysregulation, polyendocrinopathy, enteropathy, X-linked syndrome), highlighting the crucial role of Foxp3 for Treg function [4—6]. In humans, activated T cells can express low

[1]Institute for Diabetes Research, Group Immune Tolerance in Diabetes, Helmholtz Diabetes Center at Helmholtz Zentrum München, German Research Center for Environmental Health, Munich-Neuherberg, Germany [2]German Center for Diabetes Research (DZD), Munich, Germany [3]Institute for Diabetes and Obesity, Helmholtz Diabetes Center at Helmholtz Zentrum München, Munich-Neuherberg, Germany [4]ZIEL-Institute for Food & Health, Else Kröner-Fresenius Zentrum für Ernährungsmedizin, Technische Universität München, Freising-Weihenstephan, Germany [5]Department of Medicine, University of Leipzig, Leipzig, Germany [6]Department of Medicine 1, University of Erlangen-Nuremberg, Kussmaul Campus for Medical Research, Erlangen, Germany [7]Institute for Nutritional Medicine, Klinikum rechts der Isar, Technical University of Munich, Munich, Germany [8]Division of Metabolic Diseases, Department of Medicine, Technische Universität München, Munich, Germany [9]Division of Clinical Pharmacology, Department of Medicine IV, Ludwig-Maximilians-Universität München, Munich, Germany

*Corresponding author. Institute for Diabetes Research, Helmholtz Zentrum München, German Research Center for Environmental Health (GmbH), Ingolstädter Landstraße 1, 85764, Neuherberg, Germany. E-mail: carolin.daniel@helmholtz-muenchen.de (C. Daniel).

Original Article

amounts of FOXP3 [7,8], while immunosuppressive Tregs are characterized by high expression of FOXP3 together with low expression of CD127 [9,10]. Here, FOXP3 confers suppressive capacity by ensuring the expression of immunosuppressive molecules such as CTLA-4, LAG3, and IL-10 [11].

Tregs can be induced in the peripheral immune system, a process referred to as Treg conversion or induction [12]. Efficient Treg induction from naïve CD4$^+$ T cells can be achieved using antigenic stimulation under so-called subimmunogenic conditions avoiding the activation of antigen-presenting cells and T cells [13,14]. In contrast, immunogenic stimulation and strong costimulatory signals activate the phosphoinositide 3 kinase (PI3K)/Akt/mechanistic target of the rapamycin (mTOR) pathway, thereby interfering with Treg induction [12,13,15—19].

In order to maintain local homeostasis, Tregs take residence in tissues such as VAT, followed by tissue-specific adaptations of their functions, e.g. by expression of the transcription factor Peroxisome proliferator-activated receptor gamma (PPARγ) [20]. Adipocytes are surrounded by several immune cell types. Immune cell type, number, and function dramatically change in VAT following overnutrition. Fat-residing Tregs control local inflammatory processes. Specifically, upon hypercaloric challenge Treg frequencies in VAT are severely reduced accompanied by increased inflammation [21].

Importantly, Tregs possess the ability to respond to environmental and metabolic signals. It is becoming increasingly evident that the disruption of these interactions between immune and environmental-metabolic responses critically contributes to the emergence of metabolic diseases.

Towards understanding the molecular underpinnings of these metabolic diseases, we have recently provided an example of how environmental-metabolic stimuli impinge on the functional interplay between Tregs and adipose tissue [22]. Specifically, and in line with a critical role of cold exposure in interfering with metabolic impairments in obesity, we recently showed that short-term cold exposure or beta3-adrenergic stimulation induce murine Tregs *in vitro* as well as *in vivo* [22].

In line with these observations, another study had suggested an impact of cold exposure on brown adipose tissue (BAT) Tregs [23]. Mechanistically, using CD4$^+$ T cell proteomes, we uncovered Treg induction and higher protein expression of Foxp3 regulatory networks following cold exposure or beta3-adrenergic stimulation [22]. Using loss- and gain-of-function studies we highlighted that a T cell-specific Stat6/ Pten axis adjusts Foxp3$^+$Treg induction and adipose tissue function according to the degree of sympathetic tone and environmental temperature [22].

In contrast to white adipose tissue, the main function of which is the storage of lipids, BAT critically contributes to non-shivering thermo-genesis (NST), burns energy, and dissipates heat. This is facilitated by the expression of uncoupling protein 1 (UCP1) that uncouples mito-chondrial respiration from ATP synthesis [1]. Upon exposure to cold or beta3-adrenergic stimulation, white adipocytes can undergo a process referred to as browning that induces the expression of UCP1 in white adipocytes [24].

In humans, recent studies have uncovered cold-inducible BAT in adults [25,26]. Stimulating BAT energy expenditure through activation of the beta3-adrenergic receptor (ADRB3), which is expressed on human adipocytes and other tissues including human peripheral blood mononuclear cells [26,27] was also achieved by the ADRB3 agonist mirabegron [28,29]. Moreover, cold exposure was shown to provide beneficial effects on whole-body and skeletal muscle insulin sensitivity in patients with obesity and T2D [30]. Accordingly, mirabegron was reported to stimulate human BAT thermogenesis and may therefore be a promising future treatment option for metabolic disease [31].

Despite these mechanistic insights in Treg adipose crosstalk in the murine setting together with research efforts focusing on metabolic readouts upon cold exposure in humans, the impact of human Tregs in guiding the functional immunometabolic interplay in response to cold exposure *in vivo* remains currently unknown.

To fill this knowledge gap, here we studied human Treg induction following beta3-adrenergic stimulation in next generation humanized mice as well as upon short-term cold exposure in humans. Specifically, we report that a short-term cold stimulus improves human Treg induction *in vitro* and *in vivo*. Mechanistically, we find that *BLOC-1 related complex subunit 6 (BORCS6)* encoding the Ragulator-interacting protein C17orf59 is significantly enhanced in human CD4$^+$ T cells upon short-term cold exposure. C17orf59 was demonstrated to interfere with mTORC1 activity [32], thereby likely supporting enhanced Treg induction.

2. MATERIAL AND METHODS

2.1. Mice

Humanized mice lack murine MHC class II and transgenically express human HLA-DQ8 or HLA-DR4 (#026561 NOD.Cg-$Prkdc^{scid}H2$-$Ab1^{tm1Doi}Il2rg^{tm1Wjl}$Tg (HLA-DQA1,HLA-DQB1)1Dv/SzJ and #017637 NOD.Cg-$Prkdc^{scid}Il2rg^{tm1Wjl}H2$-$Ab1^{tm1Doi}$Tg (HLA-DRB1)31Dmz/SzJ, Jackson Laboratories, (herein abbreviated as NSG)) were reconstituted with 10^7 PBMCs from healthy subjects. Mice were maintained group-housed on a 12 h/12 h light dark cycle at 25 °C under specific

pathogen free (SPF) conditions and had *ad libitum* access to food (Altromin, #1314, Lage, Germany) and water. Mice were randomized to test groups. For *in vivo* beta3-adrenergic stimulation, mice were injected *i.p.* with 1 mg/kg mirabegron (Selleckchem, CAS 223673-61-8) on three consecutive days two weeks after reconstitution. 0.9% NaCl was used as vehicle control. No animals were excluded due to illness or outlier results; therefore, no exclusion determination was required. The investigators were not blinded to group allocation or to the assessment of experimental end points. All animal care was executed according to guidelines established by the Institutional Animal Committees. Ethical approval for all mouse experimentations has been received by corresponding local animal welfare authorities (*approval number #ROB-55.2-2532.Vet_02-17-130*, District Government of Upper Bavaria, Germany).

2.2. Human subjects and samples

Venous blood was collected from healthy adults (n = 2, females, age 25) who consented to the Munich Bioresource project (approval number #5049/11, Technische Universität München, Munich, Germany) in heparinized blood collection tubes (BD Vacutainer Blood Collection Tubes, Becton Dickinson).

For RT-qPCR analyses of human paired samples of subcutaneous (SAT) and omental AT (VAT), samples were obtained from lean individuals (n = 6, mean BMI: 23.2 kg/m^2). Phenotypic characterization of the study participants and AT sample collection during open or laparoscopic abdominal surgery was performed as previously described [33]. The study was approved by the Ethics Committee of the University of Leipzig (*approval number #159-12-21052012* and *#017-12-23012012*) and performed in accordance to the declaration of Helsinki.

For *in vivo* cold exposure in the FREECE study, subjects were recruited at the Institute for Nutritional Medicine, Technical University of Munich, Munich, Germany. The study protocol was approved by the ethical committee of the Faculty of Medicine of the Technical University of Munich (*approval number 236/16S* and *113/19S*), and registered at the German Clinical Trials Register (*ID: DRKS00010489*). This ongoing study examines the effects of short-term mild cold exposure on thermogenesis and metabolism of healthy individuals. Inclusion criteria were healthy non-smoking adults. Exclusion criteria were severe diseases (such as diagnosed hypertension or established diabetes), pregnancy or lactation, weight gain or loss of more than 3% of body weight within 3 months and more than 10 h rigorous exercise per week. The study was conducted at both locations of the Institute for Nutritional Medicine in Munich and in Freising, Germany.

For needle aspiration fat biopsy, participants were invited one week prior to the examinations. Subjects were informed in detail about the procedure and written informed consent was obtained. Blood was drawn to test for the prothrombin time, and the abdomen was examined for sufficient SAT by the study physicians. Subjects were studied in the morning after a 10-hour overnight fast, and subjects were not allowed to exercise 24 h prior to the study nor to drink any caffeinated beverages or alcohol. Upon arrival, height was measured using a stadiometer (Seca, Hamburg, Germany) to the nearest 0.1 cm. Body weight and body composition were measured using the TANITA Body Composition Analyser Type BC-418 MA (Tanita Europe GmbH, Sindelfingen, Germany). Measurements were performed barefoot, in underwear, and after voiding the urinary bladder. Nine wireless iBut-tons were attached to the skin to measure skin temperature. Core temperature was monitored by a zero-heat flux thermometer, which was attached to the forehead.

Resting energy expenditure was determined via indirect calorimetry for 30 min under thermoneutral conditions using a ventilated hood system (COSMED Quark RMR, Fridolfing, Germany). The conversion of the measurements of VO$_2$ (consumption of oxygen (ml/min)) and VCO$_2$ (production of CO$_2$ (ml/min)) to energy expenditure [kcal/day] was done by application of the shortened Weir equation [34].

For the individualized cooling protocol, subjects lay between two water-perfused mattresses in a supine position. Water temperature was gradually decreased until subjects reported shivering. Subsequently, water temperature was increased for 2 °C to prevent muscle shivering. Subjects remained for 2 h between the mattresses at this temperature and another 30 min for the second indirect calorimetry (in total 150 min).

Blood was drawn and fat biopsy samples were taken directly after each indirect calorimetry. To obtain 1–2 g of SAT, the paraumbilical area was treated with lidocaine and tissue was obtained by needle biopsy. 0.3–0.8 g AT were used for flow cytometric analyses.

Where indicated, subjects were grouped according to their BMI in lean (BMI <25 kg/m^2), overweight (25 kg/m^2 ≤ BMI < 30 kg/m^2) and obese (BMI ≥ 30 kg/m^2).

Immediately after each indirect calorimetry, blood was taken (EDTA KE monovettes, Nümbrecht, Sarstedt) and centrifuged at 2,500 g for 10 min at room temperature. An enzyme-linked immunosorbent assay was used to determine plasma leptin levels (Duoset ELISA human, R&D, Wiesbaden, Germany).

For human studies, written informed consent was obtained from all subjects and experiments were carried out in accordance with the Declaration of Helsinki.

For subject biometrics, please see Table 1.

2.3. Isolation of CD4$^+$ T cells from murine lymphoid organs

Lymph nodes and spleens were mashed through 70 μm cell strainers in HBSS$^+$ (supplemented with 5% FCS and 10 mM HEPES) and further processed for flow cytometry.

2.4. Human T cell isolation from blood

Venous blood was collected in heparinized tubes. Peripheral blood mononuclear cells (PBMCs) were isolated by density centrifugation over Ficoll-Paque PLUS (GE Healthcare). Human CD4$^+$ T cells were isolated from fresh PBMCs via MACS enrichment with CD4$^+$ microbeads following the manufacturer's protocol. For cytospins, untouched EasySep human CD4$^+$ T cell enrichment kit (Stem Cell) was used according to the manufacturer's instructions.

2.5. Isolation of CD4$^+$ T cells from human SAT

SAT biopsies were collected by needle aspiration, washed intensively with 0.9% NaCl to remove blood contaminants, stored in PBS supplemented with 0.5% BSA and digested with collagenase II solution (4 mg/ml collagenase II, Sigma Aldrich, EC#3.4.24.3 and 10 mM CaCl$_2$) for 5–9 min at 37 °C in a water bath, slightly shaking. Cell suspensions were passed through a 200 μm nylon mesh and

Table 1 — Subject biometrics analyzed from the FREECE study.

FREECE	subjects	range
n (males/females)	29 (11/18)	
age males (mean ± SD)	29.4 ± 8.9	(22–51)
age females (mean ± SD)	30.1 ± 8.3	(20–52)
BMI males (mean ± SD)	30.2 ± 6.8	(21.5–40.6)
BMI females (mean ± SD)	32.3 ± 7.2	(19.7–47.6)

centrifuged ($380 \times g$, 5 min, 4 °C) to separate the stromal vascular fraction from adipocytes. Pelleted cells were re-suspended in HBSS$^+$ and stained for flow cytometric analysis.

2.6. Cell staining for flow cytometry

Following antibodies were used for flow cytometry (reactivity, fluorochrome, clone, manufacturer): CD11B, Pacific Blue, ICRF44, BioLegend; CD127, PE-Cy7, A019D5, BioLegend; CD14, Pacific Blue, HCD14, BioLegend; CD19, Pacific Blue, HIB19, BioLegend; CD25, APC, 2A3, BD Biosciences; CD3, PerCP-Cy5.5, HIT3a, BioLegend; CD3, Alexa Fluor 700, HI30, BioLegend; CD4, V500, RPA-T4, BD Biosciences; CD62L, PE, DREG-56, BioLegend; CD45RA, FITC, HI100, BioLegend; CD45RO, APC-H7, UCHL1, BD Biosciences; CD8A, Pacific Blue, RPA-T8, BioLegend; FOXP3, Alexa Fluor 700, PCH101, eBioscience; FOXP3, PE, 236A/E7, eBioscience; KI67, APC, 16A8, BioLegend; KI67, Brilliant Violet 605, 16A8, BioLegend. Unspecific binding of antibodies was prevented by incubation of cell suspensions with Fc-Block (Human TruStain FcX, BioLegend, 1:20) for 5 min at RT, followed by FACS staining for 20 min at RT in the dark. Cells were passed through a 40 μm cell strainer (NeoLab) to remove large debris.

To detect intracellular protein expression, T cells were fixed and permeabilized using the Foxp3 Staining Buffer Set (eBioscience) after surface staining as recommended by the manufacturer.

Cells were acquired on BD FACSArialII flow cytometer using FACSDiva software V6.1.3 or V8.0.1 with optimal compensation and gain settings based on unstained and single-color stained samples. Doublets were excluded based on SSC-A vs. SSC-W and FSC-A vs. FSC-W plots. Live cell populations were gated on the basis of cell side and forward scatter and the exclusion of cells positive for Sytox Blue (Life Technologies) or Fixable Viability Dye eFluor450 (eBioscience). Samples were analyzed using FlowJo software V7.6.1 or V10.4.2 (TreeStar Inc., OR).

2.7. In vitro Treg induction assays

96 well U-bottom plates (Greiner bio-one) were pre-coated with 5 μg/ml anti-CD3e (UCHT1, BioLegend) and 15 μg/ml anti-CD28 (CD28.2, BioLegend) in 0.1 M sodium bicarbonate buffer pH = 8.2 for 1 h at 37 °C, followed by 4 °C. Cells were sorted with a FACSArialII (BD) cell sorter for purity. Human naïve live CD8a$^-$CD11b$^-$CD14$^-$CD19$^-$CD3$^+$CD4$^+$CD45RA$^+$CD45RO$^-$CD127$^+$CD25$^-$ T cells were cultured in x-Vivo15 Medium supplemented with 2 mM glutamine, penicillin (50 U/ml), streptomycin (50 μg/ml), and 5% (vol/vol) heat-inactivated human AB serum (Invitrogen) in the presence of 100 U/ml human recombinant IL-2 (Peprotech) in an humidified incubator at 37 °C with 5% CO$_2$. TCR stimulation was limited to 18 h by transferring cells into uncoated wells. Cells were cultured for additional 36 h without further TCR stimulation.

2.8. Quantitative analysis of mRNA abundance

Total RNA was extracted from 300,000 human MACS-purified CD4$^+$ T cell populations using QIAzol Lysis Reagent/miRNeasy Micro Kit according to the manufacturer's instructions. 200 ng total RNA were converted to first strand cDNA using iScript™Advanced cDNA Synthesis Kit (Bio-Rad) in a peqStar2X thermal cycler (Peqlab). Quantitative real-time PCR (RT-qPCR) analyses were performed using SsoFast Evagreen Supermix (Bio-Rad) and gene-specific primer sets on a CFX96 Touch real time system (Bio-Rad). *HISTONE* RNA levels were used for normalization of target gene expression levels. The following primers were used for RT-qPCR analyses (mRNA target, forward primer (5′-3′), reverse primer (5′-3′), manufacturer):

HISTONE, ACTGGCTACAAAAGCCG, ACTTGCCTCCTGCAAAGCAC, Sigma Aldrich; Hs_CD4, TTGCTTCTGGTGCTGCAACT, CAGCGCGATCATT-CAGCTTG, Sigma Aldrich; Hs_FOXP3, order nr Hs_Foxp3_1_SG, Qiagen; Hs_IKZF2, GTGACGTCTGTGGCATGGT, ACCCACAGAATGGGTCCTGA, Sigma Aldrich; Mm_Cidea, TCAGACCTTAAGGGACAACACGCA, TTCTTTGGTTGCTTGCAGACTGGG, Sigma Aldrich; Mm_Ucp1, GGCCTCTACGACTCAGTCCA, TAAGCCGGCTGAGATCTTGT, Sigma Aldrich.

2.9. Immunofluorescence

CD4$^+$ T cells, enriched with the Stem Cell Kit, were fixed with 4.5% Histofix (Carl Roth) for 10 min at room temperature, washed with HBSS and used for cytospins. Stainings were carried out using rabbit-anti-human antibodies for C17orf59/BORCS6 (MyBiosource) and mouse-anti-huCD3 (BioLegend), and as secondary antibodies goat-anti-rabbit AlexaFluor594 and goat-anti-mouse AlexaFluor488 (both Thermofisher). Negative control slides were incubated with secondary antibodies only. Nuclei were stained with Hoechst-33342 before final analysis by confocal Leitz microscopy (TCS-SP5II).

2.10. Quantification and statistical analysis

Data are presented as box-and-whisker plots with min and max values for data distribution or as percentage where appropriate or as summary plots for paired analyses. Student's paired *t*-test was used for treatment analyses and Student's unpaired *t*-test to compare independent groups. For mirabegron titration, one-way ANOVA with Dunnett's multiple comparison test was used and mirabegron treated groups vs. vehicle compared. Correlations were analyzed with either Pearson or nonparametric Spearman as indicated in the respective figures and/or figure legends. For all tests, a two-tailed *p* value of <0.05 was considered to be significant. Statistical significance is shown as * = $p < 0.05$; ** = $p < 0.01$; *** = $p < 0.001$. Analyses were performed using Prism v6.0.1 or v7.04 (GraphPad).

3. RESULTS

3.1. Beta3-adrenergic stimulation induces human Tregs in humanized NSG mice

As a critical, accessible system permitting predictive *in vivo* immunology research, we recently made use of humanized NOD Scid Il2rg KO (NSG) mice and established human Treg induction experiments *in vivo* [17]. In order to dissect the translational relevance of beta3-adrenergic stimulation or cold exposure in supporting Treg induction [22], here we applied the human beta3-receptor agonist mirabegron mimicking cold exposure to humanized NSG mice *in vivo*.

To this end, humanized NSG mice received mirabegron application for 3 d (1 mg/kg, *i.p.*), which resulted in a significant enhancement of thermogenic genes including *Ucp1* and *Cidea* in adipose tissue of humanized mice (Figure 1A). Of note, flow cytometric analyses revealed significantly increased frequencies of human CD4$^+$CD127^{low}CD25^{high} Tregs upon beta3-adrenergic stimulation in humanized mice (CD25^{hi}CD127^{low} [% of CD3$^+$CD4$^+$]: vehicle = 1.998 ± 0.5289 (n = 5) vs. mirabegron = 4.946 ± 1.006 (n = 5), $p = 0.0319$, Figure 1B, C).

Moreover, we used established protocols [15,17,19] to dissect human Treg induction potential *in vitro*. Accordingly, we demonstrated that purified naïve human CD4$^+$ T cells from mirabegron-treated humanized NSG animals had significantly improved Treg-induction capacities *in vitro* (FOXP3^{hi} [% of CD25^{hi}CD127^{low}]: vehicle = 14.18 ± 1.36
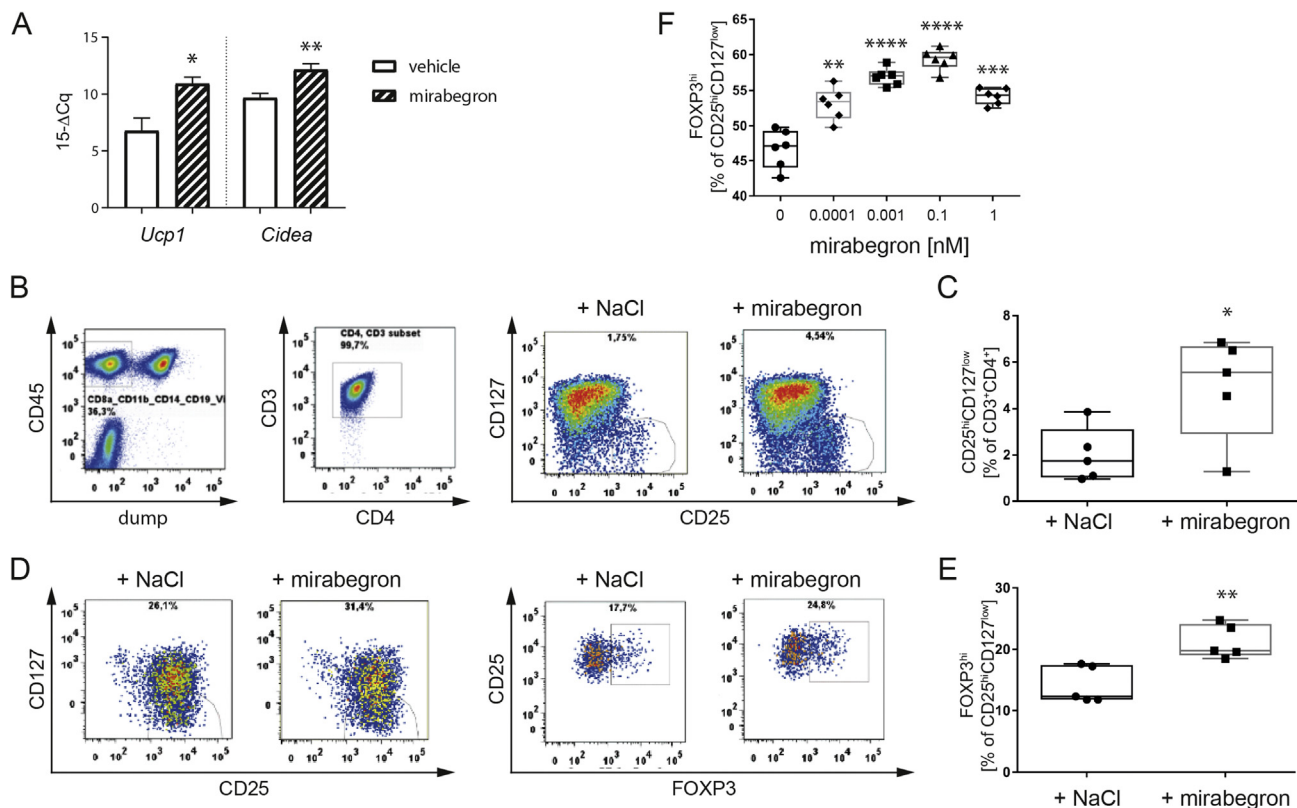
Figure 1: Beta3-adrenergic stimulation enhances Tregs in humanized mice. A) Gene expression analysis of thermogenic markers in murine VAT after vehicle or mirabegron treatment *in vivo*. B) Representative flow cytometric analysis of *ex vivo* Tregs in humanized mice after vehicle or mirabegron treatment *in vivo*. Tregs are gated as $CD8A^-CD11B^-CD14^-CD19^-eF450^-CD45^+CD3^+CD4^+CD127^{low}CD25^{hi}$. C) Summary plot of (B) with 5 mice per group from two independent experiments. D) Representative flow cytometric analysis of *in vitro* induced Tregs isolated from humanized mice after *in vivo* treatment with vehicle or mirabegron. Tregs are gated as live $CD3^+CD4^+CD127^{low}CD25^{hi}FOXP3^{hi}$. E) Summary plot of (D). F) Dose-response titration of mirabegron administered during human *in vitro* Treg induction. Two independent experiments. $* = p < 0.05$, $** = p < 0.01$, $*** = p < 0.01$, $**** = p < 0.001$; one-way ANOVA with mirabegron vs. vehicle.

(n = 5) vs. mirabegron = 21.26 ± 1.235 (n = 5), $p = 0.0049$, Figure 1D, E).

### 3.2. Beta3-adrenergic stimulation enhances human Treg induction potential *in vitro*

In line with the observations obtained in humanized NSG mice, we used human naïve $CD4^+$ T cells from healthy individuals to study the impact of beta3-adrenergic stimulation on human Treg induction *in vitro*. Media supplemented with low doses of mirabegron significantly enhanced human Treg induction *in vitro* (FOXP3^{hi} [% of CD25^{hi}CD127^{low}]: vehicle = 46.68 ± 1.115 vs. mirabegron [0.0001 nM] = 53.12 ± 0.9243, $p = 0.0013$; [0.001 nM] = 56.9 ± 0.498, $p < 0.0001$; [0.1 nM] = 59.35 ± 0.6081, $p < 0.0001$; [1 nM] = 54.18 ± 0.47, $p = 0.0001$, Figure 1F).

3.3. Short-term cold exposure *in vivo* increases human Treg induction potential

Next, to understand the importance of cold exposure for human Treg induction *in vivo* we addressed T cell samples from the FREECE study cohort. Specifically, after a 10 h overnight fast, healthy individuals were subjected to an individualized short-term cold exposure protocol for 2.5 h in the absence of muscle shivering. Blood samples were collected prior and after individualized cold exposure (For subject biometrics please see Table 1). Highly pure human naïve $CD4^+$ T cells were sort-purified before (T_0) and after (T_2) cold

exposure *in vivo* to dissect Treg induction potential *in vitro* (staining examples are provided in Figure 2A).

Cold exposure significantly enhanced Treg induction in both male and female subjects while the effect was more prominent on naïve $CD4^+$ T cells from female individuals (Figure 2B, left panel and Figure 2C, left panel, FOXP3^{hi} [% of CD25^{hi}CD127^{low}]: males $T_0 = 41.93 \pm 5.523$ vs. $T_2 = 44.09 \pm 5.689$ (n = 9), $p = 0.0457$); Figure 2B, right panel and Figure 2C, right panel, FOXP3^{hi} [% of CD25^{hi}CD127^{low}]: females $T_0 = 38.96 \pm 3.116$ vs. $T_2 = 47.58 \pm 3.415$ (n = 13), $p < 0.0001$). When female and male subjects of the FREECE study were sub-divided based on the presence or absence of obesity, it became clear that the Treg-enhancing impact of cold exposure was evident in lean, overweight and obese individuals when looking at Treg induction from naïve $CD4^+$T cells (Supplemental Figure 1, FOXP3^{hi} [% of CD25^{hi}CD127^{low}]: females lean+overweight: $T_0 = 44.14 \pm 5.808$ vs. $T_2 = 51.14 \pm 4.752$ (n = 5), $p = 0.0110$; females obese: $T_0 = 35.72 \pm 3.332$ vs. $T_2 = 45.35 \pm 4.752$ (n = 8), $p = 0.0020$); males lean+overweight: $T_0 = 35.96 \pm 9.363$ vs. $T_2 = 36.29 \pm 9.131$ (n = 4), $p = $ ns; males obese: $T_0 = 46.69 \pm 6.661$ vs. $T_2 = 50.32 \pm 6.678$ (n = 5), $p = 0.0491$). These findings therefore suggest that from an immune-metabolic perspective, cold exposure could be used to positively impinge on Treg induction also in states of overweight and obesity. In addition, we found a negative correlation between Treg induction potential and plasma leptin levels of individuals (Supplemental Figure 2). These results are in line with studies
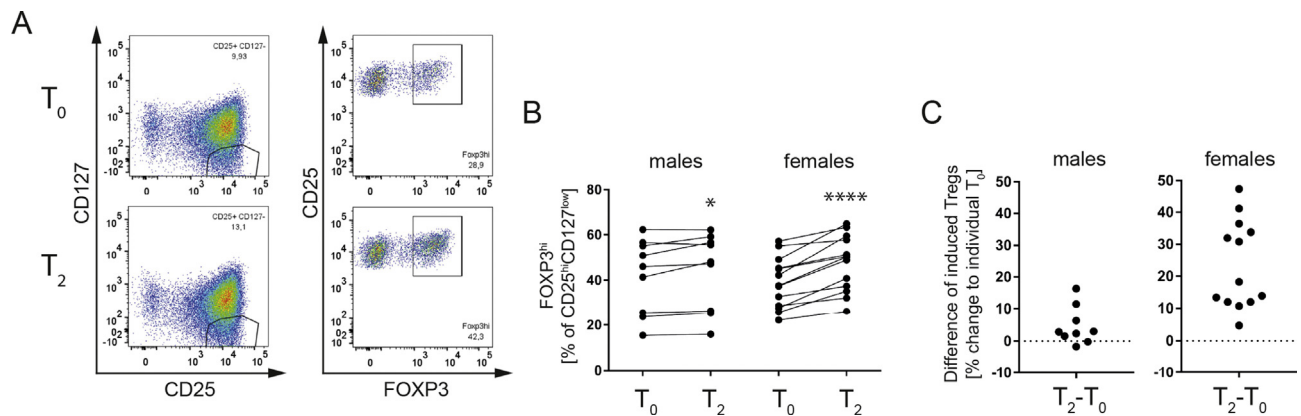
Figure 2: Short-term cold exposure *in vivo* improves human Treg induction *in vitro*. A) Representative flow cytometric analysis of *in vitro* induced Tregs before (T_0) and after (T_2) *in vivo* cold exposure. B) Paired analyses of (A). Each dot represents the mean of 3—4 replicates and an individual experiment performed with paired samples. C) Fold change of *in vitro* induced Tregs normalized to individual T_0. * = $p < 0.05$, ** = $p < 0.01$, *** = $p < 0.01$, **** = $p < 0.001$; paired *t*-test.

indicating that leptin can exert pro-inflammatory characteristics that promote inflammation [35—37]. Accordingly, additional observations have demonstrated an inhibitory effect of leptin on Treg proliferation, thereby further supporting the pro-inflammatory role of leptin [38].

3.4. Short-term cold exposure *in vivo* enhances human Tregs *ex vivo*

Given the increase seen in human *de novo* Treg induction potential upon human cold exposure *in vivo*, especially in female individuals, we
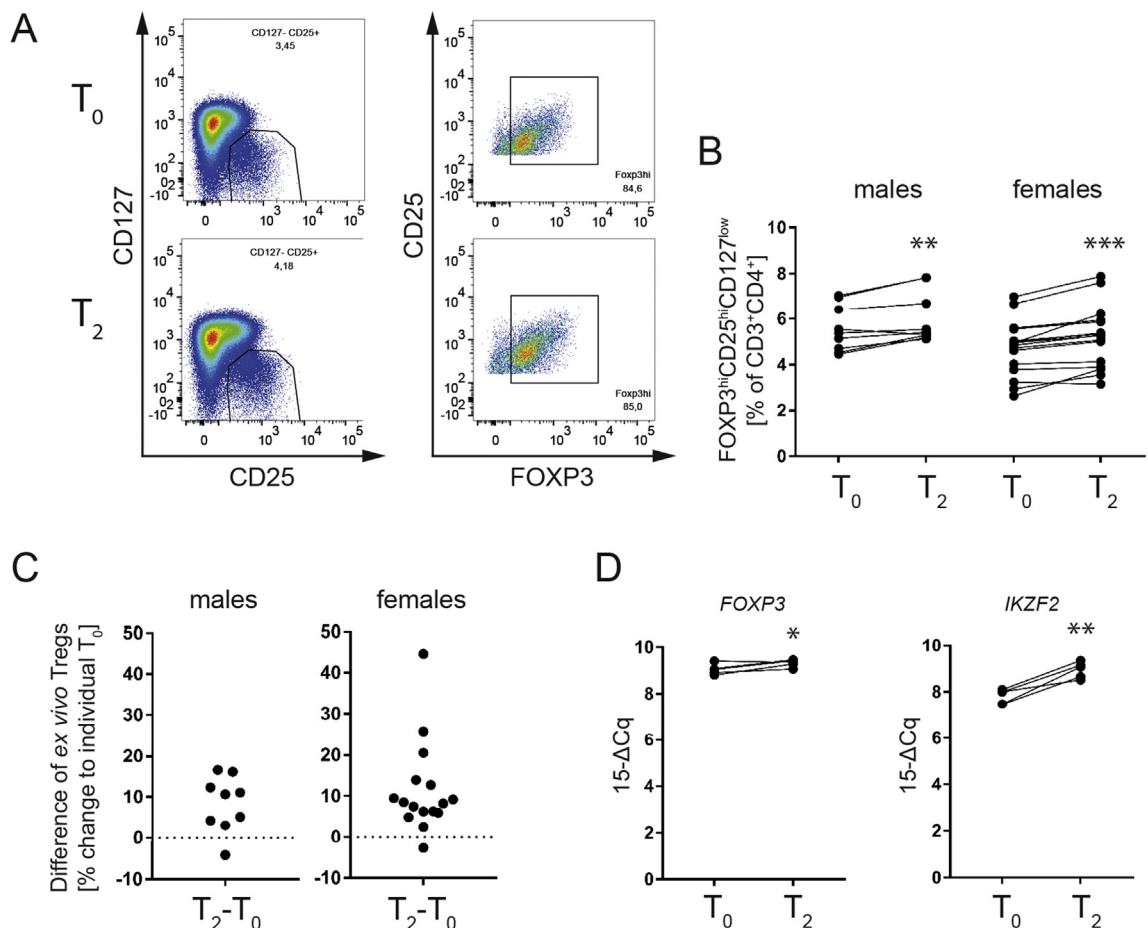
Figure 3: *In vivo* cold increases *ex vivo* Treg frequencies in human peripheral blood. A) Representative flow cytometric analysis of *ex vivo* Tregs in human peripheral blood before (T_0) and after (T_2) *in vivo* cold exposure. B) Paired analyses of (A). Each dot represents an individual experiment performed with paired samples. C) Fold change of (A) *ex vivo* Tregs normalized to individual T_0. D) RT-qPCR analysis of human $CD4^+$ T cells isolated before (T_0) and after (T_2) *in vivo* cold exposure. * = $p < 0.05$, ** = $p < 0.01$, *** = $p < 0.001$; paired *t*-test.

next assessed human Treg frequencies prior and post cold exposure *ex vivo* (Figure 3, staining examples are provided in Figure 3A). Short-term cold exposure resulted in a significant enhancement of human Tregs in peripheral blood, especially in female individuals (Figure 3B, C, FOXP3^{hi}CD25^{hi}CD127^{low} [% of CD3$^+$CD4$^+$]: males $T_0 = 5.574 \pm 0.3362$ vs. $T_2 = 6.02 \pm 0.3752$ (n = 9), $p = 0.0061$; females $T_0 = 4.72 \pm 0.3012$ vs. $T_2 = 5.211 \pm 0.3344$ (n = 16), $p < 0.0001$). In Supplemental Figure 3 subjects were grouped according to their sex and BMI and as observed for the *in vitro* Treg induction depicted in Supplemental Figure 2, the positive effect of cold showed a trend towards increased *ex vivo* Treg frequencies in all subgroups and was more pronounced in the obese sub-cohort (FOXP3^{high}CD25^{high}CD127^{low} [% of CD3$^+$CD4$^+$] of T_0 vs. T_2: lean+overweight females: $T_0 = 3.74 \pm 0.385$ vs. $T_2 = 4.152 \pm 0.339$ (n = 6), $p = 0.0705$; obese females: $T_0 = 5.309 \pm 0.2996$ vs. $T_2 = 5.846 \pm 0.3745$ (n = 10), $p = 0.0012$; lean+overweight males: $T_0 = 5.52 \pm 0.5368$ vs. $T_2 = 6.013 \pm 0.6048$ (n = 4), $p = 0.0532$; obese males: $T_0 = 5.618 \pm 0.4827$ vs. $T_2 = 6.026 \pm 0.5359$ (n = 5), $p = 0.09$. Accordingly, the numerical increase in human Tregs post cold exposure was accompanied by a significantly increased abundance of Treg signature genes such as *FOXP3* (Figure 3D, *FOXP3* expression [15-ΔCq]: $T_0 = 9.056 \pm 0.1014$; vs. $T_2 = 9.324 \pm 0.07054$ (n = 5); $p = 0.0495$) or *IKZF2* (Figure 3D, *IKZF2* expression [15-ΔCq]: $T_0 = 7.812 \pm 0.1387$; vs. $T_2 = 8.952 \pm 0.1559$ (n = 5); $p = 0.0030$.

### 3.5. Short-term cold exposure directly impacts human adipose tissue Tregs

Given the critical role of adipose tissue Treg cells in safeguarding tissue homeostasis and function, we next asked whether a short-term cold exposure stimulus can impinge on adipose tissue Tregs. To this end, biopsies from subcutaneous adipose tissue (SAT) were taken prior and post cold exposure.

First, to validate the relevance of Treg analyses from SAT we investigated *FOXP3/CD4* mRNA ratios in SAT vs. VAT from lean healthy individuals in the steady state. Here, we identified higher ratios of human *FOXP3/CD4* mRNA in SAT when compared to their VAT (*FOXP3/CD4* ratios in SAT $= 0.6465 \pm 0.02387$ (n = 20) vs. VAT $= 0.5464 \pm 0.04857$ (n = 11); $p = 0.0462$, Figure 4A). These findings are in line with the assumption that SAT is less prone towards obesity-induced inflammation when compared to VAT [1].

Next, we purified CD4$^+$ T cells in SAT biopsies from individuals prior (T_0) and 2.5 h post cold exposure (T_2) based on live CD8a$^-$CD11b$^-$CD14$^-$CD19$^-$CD3$^+$CD4$^+$T cells (see Figure 4B for staining example). In the SAT tissue context, the frequencies of locally residing Tregs after 2.5 h of cold exposure did not yet show any significant changes (Figure 4B, C). These findings are in line with previous data from the murine setting in which cold exposure supported a local increase in adipose tissue Tregs earliest after 24 h post cold exposure [22].

3.6. Human Treg induction by cold exposure involves *BORCS6/C17orf59* signaling

Mechanistically and in accordance with findings in the murine setting [22], we observed *BORCS6* mRNA to be significantly induced in human CD4$^+$ T cells upon cold exposure *in vivo* (Figure 5A). *BORCS6* encodes for C17orf59, a Ragulator-interacting protein that blocks mTORC1 activity by interacting with Ragulator at the lysosome [32]. In line with these results, inhibition of mTORC1 was demonstrated in previous studies to support Treg induction [15,19,22]. To validate the results seen for *BORCS6* mRNA expression in human CD4$^+$ T cells following
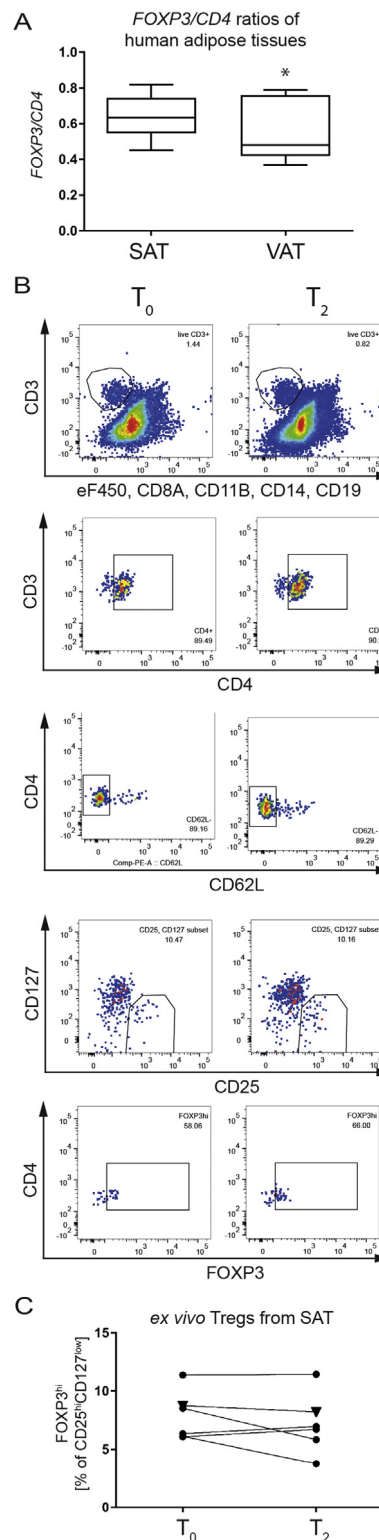
Figure 4: Human adipose tissue harbors FOXP3$^+$ Tregs that can be targeted by cold exposure or beta3-adrenergic stimulation. A) *FOXP3/CD4* gene expression ratios in human adipose tissue biopsies. SAT = subcutaneous adipose tissue, VAT = visceral adipose tissue. B) Representative flow cytometric analysis of human SAT biopsies obtained before (T_0) and after (T_2) *in vivo* cold exposure. Each dot represents an individual experiment with paired samples. C) Paired analyses of (B). * = $p < 0.05$; (A) unpaired *t*-test.
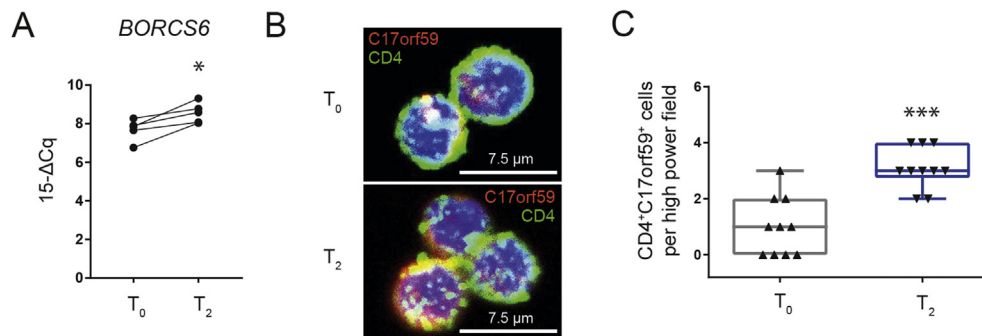
Figure 5: *In vivo* cold exposure increases *BORCS6*/C17orf59 abundance in human CD4$^+$ T cells. A) RT-qPCR analysis of *BORCS6* abundance in human CD4$^+$ T cells before (T$_0$) and after (T$_2$) *in vivo* cold. B) Magnetically enriched human CD4$^+$ T cell cytospins were stained for C17orf59 abundance before (T$_0$) and after (T$_2$) *in vivo* cold. C) Quantification of (B): CD4$^+$ C17orf59$^+$ per high power field. * = $p < 0.05$, *** = $p < 0.001$; paired *t*-test.

cold exposure, we used immunofluorescence for C17orf59 in CD4$^+$ T cells together with confocal microscopy. We found C17orf59 protein expression to be significantly upregulated following cold exposure *in vivo* (CD4$^+$C17orf59$^+$T cells per high power field: T$_0$ = 1.0 ± 0.33; T$_2$ = 3.1 ± 0.23 (n = 10 each); $p < 0.0001$; Figure 5B, C).

4. DISCUSSION

Here, we provide first direct, translational evidence that short-term cold exposure enhances human FOXP3$^+$ Tregs and their induction from naïve CD4$^+$ T cells *in vivo*. We used humanized mice, human *in vitro* Treg induction together with *ex vivo* and *in vitro* analyses of T cells from the FREECE study to demonstrate an important role of low dose beta3-adrenergic stimulation or short-term cold exposure in supporting human FOXP3$^+$Tregs. These findings highlight an important layer of immune-metabolic crosstalk in humans. Specifically, given the recent interest in cold exposure as one critical determinant of energy expenditure together with the identification of cold-inducible BAT in adult humans [25,26], the results obtained here support the concept that metabolic targeting of energy expenditure and adipose tissue will be accompanied by a significant impact on immune regulation that is mainly executed by immune-suppressive Tregs.

Metabolically, cold exposure triggers the release of catecholamines via the sympathetic nervous system (SNS) and thereby, induces beta3-adrenergic signaling. Catecholamine release in adipose tissues plays a substantial role in inducing metabolic activity upon cold exposure and the SNS is critically involved in integrating afferent signals related to metabolism and environment and responding to them via efferent signaling. With regard to the environmental stimulus cold, this includes signaling with noradrenaline and adrenaline (i.e. catecholamines), as it was shown that mice lacking both signaling molecules (due to a knockout of the synthesizing enzyme dopamine beta-hydroxylase) cannot respond to thermal stress in an adequate manner [39]. These mice are unable to increase *Ucp1* expression in BAT upon cold exposure and when being exposed to prolonged environmental cold, the constant heat loss leads to lethargy, shivering and ultimately to death due to hypothermia [39]. From an immunometabolic perspective, in previous experiments in the murine setting we aimed to assess the question whether the observed Treg-adipose-crosstalk in BAT includes a functional programming of BAT-residing T cells. When using UCP1 KO mice as a BAT loss-of-function model, we observed that local Treg induction was reduced [22]. Specifically, these results suggest that the local adipose tissue environment can co-opt local T cell differentiation programs and thereby influence tissue function. These findings are also in line with the concept that Treg induction by

sympathetic drive is critically involved in the regulation of normal adipose tissue function. In addition, to mechanistically dissect these findings, we had studied mice lacking all three beta-adrenergic receptors (betaless mice) [40]. These animals presented with significantly reduced Treg frequencies in inguinal lymph nodes and subcutaneous fat depots. As one potential means to integrate sympathetic tone with reduced Treg abundance seen in betaless mice when compared to WT mice, we observed distinctly reduced proliferation of Tregs in subcutaneous fat of betaless mice. These results therefore underline an impairment of Treg induction in the absence of beta-adrenergic receptors *in vivo* [22]. Overall, our previous findings in the murine setting support the concept that Treg induction and adipose tissue function are adjusted according to the degree of sympathetic tone and environmental temperature [22].

Immunologically, the investigation of *FOXP3/CD4* mRNA ratios in SAT vs. VAT from lean healthy individuals in the steady state revealed higher ratios of human *FOXP3/CD4* mRNA in SAT when compared to their VAT. However, as a potential limitation it is important to consider that *FOXP3* mRNA levels may not directly correlate with protein expression levels and therefore changes in *FOXP3* alone cannot be solely equated to changes in Treg frequency.

Moreover, the Treg-enhancing impact of cold exposure can contribute critically to supporting adipose tissue and metabolic functions as well as to the reduction of local inflammatory responses [22,23,41−45]. In line with these assumptions, it is important to note that the beneficial effects of cold exposure on Treg induction and frequencies *ex vivo* were likewise evident in obese individuals suggesting a broader window of potential intervention for immune-metabolic targeting of adipose tissue function and inflammation by enhancing Tregs.

Future studies will be required to dissect potential differences in female vs. male subjects in response to the beneficial effect of cold exposure on Tregs also in the context of discussed alterations in pro-inflammatory characteristics of male vs. female adipose tissue [46,47]. Here, we have focused our analyses on the direct isolation of Tregs from human adipose tissue biopsies prior and following cold exposure using cell sorting and multi-color flow cytometry. The time frame of two hours of cold exposure, however, might be rather short for the identification of local tissue-specific changes in Treg frequencies in human SAT, given recent insights and kinetics from murine adipose tissue analyses following cold exposure where a significant change in local Tregs was first observed 24 or 48 h post cold acclimation [22,23]. However, from an immunological perspective, more rapid changes are expected to be visible in peripheral blood; in fact we identified a significant increase in Tregs purified from peripheral blood individuals after this short-term cold exposure. Mechanistically, and in line with

murine data upon cold exposure [22], we found *BORCS6* mRNA levels to be significantly increased in human CD4$^+$ T cells following cold exposure. *BORCS6* was recently identified to encode for C17orf59 that functions as a critical player in interacting with Ragulator at the lysosome [32,48,49]. mTORC1 activation requires its co-localization with the Rag—Ragulator complex at lysosomal surfaces. Over-expression of C17orf59 has been demonstrated to disrupt the Rag—Ragulator complex, thereby interfering with Rag lysosomal localization [32,48,49]. Thus, C17orf59 overexpression results in reduced mTORC1 activity. Strong mTOR signaling was shown to limit successful Treg induction [14,15] and consequently, more *BORCS6* mRNA expression and higher C17orf59 abundance improves Treg induction due to reduced mTOR signaling. Established mTORC1 inhibitors such as rapamycin or everolimus have shown a direct enhancement of FOXP3$^+$Tregs due to blockade of mTORC1 activity [14,15]. The increased *BORCS6* mRNA abundance in human CD4$^+$ T cells exposed to short-term cold is in line with a concept in which physiological levels of beta3-adrenergic stimulation can exert mTORC1-inhibiting activity, thereby directly supporting the induction of human FOXP3$^+$Tregs.

5. CONCLUSION

In sum, here we demonstrate that a short-term cold stimulus induces human Treg induction *in vitro* and *in vivo*. Mechanistically, we identify *BORCS6* encoding the Ragulator-interacting protein C17orf59 to be significantly induced in human CD4$^+$ T cells upon short-term cold exposure. These novel insights into the molecular underpinnings of human Treg induction suggest an important role of Tregs in linking sympathetic tone and the environmental stimulus cold with immune and adipose function. Moreover, these discoveries shed new light on potential approaches toward tailored anti-inflammatory concepts to support human adipose tissue homeostasis.

AUTHOR CONTRIBUTIONS

MB performed *in vivo* and *in vitro* experiments, gene expression analyses, analyzed and interpreted data and wrote manuscript. IS performed *in vivo* and *in vitro* experiments. VKS performed dose-response titration. VBO analyzed human SAT/VAT gene expression. LM recruited subjects to and performed the FREECE study. MatBl is PI of the Leipzig Obesity Cohort. HH is PI of the FREECE study. MHT supported conception of the manuscript. CD analyzed data, conceptualized and wrote the manuscript.

FUNDING

CONFLICTS OF INTEREST

None declared.

APPENDIX A. SUPPLEMENTARY DATA

Supplementary data to this article can be found online at https://doi.org/10.1016/j.molmet.2019.08.002.

REFERENCES

[1] Rosen, E.D., Spiegelman, B.M., 2014. What we talk about when we talk about fat. Cell 156(1—2):20—44.

[2] Fontenot, J.D., Gavin, M.A., Rudensky, A.Y., 2003. Foxp3 programs the development and function of CD4+CD25+ regulatory T cells. Nature Immunology 4(4):330—336.

[3] Hori, S., Nomura, T., Sakaguchi, S., 2003. Control of regulatory T cell development by the transcription factor Foxp3. Science 299(5609):1057—1061.

[4] Bennett, C.L., Brunkow, M.E., Ramsdell, F., O'Briant, K.C., Zhu, Q., Fuleihan, R.L., et al., 2001. A rare polyadenylation signal mutation of the FOXP3 gene (AAUAAA—>AAUGAA) leads to the IPEX syndrome. Immunogenetics 53(6):435—439.

[5] Brunkow, M.E., Jeffery, E.W., Hjerrild, K.A., Paeper, B., Clark, L.B., Yasayko, S.A., et al., 2001. Disruption of a new forkhead/winged-helix protein, scurfin, results in the fatal lymphoproliferative disorder of the scurfy mouse. Nature Genetics 27(1):68—73.

[6] Lahl, K., Loddenkemper, C., Drouin, C., Freyer, J., Arnason, J., Eberl, G., et al., 2007. Selective depletion of Foxp3+ regulatory T cells induces a scurfy-like disease. Journal of Experimental Medicine 204(1):57—63.

[7] Walker, M.R., Kasprowicz, D.J., Gersuk, V.H., Benard, A., Van Landeghen, M., Buckner, J.H., et al., 2003. Induction of FoxP3 and acquisition of T regulatory activity by stimulated human CD4+CD25- T cells. Journal of Clinical Investigation 112(9):1437—1443.

[8] Morgan, M.E., van Bilsen, J.H., Bakker, A.M., Heemskerk, B., Schilham, M.W., Hartgers, F.C., et al., 2005. Expression of FOXP3 mRNA is not confined to CD4+CD25+ T regulatory cells in humans. Human Immunology 66(1):13—20.

[9] Liu, W., Putnam, A.L., Xu-Yu, Z., Szot, G.L., Lee, M.R., Zhu, S., et al., 2006. CD127 expression inversely correlates with FoxP3 and suppressive function of human CD4+ T reg cells. Journal of Experimental Medicine 203(7):1701—1711.

[10] Ruprecht, C.R., Gattorno, M., Ferlito, F., Gregorio, A., Martini, A., Lanzavecchia, A., et al., 2005. Coexpression of CD25 and CD27 identifies FoxP3+ regulatory T cells in inflamed synovia. Journal of Experimental Medicine 201(11):1793—1803.

[11] Wing, J.B., Tanaka, A., Sakaguchi, S., 2019. Human FOXP3(+) regulatory T cell heterogeneity and function in autoimmunity and cancer. Immunity 50(2):302—316.

[12] von Boehmer, H., Daniel, C., 2013. Therapeutic opportunities for manipulating T(Reg) cells in autoimmunity and cancer. Nature Reviews Drug Discovery 12(1):51—63.

[13] Daniel, C., Weigmann, B., Bronson, R., Boehmer, H.V., 2011. Prevention of type 1 diabetes in mice by tolerogenic vaccination with a strong agonist insulin mimetope. Journal of Experimental Medicine 208(7):1501–1510.

[14] Daniel, C., Wennhold, K., Kim, H.J., von Boehmer, H., 2010. Enhancement of antigen-specific Treg vaccination in vivo. Proceedings of the National Academy of Sciences of the United States of America 107(37):16246–16251.

[15] Sauer, S., Bruno, L., Hertweck, A., Finlay, D., Leleu, M., Spivakov, M., et al., 2008. T cell receptor signaling controls Foxp3 expression via PI3K, Akt, and mTOR. Proceedings of the National Academy of Sciences of the United States of America 105(22):7797–7802.

[16] Gottschalk, R.A., Corse, E., Allison, J.P., 2010. TCR ligand density and affinity determine peripheral induction of Foxp3 in vivo. Journal of Experimental Medicine 207(8):1701–1711.

[17] Serr, I., Furst, R.W., Achenbach, P., Scherm, M.G., Gokmen, F., Haupt, F., et al., 2016. Type 1 diabetes vaccine candidates promote human Foxp3(+) Treg induction in humanized mice. Nature Communications 7:10991.

[18] Haxhinasto, S., Mathis, D., Benoist, C., 2008. The AKT-mTOR axis regulates de novo differentiation of CD4+Foxp3+ cells. Journal of Experimental Medicine 205(3):565–574.

[19] Serr, I., Scherm, M.G., Zahm, A.M., Schug, J., Flynn, V.K., Hippich, M., et al., 2018. A miRNA181a/NFAT5 axis links impaired T cell tolerance induction with autoimmune type 1 diabetes. Science Translational Medicine 10(422).

[20] Cipolletta, D., Feuerer, M., Li, A., Kamei, N., Lee, J., Shoelson, S.E., et al., 2012. PPAR-gamma is a major driver of the accumulation and phenotype of adipose tissue Treg cells. Nature 486(7404):549–553.

[21] Feuerer, M., Herrero, L., Cipolletta, D., Naaz, A., Wong, J., Nayer, A., et al., 2009. Lean, but not obese, fat is enriched for a unique population of regulatory T cells that affect metabolic parameters. Nature Medicine 15(8):930–939.

[22] Kalin, S., Becker, M., Ott, V.B., Serr, I., Hosp, F., Mollah, M.M.H., et al., 2017. A stat6/pten Axis links regulatory T cells with adipose tissue function. Cell Metabolism 26(3):475–492 e7.

[23] Medrikova, D., Sijmonsma, T.P., Sowodniok, K., Richards, D.M., Delacher, M., Sticht, C., et al., 2015. Brown adipose tissue harbors a distinct sub-population of regulatory T cells. PLoS One 10(2):e0118534.

[24] Wu, J., Bostrom, P., Sparks, L.M., Ye, L., Choi, J.H., Giang, A.H., et al., 2012. Beige adipocytes are a distinct type of thermogenic fat cell in mouse and human. Cell 150(2):366–376.

[25] Saito, M., Okamatsu-Ogura, Y., Matsushita, M., Watanabe, K., Yoneshiro, T., Nio-Kobayashi, J., et al., 2009. High incidence of metabolically active brown adipose tissue in healthy adult humans: effects of cold exposure and adiposity. Diabetes 58(7):1526–1531.

[26] Cypess, A.M., White, A.P., Vernochet, C., Schulz, T.J., Xue, R., Sass, C.A., et al., 2013. Anatomical localization, gene expression profiling and functional characterization of adult human neck brown fat. Nature Medicine 19(5):635–639.

[27] Yu, X.Y., Lin, S.G., Wang, X.M., Liu, Y., Zhang, B., Lin, Q.X., et al., 2007. Evidence for coexistence of three beta-adrenoceptor subtypes in human peripheral lymphocytes. Clinical Pharmacology and Therapeutics 81(5):654–658.

[28] Malik, M., van Gelderen, E.M., Lee, J.H., Kowalski, D.L., Yen, M., Goldwater, R., et al., 2012. Proarrhythmic safety of repeat doses of mirabegron in healthy subjects: a randomized, double-blind, placebo-, and active-controlled thorough QT study. Clinical Pharmacology and Therapeutics 92(6):696–706.

[29] Takasu, T., Ukai, M., Sato, S., Matsui, T., Nagase, I., Maruyama, T., et al., 2007. Effect of (R)-2-(2-aminothiazol-4-yl)-4'-{2-[(2-hydroxy-2-phenylethyl) amino]ethyl} acetanilide (YM178), a novel selective beta3-adrenoceptor agonist, on bladder function. Journal of Pharmacology and Experimental Therapeutics 321(2):642–647.

[30] Hanssen, M.J., Hoeks, J., Brans, B., van der Lans, A.A., Schaart, G., van den Driessche, J.J., et al., 2015. Short-term cold acclimation improves insulin sensitivity in patients with type 2 diabetes mellitus. Nature Medicine 21(8):863–865.

[31] Cypess, A.M., Weiner, L.S., Roberts-Toler, C., Franquet Elia, E., Kessler, S.H., Kahn, P.A., et al., 2015. Activation of human brown adipose tissue by a beta3-adrenergic receptor agonist. Cell Metabolism 21(1):33–38.

[32] Schweitzer, L.D., Comb, W.C., Bar-Peled, L., Sabatini, D.M., 2015. Disruption of the rag-ragulator complex by c17orf59 inhibits mTORC1. Cell Reports 12(9):1445–1455.

[33] Kloting, N., Fasshauer, M., Dietrich, A., Kovacs, P., Schon, M.R., Kern, M., et al., 2010. Insulin-sensitive obesity. American Journal of Physiology Endocrinology and Metabolism 299(3):E506–E515.

[34] Weir, J.B., 1949. New methods for calculating metabolic rate with special reference to protein metabolism. Journal of Physiology 109(1–2):1–9.

[35] Reis, B.S., Lee, K., Fanok, M.H., Mascaraque, C., Amoury, M., Cohn, L.B., et al., 2015. Leptin receptor signaling in T cells is required for Th17 differentiation. The Journal of Immunology 194(11):5253–5260.

[36] Matarese, G., Procaccini, C., De Rosa, V., Horvath, T.L., La Cava, A., 2010. Regulatory T cells in obesity: the leptin connection. Trends in Molecular Medicine 16(6):247–256.

[37] Lord, G.M., Matarese, G., Howard, J.K., Baker, R.J., Bloom, S.R., Lechler, R.I., 1998. Leptin modulates the T-cell immune response and reverses starvation-induced immunosuppression. Nature 394(6696):897–901.

[38] De Rosa, V., Procaccini, C., Cali, G., Pirozzi, G., Fontana, S., Zappacosta, S., et al., 2007. A key role of leptin in the control of regulatory T cell proliferation. Immunity 26(2):241–255.

[39] Thomas, S.A., Palmiter, R.D., 1997. Thermoregulatory and metabolic phenotypes of mice lacking noradrenaline and adrenaline. Nature 387(6628):94–97.

[40] Bachman, E.S., Dhillon, H., Zhang, C.-Y., Cinti, S., Bianco, A.C., Kobilka, B.K., et al., 2002. βAR signaling required for diet-induced thermogenesis and obesity resistance. Science 297(5582):843–845.

[41] Guillot, X., Martin, H., Seguin-Py, S., Maguin-Gate, K., Moretto, J., Totoson, P., et al., 2017. Local cryotherapy improves adjuvant-induced arthritis through down-regulation of IL-6/IL-17 pathway but independently of TNFalpha. PLoS One 12(7):e0178668.

[42] Guillot, X., Tordi, N., Mourot, L., Demougeot, C., Dugue, B., Prati, C., et al., 2014. Cryotherapy in inflammatory rheumatic diseases: a systematic review. Expert Review of Clinical Immunology 10(2):281–294.

[43] Lange, U., Uhlemann, C., Muller-Ladner, U., 2008. Serial whole-body cryotherapy in the criostream for inflammatory rheumatic diseases. A pilot study. Medizinische Klinik (Munich) 103(6):383–388.

[44] Miller, E., Mrowicka, M., Malinowska, K., Zolynski, K., Kedziora, J., 2010. Effects of the whole-body cryotherapy on a total antioxidative status and activities of some antioxidative enzymes in blood of patients with multiple sclerosis-preliminary study. The Journal of Medical Investigation 57(1,2):168–173.

[45] Miller, E., Kostka, J., Wlodarczyk, T., Dugue, B., 2016. Whole-body cryo-stimulation (cryotherapy) provides benefits for fatigue and functional status in multiple sclerosis patients. A case-control study. Acta Neurologica Scandinavica 134(6):420–426.

[46] Karastergiou, K., Smith, S.R., Greenberg, A.S., Fried, S.K., 2012. Sex differences in human adipose tissues - the biology of pear shape. Biology of Sex Differences 3(1):13.

[47] Jeffery, E., Wing, A., Holtrup, B., Sebo, Z., Kaplan, J.L., Saavedra-Pena, R., et al., 2016. The adipose tissue microenvironment regulates depot-specific adipogenesis in obesity. Cell Metabolism 24(1):142–150.

[48] Zhang, T., Wang, R., Wang, Z., Wang, X., Wang, F., Ding, J., 2017. Structural basis for Ragulator functioning as a scaffold in membrane-anchoring of Rag GTPases and mTORC1. Nature Communications 8(1):1394.

[49] Filipek, P.A., de Araujo, M.E.G., Vogel, G.F., De Smet, C.H., Eberharter, D., Rebsamen, M., et al., 2017. LAMTOR/Ragulator is a negative regulator of Arl8b- and BORC-dependent late endosomal positioning. The Journal of Cell Biology 216(12):4199–4215.